The Role of Intracellular Trafficking of Alzheimer's Disease Amyloid Precursor Protein in Beta-Amyloid Peptide Formation

by

Wai Yan Choy

A dissertation submitted in partial satisfaction of the

requirements for the degree of

Doctor of Philosophy

in

Molecular and Cell Biology

in the

Graduate Division

of the

University of California, Berkeley

Committee in charge:

Professor Randy Schekman, Chair
Professor David Bilder
Professor Lu Chen
Professor William Jagust

Fall 2011

The Role of Intracellular Trafficking of Alzheimer's Disease Amyloid Precursor Protein in Beta-Amyloid Peptide Formation

by

Wai Yan Choy

Abstract

The Role of Intracellular Trafficking of Alzheimer's Disease Amyloid Precursor Protein in Beta-Amyloid Peptide Formation

by

Wai Yan Choy

Doctor of Philosophy in Molecular and Cell Biology

University of California, Berkeley

Professor Randy Schekman, Chair

Amyloid precursor protein (APP) is processed sequentially by β-site APP cleaving enzyme (BACE) and γ-secretase to generate amyloid β (Aβ) peptides, one of the hallmarks of Alzheimer's disease. Endosomes or the *trans*-Golgi network (TGN) are suggested as major subcellular compartments favorable for Aβ production; however, it is still controversial where this process actually occurs. In this study, we investigated the role of different post-endocytic trafficking events in Aβ production using an RNA interference (RNAi) approach. Depletion of Hrs and Tsg101 acting early in the multivesicular bodies (MVB) pathway retained APP in early endosomes and reduced Aβ production. Conversely, depletion of CHMP6 and VPS4 acting late in the pathway rerouted endosomal APP to the TGN for enhanced APP processing. We also showed that VPS35-mediated APP recycling to the TGN was required for efficient Aβ production. Interfering with the bidirectional trafficking of APP between the TGN and endosomes, particularly retromer-mediated retrieval of APP from early endosomes to the TGN, resulted in the accumulation of endocytosed APP in early endosomes with reduced APP processing. These data suggested that Aβ was generated predominantly in the TGN, from the endocytosed pool of APP that had recycled from early endosomes to the TGN.

To Mother, Father, Nam, and Ethan

TABLE OF CONTENTS

LIST OF FIGURES

CHAPTER FIVE

ACKNOWLEDGEMENTS

First and foremost I would like to express my sincerest gratitude to my supervisor, Professor Randy Schekman, for his guidance and support throughout my graduate school years. Randy is an enthusiastic, supportive, and down-to-earth mentor. He gave me the freedom to explore and pursue an ambitious project on my own. He provided me with the best training needed to become an independent researcher. I am honored to be a part of the Schekman Lab.

I am deeply grateful to the Croucher Foundation in Hong Kong for granting me a Ph.D. fellowship (as well as a future postdoctoral fellowship) that allowed me to pursue my dreams at UC Berkeley. I appreciate the late Noel Croucher, founder of the Croucher Foundation, for his generosity and great vision to support the next generation scientists from Hong Kong.

I would like to thank my thesis committee members: Professor David Bilder, Professor Lu Chen, and Professor William Jagust for their helpful advice on my thesis. I want to also thank Professor Jeremy Thorner and Professor Nilabh Shastri for their guidance and support during my rotations in their laboratories.

I would like to thank the past and present members of the Schekman lab for all their help. I want to thank John Tran and Kanika Bajaj for their support and friendship through the years. Special thanks are given to John for helping with my thesis writing, and all his invaluable advice on surviving graduate school. I also want to thank Kanika for all her care and encouragement. I appreciate all the useful parenting advice from experts of the Mom's Group in Schekman Lab. They made me learn that you can be a good parent and a successful scientist at the same time. Special thanks to Yusong Guo for useful suggestions in science and life, who will soon join the Mom's Group. I enjoyed the discussions with many great former lab members: Robyn Barfield, Chris Fromme, Shoomin Shim, Jinoh Kim, and Bertrand Kleizen. I want to especially thank Bob Lesch, Susan Hamamoto, and Peggy McCutchan Smith for their technical support. I would also like to thank Jason Lam for all our conversations related to Hong Kong.

I would like to thank Ann Fischer and Michelle Richner for their excellent tissue culture support that is important for good experiments, and their genuine friendship that is important in life. I want to especially thank my graduate school classmates and best friends Jason Chien and Deng Pan for making my graduate school life outside science enjoyable and memorable. I would also like to thank many good friends in the department: Aaron Cheng, Heshu Lu, Nanhai He, Isabelle Le Blanc, and Weiliang Fan.

I dedicate this thesis to my beloved family. I am eternally grateful to my parents Rosa and Igino for their unconditional love, support, patience and prayers over the years. I know that they are always there for me; no matter if I cry or smile. I would like to thank my loving and supportive husband Nam for his love, encouragement and patience.

He is a wonderful husband, soulmate, and mentor to me. He gives me the strength and courage to persist in my graduate studies. I want to thank my lovely son Ethan for bringing me infinite happiness and make me understand the true meaning of life. I cherish all the moments I spend with my family. I would also like to thank my brother Vincent and my cousin and best friend Catherine for their love and support.

Last but not least, I praise God everyday for his endless love and grace. *The Lord is my shepherd, I shall not want (Psalm 23).* I am looking forward to the amazing journey that God has planned for me after my graduation.

CHAPTER ONE
INTRODUCTION

Overview of Alzheimer's disease

Alzheimer's disease, the leading cause of dementia in the elderly, is a progressive and irreversible neurodegenerative defect that is characterized by impairments in cognition, memory and behavior. More than 5 million Americans over age 65 were estimated to have Alzheimer's disease in 2010, and this number is projected to increase tremendously to over 13 million in 2015, according to a report published by the Alzheimer's Association in 2010 (http://www.alz.org/alzheimers_disease_trajectory.asp). Although there are drugs that may reduce certain symptoms or delay the progression of Alzheimer's disease in some patients, there are currently no known treatments that can prevent or completely cure Alzheimer's disease, despite the fact that research on Alzheimer's disease has already been conducted for a century. More than a hundred years ago, Dr. Alois Alzheimer, a German psychiatrist and neuropathologist, first described senile plaques and neurofibrillary tangles as the histopathological hallmarks found in brains of patients with Alzheimer's disease (Burns et al., 2002). It was later discovered that these senile plaques are extracellular protein aggregates that are composed mainly of β-amyloid (Aβ) peptides (Kang et al., 1987), whereas neurofibrillary tangles are intracellular paired helical filaments primarily consisting of the hyperphosphorylated form of the microtubule-associated protein tau (Lee et al., 1991). The most commonly view accepted has been the "amyloid cascade hypothesis", which posits that the deposition of Aβ peptides in the brain would trigger a cascade of events such as oxidative stress and synaptic loss, leading to eventual neuronal dysfunction and cell death in the brain and Alzheimer's disease (Hardy and Selkoe, 2002; Hardy and Higgins, 1992). However, the primary cause of Alzheimer's disease remains unclear and controversial, since it is a complex disease that can be caused by a combination of different genetic and environmental risk factors. Due to the lack of an effective cure for Alzheimer's disease and the extended life expectancy of the aging population, the financial burden associated with Alzheimer's disease is projected to increase exponentially as estimated by the Alzheimer's Association. Therefore, there is an urgent need to gain better understanding of the molecular mechanism underlying the pathology of this devastating disease in hopes of providing insights into the development of better therapies to prevent and cure Alzheimer's disease.

Proteolytic processing of β-amyloid precursor protein (APP)

According to the "amyloid cascade hypothesis", enhanced production of Aβ peptides is the underlying cause of the pathology of Alzheimer's disease (Hardy and Selkoe, 2002; Hardy and Higgins, 1992). Aβ peptides of 39 to 43 amino acids in length are the cleaved fragments of β-amyloid precursor protein (APP) through sequential proteolytic processing. APP is a type-I transmembrane protein with a large extracellular domain and a short cytosolic tail. There are 3 common alternatively spliced forms of APP, including the shorter APP_{695} isoform that is expressed predominantly in neurons, and the APP_{751} and APP_{770} isoforms that are widely expressed throughout the body (O'Brien and Wong, 2011).

APP can be processed either in the non-amyloidogenic or amyloidogenic pathways. In the non-amyloidogenic pathway, also known as the α-secretase pathway, APP is cleaved primarily by the metalloproteinases ADAM-9, ADAM-10 and TACE/ADAM-17 at the cell surface which results in the secretion of soluble sAPPα fragments into the extracellular space (Buxbaum et al., 1998). No Aβ peptides are formed in the non-amyloidogenic pathway since α-secretase cleavage happens within the Aβ sequence of APP. Alternatively, APP in the amyloidogenic pathway undergoes sequential steps of proteolytic processing first by the β-site APP cleaving enzyme (BACE), or the β-secretase (Lin et al., 2000; Sinha et al., 1999; Vassar et al., 1999), and then by γ-secretase to yield Aβ peptides primarily of either a 40-residue form ($A\beta_{40}$) or a 42-residue form ($A\beta_{42}$) (Fig. 1-1).

BACE is a type-I transmembrane aspartyl protease that initially cleaves within the extracellular domain of APP to produce a membrane-bound C-terminal fragment CTFβ, also known as C99, the substrate for subsequent intramembranous proteolytic processing by γ-secretase (Lin et al., 2000; Sinha et al., 1999; Vassar et al., 1999). Knockout of BACE gene abolishes Aβ production (Cai et al., 2001; Luo et al., 2001). γ-Secretase is a multisubunit aspartyl protease complex that is composed of four membrane proteins, including presenilin-1 (PSEN-1) or its homolog presenilin-2 (PSEN-2), nicastrin (NCT), anterior pharynx defective-1 (APH-1) and presenilin enhancer-2 (PEN-2) (Kaether et al., 2006; Takasugi et al., 2003). The catalytic subunit of γ-secretase is believed to be PSEN-1, in which PSEN-1-knockout mice are shown to significantly reduce γ-secretase cleavage of APP into Aβ peptides (De Strooper et al., 1998). PSEN-1 contains nine transmembrane domains (TMDs), with two conserved catalytic aspartate residues embedded in TMD6 and TMD7 (Laudon et al., 2005; Spasic et al., 2006), and the substrate-binding site located in TMD9 (Sato et al., 2008). It has been suggested that the full length PSEN-1 remains catalytically inactive until it is endoproteolytically processed between TMD6 and TMD7 to yield a heterodimer of the PSEN-1 N-terminal fragment (NTF) and the C-terminal fragment (CTF), in which the endoproteolysis of PSEN-1 and the formation of active γ-secretase complex are regulated by the stepwise assembly of PSEN-1, NCT, APH-1 and PEN-2 (Kaether et al., 2006; Wolfe et al., 1999).

The amyloidogenic pathway is not unique to Alzhiemer's disease patients; it happens under normal physiological condition in healthy people. APP is processed in both the non-amyloidogenic and non-amyloidogenic pathways, in which about 90-95% of the total secreted Aβ peptides comprise the innocuous and soluble $A\beta_{40}$ (Seubert et al., 1992). Despite the fact that $A\beta_{42}$ peptides are produced in minute quantities, they are highly aggregation-prone. Mutations in the genes that encode APP and the catalytic subunits of γ-secretase are known to cause the early-onset form of Alzheimer's disease known as familial Alzheimer's disease (FAD). In many cases, there is also an increase in the relative ratio between the highly aggregation-prone $A\beta_{42}$ peptides and the soluble $A\beta_{40}$ peptides (Scheuner et al., 1996), in which $A\beta_{42}$ peptides accumulate to high levels in the brain regions to induce neurodegeneration. However, the specific mechanism that leads to selective elevation of the $A\beta_{42}/A\beta_{40}$ ratio by these FAD-linked mutations still

remains elusive (Hardy and Selkoe, 2002; LaFerla, 2002; Walsh and Selkoe, 2004). It is also unclear how the "amyloid cascade hypothesis" could explain the more common late-onset sporadic form of Alzheimer's disease, because an increase of $A\beta_{42}/A\beta_{40}$ ratio is not necessarily observed in all late-onset Alzheimer's disease patients.

Genes associated with Alzheimer's disease

Genetic analyses of patients having early-onset familial Alzheimer's disease (FAD) revealed autosomal dominant mutations in three genes: APP on chromosome 21 (St George-Hyslop et al., 1987), PSEN-1 on chromosome 14 (Sherrington et al., 1995) and its homolog PSEN-2 on chromosome 1 (Levy-Lahad et al., 1995); not surprisingly, these are all important players central to the amyloidogenic pathway. According to the Alzheimer Disease & Frontotemporal Dementia Mutation Database, there are 32 mutations found in APP, 185 mutations found in PSEN-1, and 13 mutations found in PSEN-2 to date (Cruts and Van Broeckhoven, 1998a, b) (http://www.molgen.ua.ac.be/ADMutations). All of these autosomal dominant mutations lead to an increase in the $A\beta_{42}/A\beta_{40}$ ratio (Cruts and Van Broeckhoven, 1998a, b), which forms the basis of the significant role of Aβ in the "amyloid cascade hypothesis". However, since FAD-linked mutations in APP, PSEN-1, and PSEN2 only constitute less than 5% of all Alzheimer's disease cases, further genetic studies are necessary to identify additional genes that underlie the more common late-onset sporadic Alzheimer's disease.

By using genetic linkage analysis to associate common polymorphism with increased risk for late-onset Alzheimer's disease, the first and major susceptibility gene was found to be apolipoprotein E (APOE) on chromosome 19 (Pericak-Vance et al., 1991; Schmechel et al., 1993; Strittmatter et al., 1993). APOE is a major lipoprotein component of the very low density lipoprotein (VLDL) complexes that regulates lipid metabolism by transporting cholesterol and other lipids in different cell types (Mahley and Rall, 2000). It has been suggested that APOE promotes the conversion of monomeric Aβ peptides into the more neurotoxic Aβ oligomers and fibrils (Ma et al., 1994). Although APOE is regarded as the most important genetic risk factor for late-onset Alzheimer's disease, it still does not account for all cases of Alzheimer's disease, suggesting that there are other susceptibility genes yet to be identified. Other potential risk factors such as angiotensin-converting enzyme (ACE) (Kehoe et al., 1999) and SORLA (sortilin-related receptor) (Rogaeva et al., 2007) have been reported to be associated with late-onset Alzheimer's disease using the classical candidate gene approach; yet, they only show modest statistical support. More recently, several researchers have performed genome-wide association studies (GWAS) in Alzheimer's disease and successfully identified new and more significant loci associated with late-onset Alzheimer's disease. To date, except for APOE that was identified two decades ago, all other risk factors in Alzheimer's disease on the top ten list of the Alzheimer Research Forum ALZGENE database (http://www.alzgene.org/TopResults.asp) were discovered using this massive testing, unbiased and hypothesis-free GWAS approach. These novel genome-wide significant risk loci includes clusterin (CLU, also known as apolipoprotein J), complement component (3b/4b) receptor 1 (CR1), phosphatidylinositol

binding clathrin assembly protein (PICALM), and bridging integrator 1 (BIN1) (Harold et al., 2009; Hollingworth et al., 2011; Lambert et al., 2009). Identification of more susceptible genes in late-onset Alzheimer's disease and follow-up functional studies will help us to understand more about the molecular mechanisms underlying this disease.

Intracellular trafficking and diseases

Intracellular trafficking of biomolecules such as proteins and lipids to correct destinations is essential to maintain normal cellular functions. Retention of these molecules in upstream compartments, or the mistargeting to wrong compartments may prevent them from reaching the desired compartments in which they function optimally, or may disturb the balance in other compartments by accumulation of unwanted molecules. Hence, defects in intracellular trafficking could lead to diseases.

Protein retention in the secretory pathway, primarily in the endoplasmic reticulum, is a common cause of many diseases. The ER is the site of protein synthesis, and its intrinsic quality control machinery ensures only properly folded proteins are transported from the ER to downstream organelles. In cystic fibrosis patients, the ΔF508 mutation in the chloride channel, the cystic fibrosis transmembrane conductance regulator (CFTR), causes incomplete CFTR folding, thereby inhibiting ER export of CFTR and proper transport to the plasma membrane, which results in defective chloride transport across the apical epithelial membrane (Bertrand and Frizzell, 2003). Other diseases that are related to defective ER exit due to protein misfolding include nephrogenic diabetes insipidus (Tamarappoo and Verkman, 1998), congenital hyperinsulinism (Cartier et al., 2001), and Menkes' disease (Lutsenko and Petris, 2003).

In addition to protein folding defects, mutations in the COPII coat complex that mediates protein export from the ER can also lead to disease-causing protein retention in the ER. The COPII coat consists of a small GTP binding protein Sar1, and two heterodimeric sub-complexes, with Sec23/Sec24 in the inner coat and Sec13/Sec31 in the outer coat (Jensen and Schekman, 2011). Mutations in Sar1B are found in chylomicron retention disease and Anderson disease, in which lipoprotein-containing chylomicrons cannot be secreted from intestinal epithelial cells into the bloodstream, leading to a disorder in fat absorption (Jones et al., 2003). ER export of a planar cell polarity protein Vangl2 is inhibited by Sec24B mutations in a mouse model of craniorachischisis, an extreme neural tube defect (Merte et al., 2010). Other COPII-related diseases include Sec23A mutation in cranio-lenticulo-sutural dysplasia (CLSD) (Boyadjiev et al., 2006) and Sec23B mutations in congenital dyserythropoietic anemia type II (CDAII) (Schwarz et al., 2009). Along the secretory pathway, some proteins are retained in the Golgi complex resulting in diseases such as Dent's disease (Ludwig et al., 2005), and autosomal dominant retinitis pigmentosa (Deretic et al., 2005).

Abnormal trafficking through the endosomal and lysosomal pathways also gives rise to different diseases. In Niemann-Pick type C disease (NPC), a neurodegenerative disease, mutations in the NPC-1 and NPC-2 genes inhibit the export of cholesterol and

glycosphingolipids out of late endosomes and lysosomes, leading to the lysosomal accumulation of lipids in neurons that eventually causes brain dysfunction (Karten et al., 2009). Mutations in GlcNAc-1-phosphotransferase in patients with mucolipidosis type II (MLII) and III (MLIII) diseases, also known as I-cell disease, inhibit the trafficking of lysosomal enzymes to the lysosome due to impairment in the formation of mannose-6 phosphate, resulting in the secretion of lysosomal enzymes, and hence lysosome dysfunction (Kollmann et al., 2010).

Defective protein targeting in polarized cells is also associated with some diseases. Primary cilium dysfunction is the underlying cause of Bardet-Biedl syndrome (BBS), in which mutations in some BBS genes such as BBS3/Arl6 lead to impaired sorting of cell surface proteins including signaling receptors to the cilium (Fliegauf et al., 2007; Jin et al., 2010). Missorting of proteins to the apical or basolateral membranes can also cause diseases such as Bartter syndrome, congenital sucraseisomaltase deficiency, retinitis pigmentosa, and familial hypercholesterolaemia (Mellman and Nelson, 2008).

Intracellular trafficking of APP and Aβ production

The three key players in the amyloidogenic pathway, namely APP, BACE, γ-secretase, are transmembrane proteins that traffic through the secretory pathway as well as the endocytic pathway, which involves trafficking of proteins from the plasma membrane to the lysosomes via early and late endosomes. Hence, it is in theory equally possible that APP could be cleaved into Aβ in any of the organelles along these pathways, including the ER, the Golgi apparatus, the plasma membrane, early or late endosomes, the lysosome, and the recycling compartments (Small and Gandy, 2006; Thinakaran and Koo, 2008). Therefore, the subcellular compartment in which APP is processed to generate Aβ has been controversial.

Although PSEN-1, the catalytic subunit of γ-secretase, localizes predominantly in the ER, there is a spatial paradox phenomenon that the subcellular localization of PSEN-1 may not necessary overlap with the subcellular compartments where γ-secretase actively generates Aβ peptides (Cupers et al., 2001). Endoproteolysis of full length PSEN1 into N-terminal fragment (NTF) and the C-terminal fragment (CTF) is required to maximize γ-secretase activity by stabilizing the conformation of two catalytic aspartate residues embedded in TMD6 and TMD7 of PSEN1 (Kaether et al., 2006; Steiner et al., 2008). We were interested in examining whether PSEN-1 is exported from the ER in a precursor or proteolytically activated form. In Kim et al., we used a cell-free COPII vesicle budding assay to detect the capture of cargo proteins en route to the Golgi complex (Kim et al., 2007). This *in vitro* budding assay is performed by incubating semi-intact mammalian cells as the source of ER membrane, rat liver cytosol, purified recombinant COPII components, an ATP regenerating system and GTP as energy source, and the budded vesicle fraction is separated by high speed centrifugation for analysis (Barlowe et al., 1994; Kim et al., 2005; Matsuoka et al., 1998). Using this COPII budding assay, it was shown previously by our laboratory that PSEN-1 exited the ER without undergoing the endoproteolysis required to maximize γ-secretase activity, suggesting that Aβ production

is likely to occur after exiting the ER (Kim et al., 2007). Along the secretory pathway, several groups suggested the Golgi apparatus or the *trans*-Golgi network (TGN) as the major Aβ-producing organelle (Burgos et al., 2010; Siman and Velji, 2003; Xu et al., 1997) based on subcellular fractionation and localization analyses, whereas the plasma membrane was demonstrated to be the predominant site for non-amyloidogenic processing of APP by α-secretase

In addition to the TGN, the endocytic pathway has also been shown to play significant roles in the proper processing of APP into Aβ. Endocytosis of APP is dependent on a C-terminal cytoplasmic endocytic sorting signal, GYENPTY (amino acids 737–743). Mutations of this endocytic motif or deletion of the whole cytoplasmic domain significantly abolished the internalization of APP from the cell surface (Perez et al., 1999). Inhibition of endocytosis by mutating the endocytic signal of APP or by expressing a dominant negative mutant of dynamin reduces Aβ level dramatically (Carey et al., 2005; Perez et al., 1999), suggesting that endocytosis of APP is required for Aβ production. In addition, it is generally believed that the first enzymatic cleavage of APP by BACE to form the membrane-bound APP C-terminal fragment (β-CTF), an intermediate substrate for γ-secretase to produce Aβ, occurs predominantly in early endosomes, based on evidence showing that the acidic environment in endosomes is optimum for β-secretase activity, and the strong interaction between APP and BACE in endosomal compartments as demonstrated by fluorescence resonance energy transfer (FRET) analysis (Huse et al., 2000; Kinoshita et al., 2003). Electron microscopy (EM) analysis has demonstrated that $A\beta_{42}$ peptides are localized predominantly to multivesicular bodies (MVB) (Takahashi et al., 2002). It has also been reported that agonist-induced endocytosis of β2-adrenergic receptor could stimulate γ-secretase activity possibly by promoting the localization of PSEN-1 to late endosomal compartments (Ni et al., 2006). Hence, converging evidence confirmed the importance of the endocytic pathway in the regulation of Aβ production. To date, there has been limited detailed analysis dissecting the different downstream steps following endocytosis to reveal the actual location in which Aβ is ultimately produced. It is yet to be determined whether this reaction occurs early, right after endocytosis, or during subsequent stages along the MVB pathway that sorts proteins towards the lysosome, or the recycling pathway back to the TGN.

In recent years, there have been active debates regarding whether the TGN or endosomes (more specifically, early endosomes) would be the actual subcellular site for Aβ production. Both the TGN and early endosomes have been regarded as the sorting stations for proteins that traffic through the secretory and endocytic pathways, respectively. These pathways are directly connected through the bidirectional flow of transport vesicles between the two compartments (Pfeffer, 2009; Puertollano et al., 2001; Waguri et al., 2003). It is possible that cleavage of APP into Aβ can actually occur in both compartments, depending on differences in cell lines with variations in the steady state distribution of APP and other components in the amyloidogenic pathway (Small and Gandy, 2006). Such variations could alter the dynamics between the TGN and the

endosomes, resulting in a shift in the location of APP processing between these two organelles.

A more comprehensive study on each trafficking step in the secretory and endocytic pathways is required to establish the normal location of Aβ peptide generation. In this study, I investigated the importance of different post-endocytic trafficking steps including the endosomal and recycling pathways in the production of Aβ using an RNA interference (RNAi) approach. I observed distinct effects in both the early and late stages of the MVB pathway on Aβ production as well as on APP localization. Furthermore, I demonstrated that the majority of APP is processed in the TGN to produce Aβ, with the requirement of the endocytic population of APP being recycled from endosomes to the TGN in a retromer-dependent manner for efficient cleavage to occur. I believe this study enhances our understanding of the subcellular site of Aβ generation, and its role in the development of Alzheimer's disease.

Figure 1-1. Schematic illustration of the non-amyloidogenic and amyloidogenic pathways of APP. Arrows indicate the site for proteolytic processing of APP. In the non-amyloidogenic pathway (as shown in blue), the extracellular domain of APP is cleaved by α-secretase at the plasma membrane to release a soluble fragment known as sAPPα. Production of Aβ is precluded in this pathway, since α-secretase cleavage happens within the Aβ sequence of APP. In the amyloidogenic pathway (as shown in red), APP is first cleaved by BACE to produce the soluble sAPPβ fragment and the membrane-bound C-terminal fragment CTFβ, as known as C99. The second enzymatic step in amyloidogenic pathway involves the intramembranous processing of CTFβ fragment of APP by γ-secretase to yield Aβ peptides and APP intracellular domain (AICD).

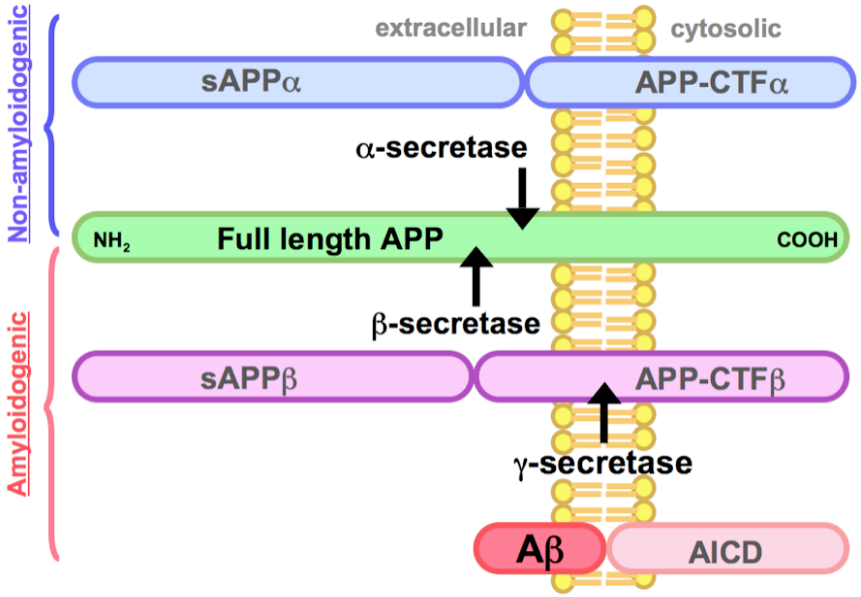
Non-amyloidogenic
Amyloidogenic
extracellular
cytosolic
sAPPα
APP-CTFα
α-secretase
NH2
Full length APP
COOH
β-secretase
sAPPβ
APP-CTFβ
γ-secretase
Aβ
AICD

Figure 1-2. Possible subcellular compartments for APP processing and Aβ production. The three major players in the amyloidogenic pathway, namely APP, BACE, and γ-secretase, are all integral membrane proteins that travel along the secretory and endocytic pathways, which are sorted through the membranes of intracellular organelles and the plasma membrane. Therefore, APP processing could possibly occur in any of the organelles along the secretory and the endocytic pathways, including the ER, TGN, early endosomes (EE), MVB, recycling endosomes, and lysosome.

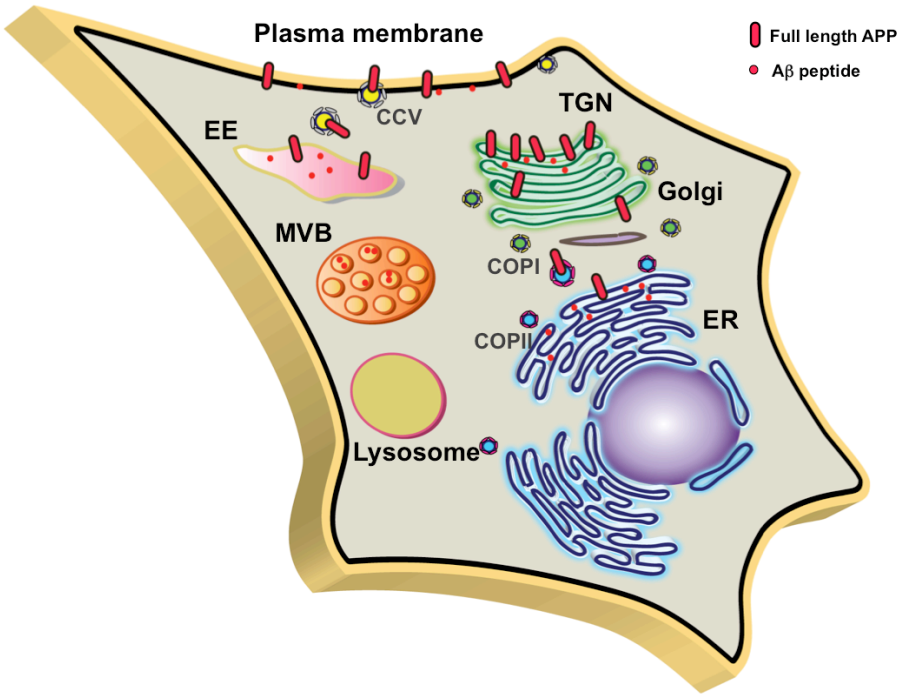
Plasma membrane
Full length APP
Aβ peptide
CCV
EE
TGN
Golgi
MVB
COPI
ER
COPII
Lysosome

CHAPTER TWO
DEPLETION OF ESCRTS AFFECTS Aβ PRODUCTION

INTRODUCTION

Endocytosis of APP has been shown to be important in the production of Aβ, yet the involvement of different post-endocytic trafficking steps in APP processing has not been thoroughly assessed. Membrane proteins at the plasma membrane are sorted into the MVB and lysosomal degradation pathways by endosomal sorting complexes required for transport (ESCRT) (Henne et al., 2011; Hurley and Hanson, 2010). The ESCRT-0 complex mediates sorting and concentrating of cargoes to this pathway, the ESCRT-I and ESCRT-II complexes are important for membrane budding, the ESCRT-III complex is involved in membrane scission to form internal vesicles of MVBs, while the AAA+ ATPase VPS4 dissembles and recycles ESCRT-III components to sustain subsequent rounds of the pathway (Henne et al., 2011; Hurley and Hanson, 2010). To ascertain the involvement of the endosomal MVB pathway happening downstream of the endocytic event in APP processing, I investigated the effects of depleting different ESCRT complex subunits on Aβ production and APP localization.

RESULTS

Generation of a stable cell line overexpressing APP

A stable human cell line that overexpresses APP would be useful for analyzing APP localization and Aβ production. Since APP is not robustly expressed in most of the cell types, minute quantity of endogenous Aβ secreted by the cells were difficult to be detected even with a sensitive enzyme-linked immunosorbent assay (ELISA) method. Also, endogenous APP is not readily labeled and detected by immunofluorescence microscopy and immunoelectron microscopy. Therefore, a stable cell line expressing APP was used throughout this study.

Primary neurons or mammalian cell lines of neuronal origin are ideal for studying the molecular mechanisms underlying neurodegenerative diseases such as Alzheimer's disease. However, these primary neurons and common neuronal lines such as human derived neuroblastoma cell lines SH-SY5Y and SK-N-DZ, and mouse derived neuroblastoma cell line Neuro-2a (N2a) have relatively low transfection efficiency. In this study, I chose to use the human embryonic kidney line HEK293 for the generation of a stable APP expressing cell line. Although HEK293 cells are derived from kidney, it has been suggested that these cells may have a neuronal lineage, with evidence showing the expression of neurofilament proteins and many other neuron-specific proteins (Shaw et al., 2002). Owing to the proposed neuronal lineage and extremely high transfection efficiency of these cells, HEK293 is widely used in studying Alzheimer's disease (Small and Gandy, 2006).

Here, I generated a stable cell line of HEK293 overexpressing the wildtype APP_{695}, the isoform that is expressed predominantly in neurons (O'Brien and Wong, 2011). Although many researchers in this field use the Swedish mutant of APP instead of the wildtype form due to robust production of Aβ (Citron et al., 1992), I preferred to study the wildtype form of APP because the trafficking and processing of Swedish APP may be altered. Following antibiotic selection for 2 weeks after transfection of wildtype

APP_{695} into parental HEK293 cells, I performed limiting dilution cloning to obtain single cell clones stably expressing APP_{695}. A total of 16 different single-clone derived HEK293.APP_{695} stable cell lines were generated and analyzed for exogenous APP expression by immunoblotting. The levels of APP overexpression in different stable clones were compared to the endogenous APP level in the control parental HEK293 cells. As shown in Fig 2-1, clone #A6 has the highest level of APP expression, thus it was designated as the major HEK293.APP_{695} stable cell line that was used in this study. Other stable clones with various APP expression level, namely #A1, #A3, #A4, #A9, #A10, and #A16, were stored as frozen stocks for future use. I used clone #A5 in part of the study. In clone #A6 cells, APP showed a predominant perinuclear localization with some cytosolic and plasma membrane staining as shown by immunofluorescence microscopy analysis (Fig. 2-2), which colocalized nicely with the TGN marker Golgin 97. This HEK293.APP_{695} stable cell line also showed a higher knockdown efficiency when compared to the neuronal SH-SY5Y cell line in short hairpin RNA (shRNA)-mediated knockdown of VPS4B (Fig. 2-3).

Depletion of ESCRT altered Aβ production and redistributed APP localization

To assess the involvement of different ESCRT complexes in Aβ production, I performed shRNA-based knockdown of Hrs (ESCRT-0), Tsg101 (ESCRT-I), CHMP6 (ESCRT-III), and VPS4A/B in HEK293 cells stably expressing APP_{695}. To collect secreted $A\beta_{40}$ peptides from the culture media, I transfected HEK293.APP_{695} cells with pSUPER shRNA constructs by Lipofactamine for 24 h. At 72 h post-transfection, cells were trypsinized and replated at same cell numbers into new tissue culture dishes. Culture media were conditioned for 24 h from 96 h to 120 h post-transfection, and collected for ELISA analysis (Fig. 2-4). I performed all shRNA knockdown experiments for 120 h to maximize the knockdown efficiency. A time-course shRNA knockdown experiment to deplete Hrs, Tsg101, and VPS4B was done, and cells were lysed from 24 h to 144 h post-transfection to analyze protein levels. As shown in Fig. 2-5, protein levels started to decrease significantly at 72 h, with the most efficient knockdown at 120 h.

After efficient knockdown of different ESCRT complexes (Fig. 2-6), the changes in secreted $A\beta_{40}$ levels in the culture media were analyzed by ELISA. Depletion of the indicated individual components of each ESCRT complex results in degradation of the respective ESCRT complex (Babst et al., 2002; Bache et al., 2003; Doyotte et al., 2005; Langelier et al., 2006; Razi and Futter, 2006). Depletion of Hrs or Tsg101 led to 22 ± 3% and 36 ± 6% decrease in $A\beta_{40}$, respectively; whereas an increase in $A\beta_{40}$ to varying degrees was observed upon depletion of CHMP6 or VPS4A/B, with more than 3-fold increase in the $A\beta_{40}$ level in double knockdowns of VPS4A and VPS4B (Fig. 2-7). It is interesting to note the differential effects on Aβ production upon depleting subunits of different ESCRT complexes that apparently function in the same endosomal sorting MVB pathway. Because these ESCRT components are involved in different stages of this pathway (Henne et al., 2011; Hurley and Hanson, 2010), depleting them may differentially affect the intracellular trafficking and steady-state distribution of APP, leading to differences in the efficiency of Aβ production. The level of Aβ may increase

if depleting a certain ESCRT subunit would direct more APP to a compartment where the secretases have optimal activities to cleave APP. On the other hand, Aβ production may be delayed when APP is retained in compartments that are less favorable for processing. Therefore, the localization of APP upon each ESCRT knockdown may provide a clue about the actual subcellular site of Aβ production.

To correlate the changes in the $A\beta_{40}$ levels with the steady-state distribution of APP upon depletion of ESCRT subunits, I used immunofluorescence microscopy to visualize APP colocalization with different organelle markers. In control cells, APP predominantly localized to the TGN as visualized by the TGN marker Golgin 97 (55 ± 7%) (Fig. 2-8 A to D), with only a subset of APP (9 ± 2%) colocalized with the early endosome marker EEA1 (Fig. 2-8 E to H), while the remaining signals of APP distributed throughout the cytosol, the endoplasmic reticulum (ER) and the plasma membrane. Interestingly, in Hrs- or Tsg101-depleted cells, APP was redistributed from the TGN to enlarged (with varying sizes), ring-like structures that were labeled by EEA1 (24 ± 6%) (Fig. 2-9). Epidermal growth factor receptor (EGFR) also colocalized with APP in these early endosomal structures in Hrs-depleted cells (Fig. 2-9). Colocalization of APP with EEA1 in Hrs-depleted cells was also confirmed by thin section immunoelectron microscopy analysis (Fig. 2-11). With the deficiency of these early ESCRT subunits, APP was likely to be retained in enlarged endosomal compartments that were defective in progression further along the MVB pathway, thus delaying APP transport to late endosomes, MVBs and lysosomes, as well as its retrograde transport to the TGN. The decrease in the Aβ levels accompanied by the accumulation of APP in these compartments suggested that Aβ production may be less efficient in early endosomes, such that APP has to traffic beyond early endosomes to gain access to a downstream organelle that presents favorable conditions for the generation of Aβ.

In CHMP6-, or VPS4A/B-depleted cells, APP did not colocalize well with subcellular markers in the endosomal or lysosomal pathways including the early endosome marker EEA1, late endosome/MVB markers Rab7 and LBPA, and lysosome markers CD63, LAMP1, and LAMP2. Instead of accumulating in endosomes or lysosomes, APP localized predominantly to the TGN (CHMP6: 55 ± 7%; VPS4A: 54 ± 6%; VPS4B: 54 ± 5%) (Fig. 2-10), which was comparable to the control cells (55 ± 7%) (Fig. 2-8), with some dispersal of the Golgi structures as shown in VPS4A/B-depleted cells which could be a general effect of VPS4A/B knockdown. Colocalization of APP with Golgin 97 in VPS4A-depleted cells was also confirmed by thin section immunoelectron microscopy analysis (Fig. 2-11). It has been suggested the TGN may represent a favorable subcellular site for Aβ production (Burgos et al., 2010; Siman and Velji, 2003; Xu et al., 1997). Although depletion of these late ESCRT components showed the same steady-state APP localization to the TGN as in the control, I speculated the enhancement in $A\beta_{40}$ levels upon their depletion may be attributed to the redirection of more APP to the compartment that possessed optimal secretases activities, possibly be the TGN (Burgos et al., 2010; Siman and Velji, 2003; Xu et al., 1997).

Endocytosed APP was redirected to the TGN upon VPS4 depletion

The steady-state concentration of APP in the TGN after depletion of VPS4 or other late ESCRT components could be due to a delay in TGN export of APP, or to enhanced routing of APP from the endocytic pathway into the retrograde pathway back to the TGN as a result of disruption of the downstream pathways towards the lysosome. To distinguish between these possibilities, I performed a double knockdown of Hrs and VPS4A, and assessed any changes in the $A\beta_{40}$ level and APP localization. There was a slight decrease in the $A\beta_{40}$ level (Fig. 2-12), which was consistent with the notion that Aβ was produced less efficiently in these enlarged early endosomal compartments. To analyze any changes in APP localization in double knockdown cells by immunofluorescence microscopy, I used a pSUPER.puro shRNA construct for Hrs-targeting, and a pSUPER+GFP shRNA construct for VPS4A targeting. The cells were then selected in puromycin to concentrate the population of cells containing Hrs knockdown, and by searching for GFP signal, cells with VPS4A knockdown were identified. The steady-state localization of APP was redistributed to enlarged (with varying sizes), ring-like structures that were labeled by EEA1 (26 ± 10%) (Fig. 2-13 A), similar to the observation in single Hrs-depleted cells (Fig. 2-9); accompanying by a decrease in TGN localization (12 ± 3%) (Fig. 2-13 A). To confirm that the phenotypes observed in cells with double knockdown of Hrs and VPS4SA which mimicked the pheneotype of single Hrs knockdown was not due to the inefficient knockdown of VPS4A using the non-selectable pSUPER+GFP vector, I performed another double knockdown experiment using pSUPER.puro with puromycin selection for VPS4A, and pSUPER+GFP for Hrs. Consistently, APP was also redistributed to enlarged early endosomes (Fig. 2-13 B). These results demonstrated that depletion of both Hrs and VPS4A resembled the phenotypes in knockdown of Hrs alone, which suggested that APP was not retained in the TGN but was rather able to reach the cell surface and internalized to the endocytic pathway in case of VPS4 single knockdown. Therefore, APP accumulation in the TGN in single VPS4A-depleted cells appears to have derived from the endosomal population of APP that was retrieved back to the TGN where enhanced production of Aβ may occur. Endosomal APP may arise by internalization from the plasma membrane or from a biosynthetic pool that had trafficked from the TGN to endosomes directly. The apparent link between APP localization in the TGN and enhanced Aβ production upon late ESCRT knockdown suggested Aβ formation may be localized to the TGN, made possible by retrograde transport to reroute the endosomal APP towards the TGN.

DISCUSSION

In my experimental system using HEK293 cells expressing APP_{695}, I demonstrated that the processing of APP into Aβ occurs predominantly in the TGN, and less favorably in early endosomes. I observed a correlation between the increase in Aβ and the accumulation of APP in the TGN, as shown by depleting the late ESCRT components CHMP6 or VPS4A/B, which rerouted APP from the endosomal pathway to the TGN (Fig. 2-7 and 2-10). On the other hand, reduced Aβ levels were observed when there was a shift in steady state localization of APP from the TGN to early endosomes, as

shown by knockdown of the early ESCRT components Hrs or Tsg101 (Fig. 2-7 and 2.9). Surprisingly, I observed differential effects on APP processing and trafficking upon depletion of different ESCRT components (Fig. 2-7). As shown in Hrs and Tsg101 knockdown, depleting early ESCRT subunits delayed APP exit from early endosomes, in which all downstream pathways were blocked. On the contrary, upon depletion of later ESCRT components CHMP6 and VPS4A/B, APP was able to exit early endosomes and reached a later stage in which APP was rerouted towards the TGN owing to defective downstream MVB and lysosomal pathways. These differential effects could be attributed to the functionally distinct roles of the earlier and later ESCRTs in MVB biogenesis (Henne et al., 2011; Hurley and Hanson, 2010). Moreover, my findings based on the double knockdown experiment of Hrs and VPS4 suggested that the retrograde pathway that retrieved endosomal APP to the TGN might play a role in Aβ production (Fig. 2-12 and 2-13).

MATERIALS AND METHODS

Antibodies

Mouse monoclonal antibodies used were anti-Hrs (A-5; Enzo Life Sciences), anti-Tsg101 (4A10, Genetex), anti-Golgin 97 (CDF4, Life Technologies), anti-EEA1 (14, BD Transduction Laboratories), and anti-Actin (C4, MP Biomedicals). Rabbit polyclonal antibodies used were anti-CHMP6 (gift from W. I. Sundquist, University of Utah), anti-VPS4A (gift from W. I. Sundquist, University of Utah), anti-VPS4B (gift from W. I. Sundquist, University of Utah), anti-SEC23A (gift from J. P. Paccaud; Drugs of Neglected Diseases Initiative, Geneva, Switzerland) and anti-APP C-terminus (Sigma-Aldrich). IRDye 680 and 800 secondary antibodies (LICOR) were used for immunoblotting analysis. Alexa Fluor 568 and 647-conjugated secondary antibodies (Life Technologies) were used for immunofluorescence microscopy.

Stable cell line generation and maintenance

Full-length cDNA of human wildtype APP_{695} was cloned into pCI-neo mammalian expression vector (Promega) and transfected in HEK293 cells (ATCC). Cells were selected on 650 μg/mL Geneticin/G418 (Life Technologies) for 2 weeks to kill cells without stably-integrated pCI-neo.APP plasmid. Cells were trypsinized, counted, and diluted. Limiting dilution cloning was performed by plating the density of 1 cell per well of cells in100 μl G418 selection media into 96-well plates. Three days after plating into 96-well plates, single-cell clones were identified and grown under continuous selection in media contatining 650 μg/mL Geneticin/G418 until 80-90% confluent has been reached. Confluent single-cell derived cells were re-plated into 12-well plates and grown under continuous selection in media contatining 650 μg/mL Geneticin/G418 until 80-90% confluent has been reached. Cells were analyzed by immunoblot to determine APP expression levels, and by immunofluorescence microscopy to determine APP subcellular localization. Positive clones were further expanded into 100 mm culture dishes to create frozen cell stocks (in 10% DMSO/50% FBS/DMEM/high glucose/GlutaMAX without antibiotics) for storage in a liquid nitrogen freezing tank. Stable HEK293 cells expressing APP_{695} (HEK293.APP_{695}) were cultured in DMEM/high glucose/GlutaMAX

(Life Technologies) with the addition of 10% FBS (HyClone), 0.1 mM NEAA (Life Technologies), and 650 μg/mL Geneticin/G418 (Life Technologies) and maintained in a humidified incubator with 5% CO_2 at 37^{o}C. New cells were thawed every 10 passages to ensure consistency between individual experiments and to maintain good transfection efficiency of the cells.

RNAi constructs

The mRNA sequences of human Hrs, Tsg101, CHMP6, VPS4A, VPS4B, VPS35, and Rab9A were used to design short hairpin RNA (shRNA) for specific gene silencing using siDirect 2.0 web server (http://sidirect2.rnai.jp/doc) and siRNA Target Finder software from Ambion (http://www.ambion.com/techlib/misc/siRNA_finder.html).

Custom-made 62-nt DNA oligonucleotides were designed to contain a 19-nt sense strand target sequence that was linked to the 19-nt reverse complement antisense sequence by a short spacer region (5′-TTCAAGAGA-3′), followed by the RNA polymerase III termination sequence (5′-TTTTTT-3′), with the addition of BglII and BamHI restriction enzyme sites flanking the 5′ and 3′ ends, respectively.

Two pairs of complementary oligonucleotides directed towards distinct regions of mRNA sequences of each knockdown target was synthesized (Integrated DNA Technologies), as follows:

5’-GATCGAGACAAGTGGAGGTAAACTTCAAGAGAGTTTACCTCCACTTGTCTCTTTTTTGGAAA-3’ and 5’-AGCTTTTCCAAAAAAGAGACAAGTGGAGGTAAACTCTCTTGAAGTTTACCTCCACTTGTCTC-3’ for Hrs-1;

5’-GATCCCTGTACTCTTCACCTGTGTTCAAGAGACACAGGTGAAGAGTACAGGTTTTTTGGAAA-3’ and 5’-AGCTTTTCCAAAAAACCTGTACTCTTCACCTGTGTCTCTTGAACACAGGTGAAGAGTACAGG-3’ for Hrs-2;

5’-GATCCCTCCAGTCTTCTCTCGTCTTCAAGAGAGACGAGAGAAGACTGGAGGTTTTTTGGAAA-3’ and 5’-AGCTTTTCCAAAAAACCTCCAGTCTTCTCTCGTCTCTCTTGAAGACGAGAGAAGACTGGAGG-3’ for Tsg101-1;

5’-GATCGAAGTAGCCGAGGTTGATATTCAAGAGATATCAACCTCGGCTACTTCTTTTTTGGAAA-3’ and 5’-AGCTTTTCCAAAAAAGAAGTAGCCGAGGTTGATATCTCTTGAATATCAACCTCGGCTACTTC-3’ for Tsg101-2;

5’-GATCATGAGTGTCTGAACAAGATTTCAAGAGAATCTTGTTCAGACACTCATTTTTTTGGAAA-3’ and 5’-AGCTTTTCCAAAAAAATGAGTGTCTGAACAAGATTCTCTTGAAATCTTGTTCAGACACTCAT-3’ for CHMP6-1;

5’-
GATCGCGCAATCACTCAGGAACATTCAAGAGATGTTCCTGAGTGATTGCGCT
TTTTTGGAAA-3’ and 5’-
AGCTTTTCCAAAAAAGCGCAATCACTCAGGAACATCTCTTGAATGTTCCTGAG
TGATTGCGC-3’ for CHMP6-2;
5’-
GATCGGATTATTTACGAAGCAAATTCAAGAGATTTGCTTCGTAAATAATCCTT
TTTTGGAAA-3’ and 5’-
AGCTTTTCCAAAAAAGGATTATTTACGAAGCAAATCTCTTGAATTTGCTTCGT
AAATAATCC-3’ for VPS4A-1;
5’-
GATCGGCCAAGGAGAGCATTCGATTCAAGAGATCGAATGCTCTCCTTGGCCT
TTTTTGGAAA-3’ and 5’-
AGCTTTTCCAAAAAAGGCCAAGGAGAGCATTCGATCTCTTGAATCGAATGCT
CTCCTTGGCC-3’ for VPS4A-2;
5’-
GATCGGCTGGGAACTACGAAGAATTCAAGAGATTCTTCGTAGTTCCCAGCCT
TTTTTGGAAA-3’ and 5’-
AGCTTTTCCAAAAAAGGCTGGGAACTACGAAGAATCTCTTGAATTCTTCGTA
GTTCCCAGCC-3’ for VPS4B-1;
5’-
GATCGCGGTCACTATCTAACACATTCAAGAGATGTGTTAGATAGTGACCGCTT
TTTTGGAAA-3’ and 5’-
AGCTTTTCCAAAAAAGCGGTCACTATCTAACACATCTCTTGAATGTGTTAGAT
AGTGACCGC-3’ for VPS4B-2;
The complementary pair of DNA oligonucleotides was annealed and ligated into the linearized pSUPER.retro.puro (pSUPER) shRNA or pSUPER.retro.gfp+neo (pSUPER+GFP) expression vectors (OligoEngine) in between the BglII and HindIII sites.
The complementary pair of DNA oligonucleotides was annealed and ligated into the linearized pSUPER.retro.puro (pSUPER) shRNA or pSUPER.retro.gfp+neo (pSUPER+GFP) expression vectors (OligoEngine) in between the BglII and HindIII sites.

ELISA, Protein Determination, and Immunoblotting

Cells were transfected in 6-well plates with 3.5 μg pSUPER shRNA constructs using Lipofectamine 2000 (Life Technologies) in serum-free Opti-MEM (Life Technologies) for 24 h. For double knockdown experiments, I used 1.75 μg of each shRNA construct. Transfection media were replaced by complete media containing 4 μg/ml puromycin (Sigma-Aldrich) at 24 h post-transfection. At 72 h post-transfection, cells were trypsinized and cell numbers were measured by Coulter Counter (Beckman Coulter). Cells with a density of 6.5 x 10^6 were replated onto 60 mm dishes in selection media containing puromycin. At 96 h post-transfection, selection media were replaced with fresh media without puromycin, and were conditioned for 24 h. At 120 h post-transfection, conditioned media were collected with the addition of a protease inhibitor cocktail mini tablets (Roche). Media were diluted 10- to 20- fold (same dilution factor

was used for both control and knockdown samples in the same set of experiment) and subjected to $A\beta_{40}$ ELISA analysis (Life Technologies) according to the manufacturer's instructions. For immunoblotting analysis, cells were scraped and lysed in ice-cold RIPA buffer (50 mM Tris-HCl, pH 7.6, 150 mM NaCl, 0.5% sodium deoxycholate, 0.1% SDS, 1% NP40, 5 mM EDTA, and protease inhibitor cocktails mini tablets). Lysates were centrifuged at 20,800 *g* at 4°C for 30 min and protein concentration was determined by BCA protein assay (Thermo Fisher Scientific). Equal amounts of protein samples were separated by SDS-PAGE and transferred to Immobilon-FL PVDF membranes (Millipore), and analyzed and quantified by Odyssey Infrared Imaging System (LICOR). Actin or SEC23A were used as loading controls. All experiments were performed at least 3 times independently. Data represented as mean ± SEM were plotted and analyzed by Prism (GraphPad software) using paired t-test to compare control and knockdown samples. Statistical significance was represented by * $p < 0.05$, ** $p < 0.01$, and *** $p < 0.001$, only p values below 0.05 were shown.

Immunofluorescence Microscopy and Quantification

Cells were transfected in 6-well plates with 3.5 μg pSUPER+GFP shRNA constructs using Lipofectamine 2000 (Life Technologies) in serum-free Opti-MEM (Life Technologies) for 24 h. For double knockdown experiments, 1.75 μg of each shRNA constructs were used. Transfection media were replaced by complete media at 24 h post-transfection. At 96 h post-transfactions, cells were trypsinzed and replated onto polylysine-coated coverslips. At 120 h post-transfection, cells were fixed with 4% paraformaldehyde (Electron Microscopy Sciences) for 1 h at room temperature, permeabilized with 0.1% Triton X-100, stained for primary antibodies and Alexa Fluor-conjugated secondary antibodies, and mounted on microscopic slides with ProLong Gold antifade reagent containing DAPI (Life Technologies). Cells were imaged using a wide-field fluorescence microscope (AxioObserver Z1, Carl Zeiss). Images were processed and analyzed by MetaMorph image analysis software (Molecular Devices). Cells that were expressing GFP from pSUPER+GFP shRNA vector were selected for quantification. The extent of APP colocalization with subcellular markers Golgin 97 or EEA1 was determined by quantification of overlapping pixels in Alexa 568 and Alexa 647 channels. The percentage of APP pixels that overlapped with Golgin 97 or EEA1 pixels was measured and represented as mean ± SD from at least 20 cells per sample from at least 2 representative experiments that were performed multiple times with similar results.

Immuoelectron Microscopy

Cells were transfected in 6-well plates with 3.5 μg pSUPER+GFP shRNA constructs using Lipofectamine 2000 (Life Technologies) in serum-free Opti-MEM (Life Technologies) for 24 h. For double knockdown experiments, 1.75 μg of each shRNA constructs were used. Transfection media were replaced by complete media containing at 24 h post-transfection. At 96 h post-transfactions, cells were trypsinzed and replated onto polylysine-coated coverslips. At 120 h post-transfection, confluent cells were fixed with glutaraldehyde, scraped gently, and processed for thin-section preparation as previously

described (Kim et al., 2005; Wang et al., 2006). Thin sections were analyzed by immunoelectron microscopy using an anti-APP antibody and 15 nm gold-coupled secondary antibody, together with either anti-EEA1 or anti-Golgin 97 antibodies, and 10 nm gold-coupled secondary antibody as previously described (Fromme et al., 2007; Kim et al., 2005; Liou et al., 1996) .

Figure 2-1. Relative expression levels of APP in HEK293.APP$_{695}$ stable cell lines. Different single clones (#A1 to A16) of HEK293 cells stably expressing APP$_{695}$ were generated. APP expression level in the stable cell lines. Cells were lysed and proteins were analyzed by immunoblot. The levels of APP expression in the stable cell lines were compared to the endogenous APP level in the parental HEK293 line (control). Highest APP expression level was shown in clone #A6 (as shown in red).

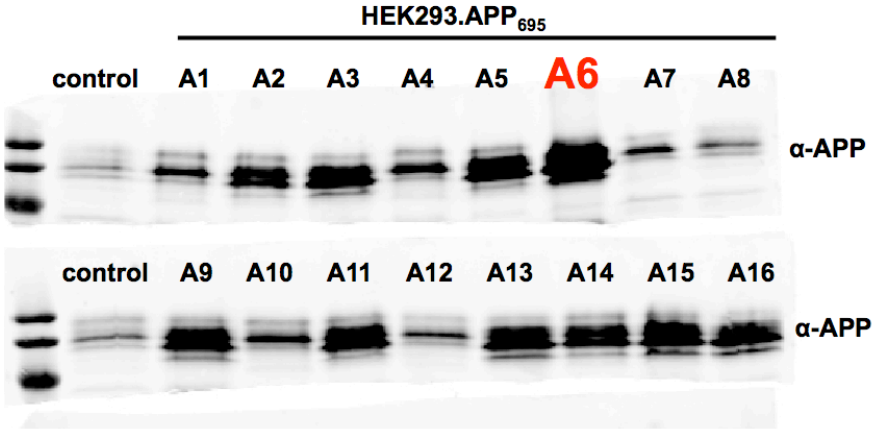
HEK293.APP695
control
A1
A2
A3
A4
A5
A6
A7
A8
α-APP
control
A9
A10
A11
A12
A13
A14
A15
A16
α-APP

Figure 2-2. APP is localized to perinuclear region and colocalized with TGN marker in HEK293.APP$_{695}$ stable line. HEK293.APP$_{695}$ clone #A6 cells were fixed and stained for (A) APP (as shown in red) and nucleus (as shown in blue); or APP (as shown in red) and Golgin 97 (as shown in green). Merged images were generated. Scale bars = 10 μm.

A

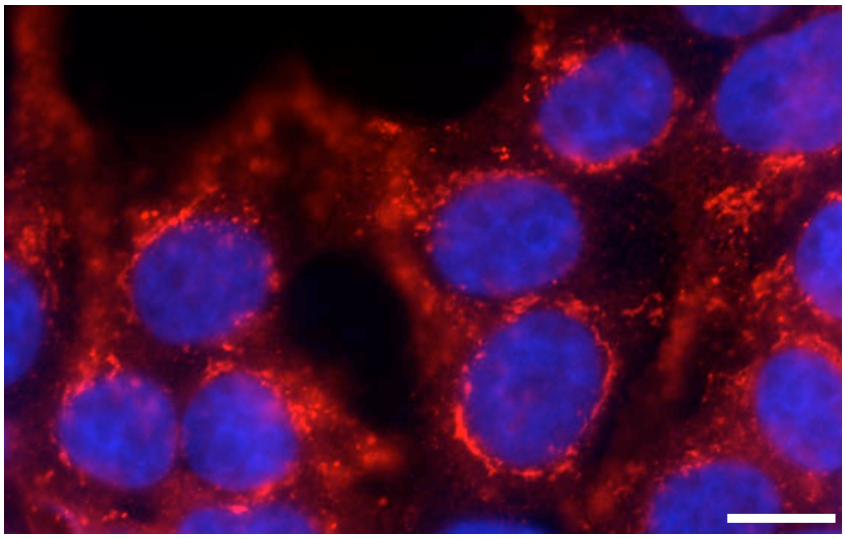

B

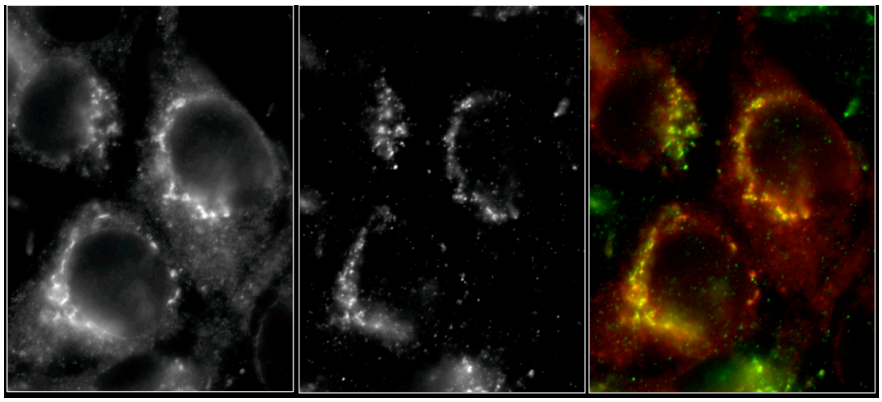

Figure 2-3. Higher knockdown efficiency in HEK293.APP stable cells than in neuronal SH-SY5Y cells after transfecting with shRNA constructs. HEK293.APP_{695} stable cells and SH-SY5Y cells were transfected with empty vector (as control) or shRNA targeting VPS4B. Cells were lysed 72 h post-transfection, and proteins were analyzed by immunoblot.

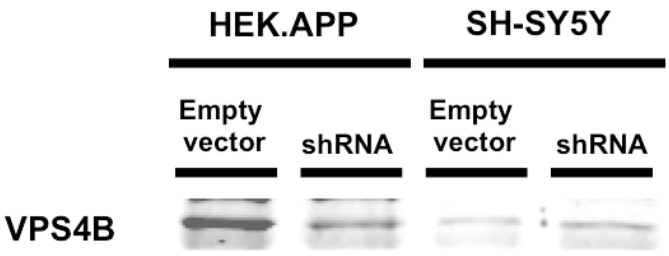
HEK.APP
SH-SY5Y
Empty vector
shRNA
Empty vector
shRNA
VPS4B

Figure 2-4. Schematic illustration of shRNA knockdown experiment.
(A) HEK293 cells stably expressing APP_{695} were transfected transiently with shRNA constructs for 120 h. Cells were lysed and the knockdown efficiency was determined by immunoblot. Levels of $A\beta_{40}$ peptides in the conditioned media were measured using ELISA assay. The localization of APP was analyzed by fluorescence microscopy. (B) To collect secreted $A\beta_{40}$ peptides from the culture media for ELISA anaylsis, I transfected HEK293.APP_{695} cells with pSUPER shRNA constructs for 24 h. Transfection media were replaced by media containing puromycin for selection. At 72 h post-transfection, cells were trypsinized, counted and replated at the same density. At 96 h post-transfection, selection media were replaced with fresh media without puromycin, and were conditioned for 24 h. At 120 h post-transfection, conditioned media were collected for ELISA assay.

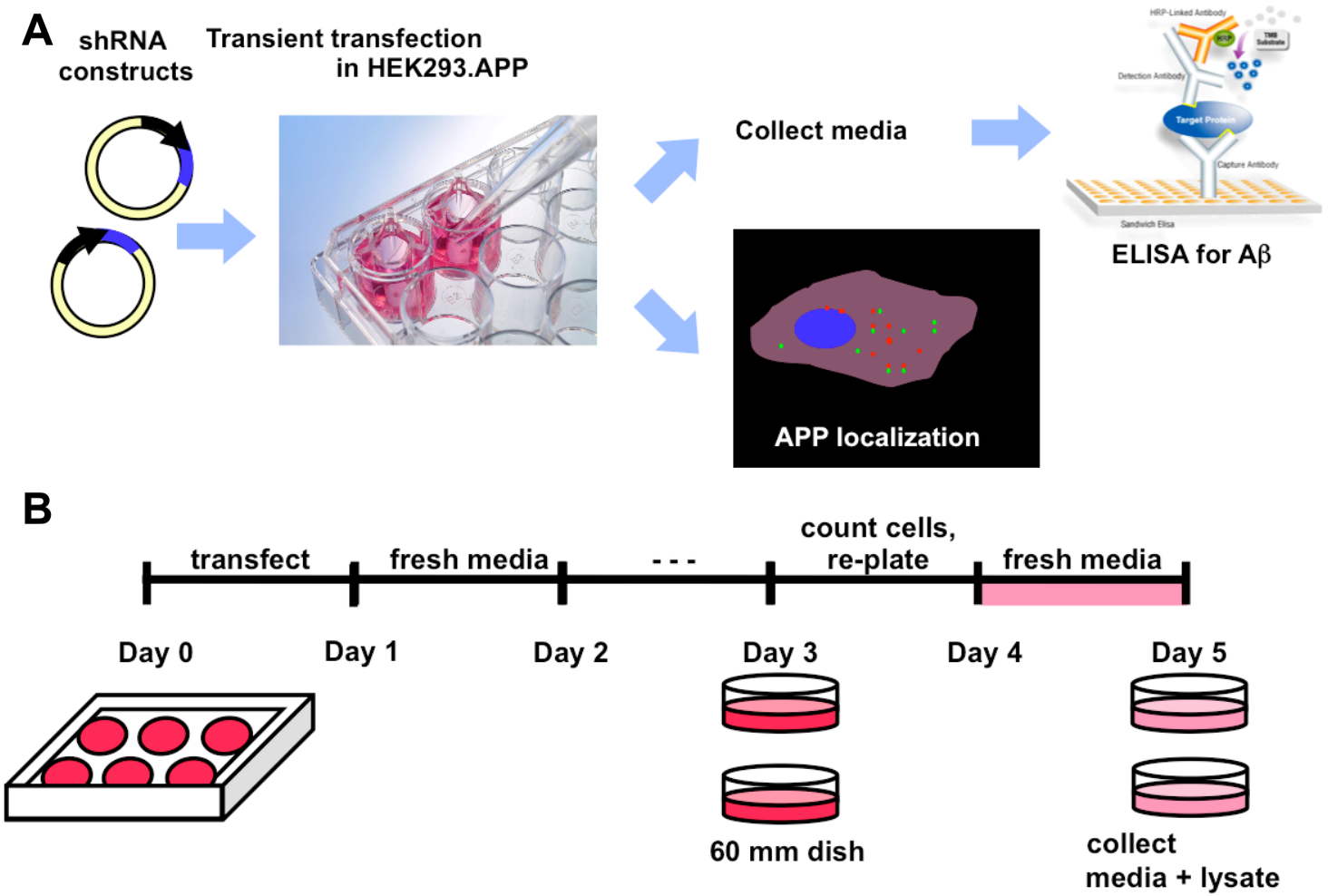
A
shRNA constructs
Transient transfection in HEK293.APP
Collect media
ELISA for Aβ
APP localization
B
transfect
fresh media
- - -
count cells, re-plate
fresh media
Day 0
Day 1
Day 2
Day 3
Day 4
Day 5
60 mm dish
collect media + lysate

Figure 2-5. Efficient knockdown at 120 h post-transfection of shRNA. HEK293 cells stably expressing APP_{695} were transfected transiently with shRNA constructs targeting Hrs, Tsg101, or VPS4B. Cells were lysed at 24 h, 48 h, 72 h, 120 h, and 144 h post-transfection, and the knockdown efficiency was determined by immunoblot. Relative protein levels in shRNA knockdown cells as a percentage of the empty vector control are shown.

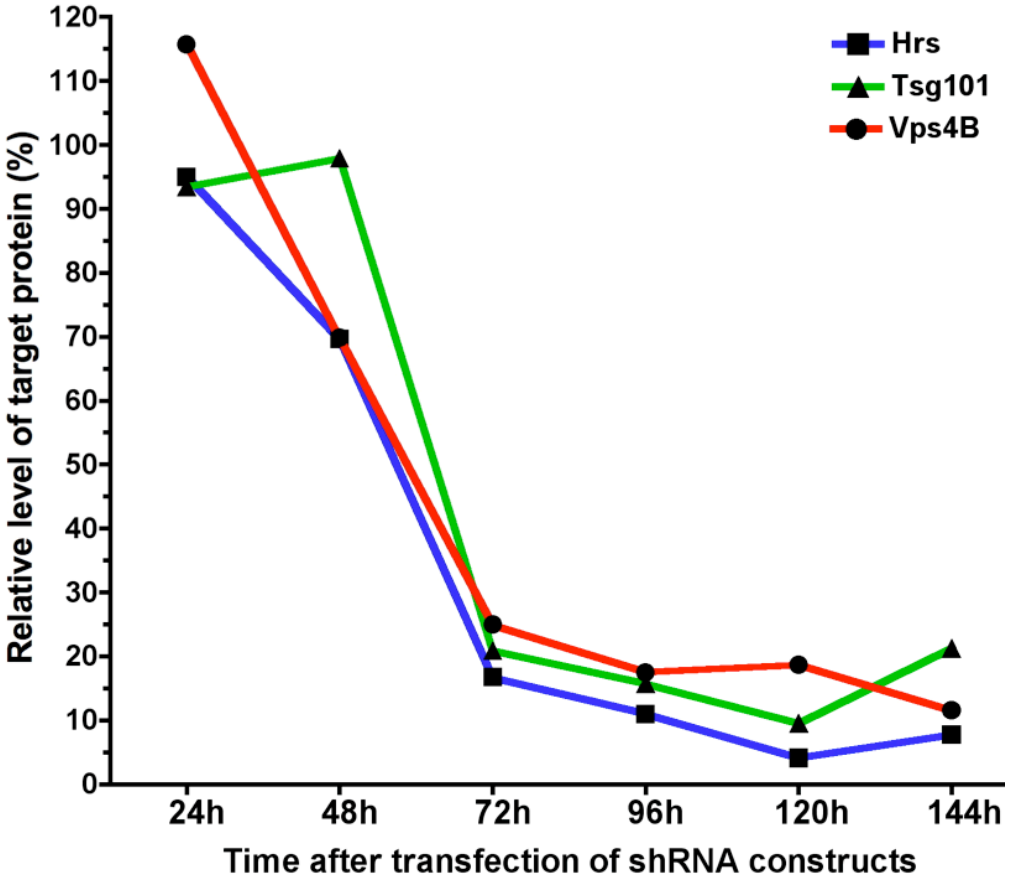
Hrs
Tsg101
Vps4B
Relative level of target protein (%)
120
110
100
90
80
70
60
50
40
30
20
10
0
24h
48h
72h
96h
120h
144h
Time after transfection of shRNA constructs

Figure 2-6. Knockdown efficiency of shRNA-mediated depletion of ESCRT components. (A) HEK293 cells stably expressing APP_{695} were transfected with empty vector pSUPER (control) or two shRNA constructs directed towards distinct regions of mRNA sequences of Hrs, Tsg101, CHMP6, VPS4A, or VPS4B (KD). Cells were lysed at 120 h post-transfection and proteins were analyzed by immunoblot. Actin or SEC23A were used as loading controls. (B) Relative protein levels of Hrs, Tsg101, CHMP6, VPS4A, or VPS4B in shRNA knockdown cells as a percentage of the control (set as 100%) were quantified by the LI-COR Odyssey Infrared Imaging System (mean ± SEM; $n \geq 3$).

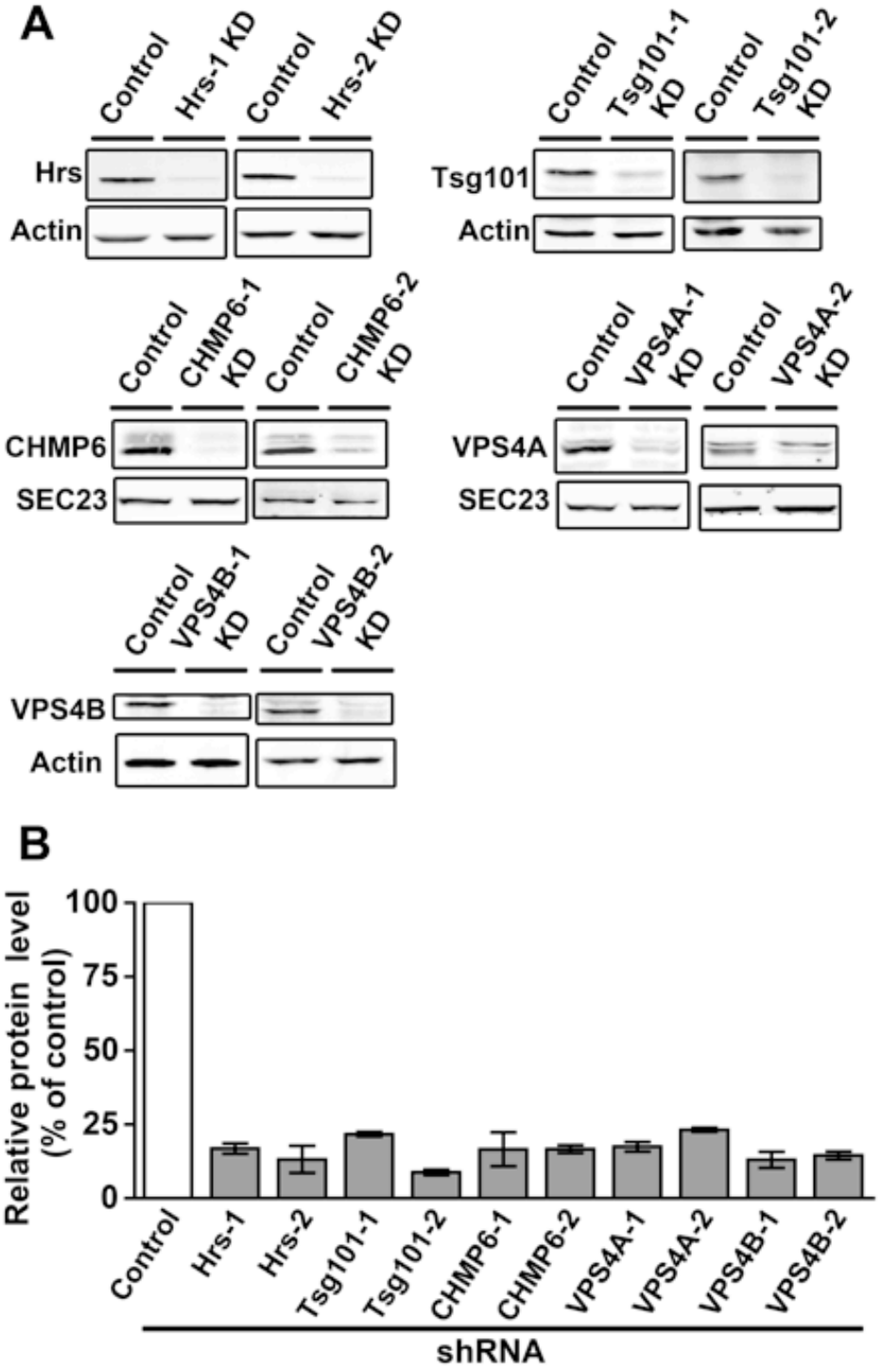
A
Control
Hrs-1 KD
Control
Hrs-2 KD
Hrs
Actin
Control
Tsg101-1 KD
Control
Tsg101-2 KD
Tsg101
Actin
Control
CHMP6-1 KD
Control
CHMP6-2 KD
CHMP6
SEC23
Control
VPS4A-1 KD
Control
VPS4A-2 KD
VPS4A
SEC23
Control
VPS4B-1 KD
Control
VPS4B-2 KD
VPS4B
Actin
B
Relative protein level (% of control)
100
75
50
25
0
Control
Hrs-1
Hrs-2
Tsg101-1
Tsg101-2
CHMP6-1
CHMP6-2
VPS4A-1
VPS4A-2
VPS4B-1
VPS4B-2
shRNA

Figure 2-7. ELISA analysis of $A\beta_{40}$ level upon ESCRTs depletion. Culture media conditioned from 96 h to 120 h post-transfection of shRNA directed towards distinct regions of mRNA sequences of Hrs, Tsg101, CHMP6, VPS4A, or VPS4B were subjected to $A\beta_{40}$ ELISA analysis. Relative normalized $A\beta_{40}$ levels as a percentage of the control (set as 100%) were plotted as mean ± SEM ($n \geq 3$). * $p < 0.05$, ** $p < 0.01$, and *** $p < 0.001$.

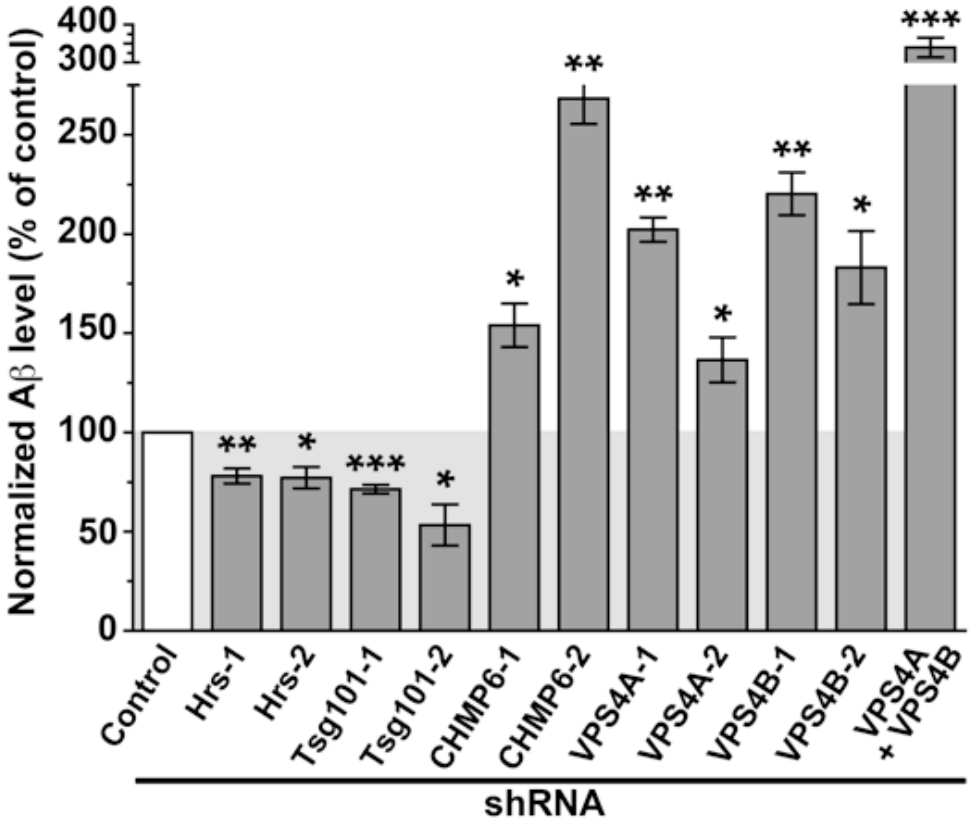
Normalized Aβ level (% of control)
400
300
250
200
150
100
50
0
**
*
***
*
*
**
**
*
**
*
***
Control
Hrs-1
Hrs-2
Tsg101-1
Tsg101-2
CHMP6-1
CHMP6-2
VPS4A-1
VPS4A-2
VPS4B-1
VPS4B-2
VPS4A + VPS4B
shRNA

Figure 2-8. APP is localized predominantly in the TGN at steady in control. HEK293 cells stably expressing APP_{695} were transfected with empty vector pSUPER+GFP (control). Cells were fixed at 120 h post-transfection and stained for APP, and subcellular markers Golgin 97 or EEA1. Merged images were generated from the Alexa 568 channel (APP signals indicated by red) and the Alexa 647 channel (Golgin 97 or EEA signals indicated by green), or 2D-deconvolved images from each channel; colocalization indicated by yellow. Scale bars = 10 μm.

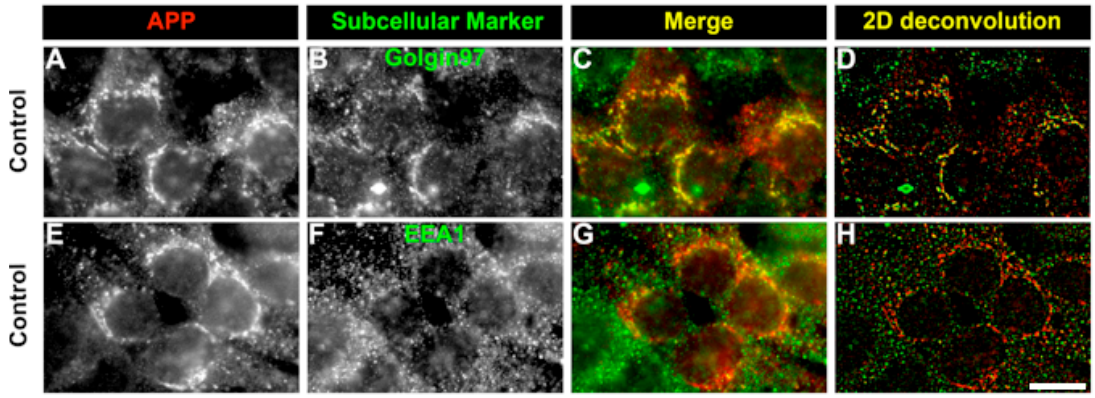
APP
Subcellular Marker
Merge
2D deconvolution
Control
Control
A
B
Golgin97
C
D
E
F
EEA1
G
H

Figure 2-9. Redistribution of APP to enlarged early endosomes upon depletion of early ESCRT components. HEK293 cells stably expressing APP_{695} were transfected with pSUPER+GFP shRNA directed to Hrs or Tsg101 (KD). Cells were fixed at 120 h post-transfection and stained for APP, and EEA1 or EGFR. Because pSUPER+GFP vector co-expressed both the shRNA and GFP, GFP signals were used to indicate knockdown cells. Representative cells with GFP signals are shown. Merged images were generated from the Alexa 568 channel (APP signals indicated by red) and the Alexa 647 channel (EEA1 or EGFR signals indicated by green), or 2D-deconvolved images from each channel; colocalization indicated by yellow. Scale bars = 10 μm.

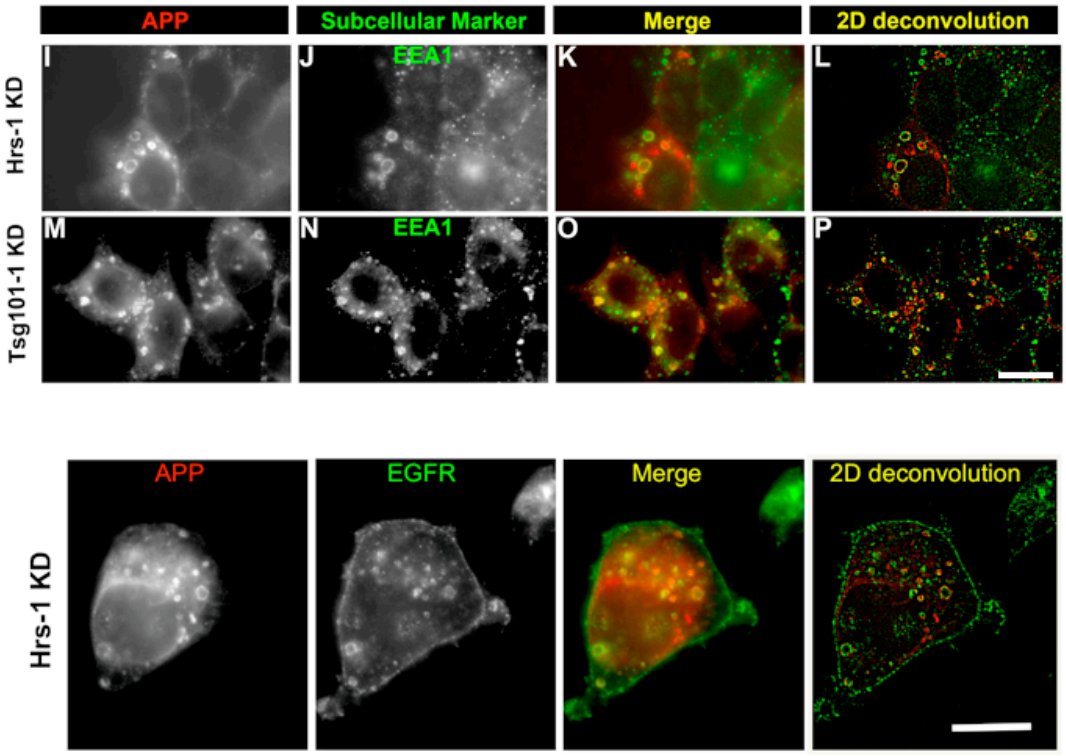
APP
Subcellular Marker
Merge
2D deconvolution
Hrs-1 KD
Tsg101-1 KD
I
J
EEA1
K
L
M
N
EEA1
O
P
Hrs-1 KD
APP
EGFR
Merge
2D deconvolution

Figure 2-10. APP localized to the TGN upon depletion of late ESCRT components. HEK293 cells stably expressing APP_{695} were transfected with pSUPER+GFP shRNA directed to CHMP6, VPS4A, or VPS4B (KD). Cells were fixed at 120 h post-transfection and stained for APP and Golgin 97. Because pSUPER+GFP vector co-expressed both the shRNA and GFP, GFP signals were used to indicate knockdown cells. Representative cells with GFP signals are shown. Merged images were generated from the Alexa 568 channel (APP signals indicated by red) and the Alexa 647 channel (Golgin 97 signals indicated by green), or 2D-deconvolved images from each channel; colocalization indicated by yellow. Scale bars = 10 μm

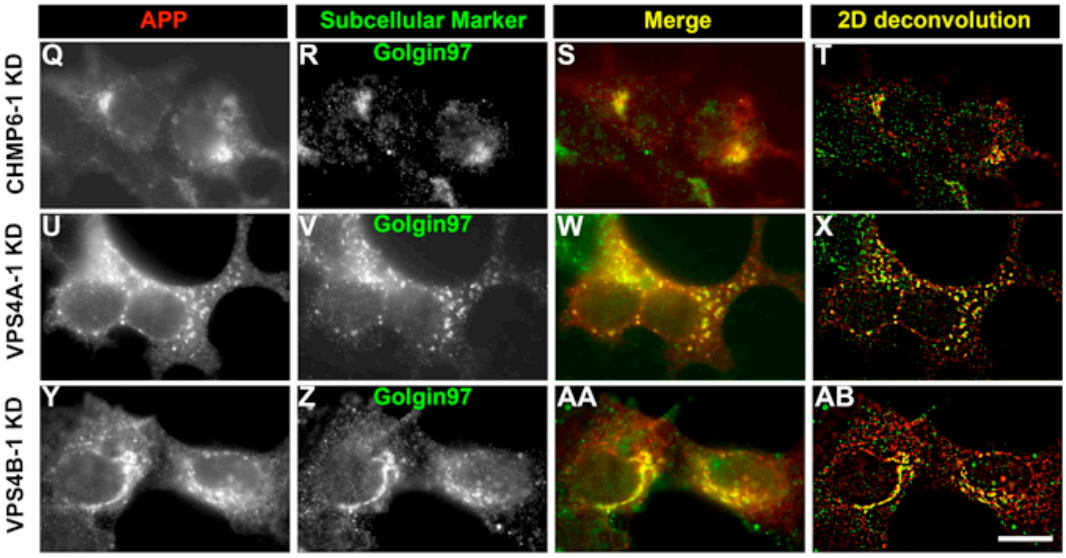
APP
Subcellular Marker
Merge
2D deconvolution
CHMP6-1 KD
VPS4A-1 KD
VPS4B-1 KD
Q
R
Golgin97
S
T
U
V
Golgin97
W
X
Y
Z
Golgin97
AA
AB

Figure 2-11. Immunoelectron microscopy analysis upon ESCRT depletion. HEK293 cells stably expressing APP_{695} were transfected with shRNA directed to Hrs or VPS4A (KD). Cells were fixed at 120 h post-transfection and processed for thin section electron microscopy. Thin sections were analyzed by immunoelectron microscopy using an anti-APP antibody and 15 nm gold-coupled secondary antibody, together with either an anti-EEA1 antibody (for Hrs-1 KD) or an anti-Golgin 97 antibody (for VPS4A-1 KD), and 10 nm gold-coupled secondary antibody. Clusters of APP with the corresponding subcellular markers were shown by blue arrows for Hrs-1 KD and red arrows for VPS4A-1 KD. Scale bars = 100 nm.

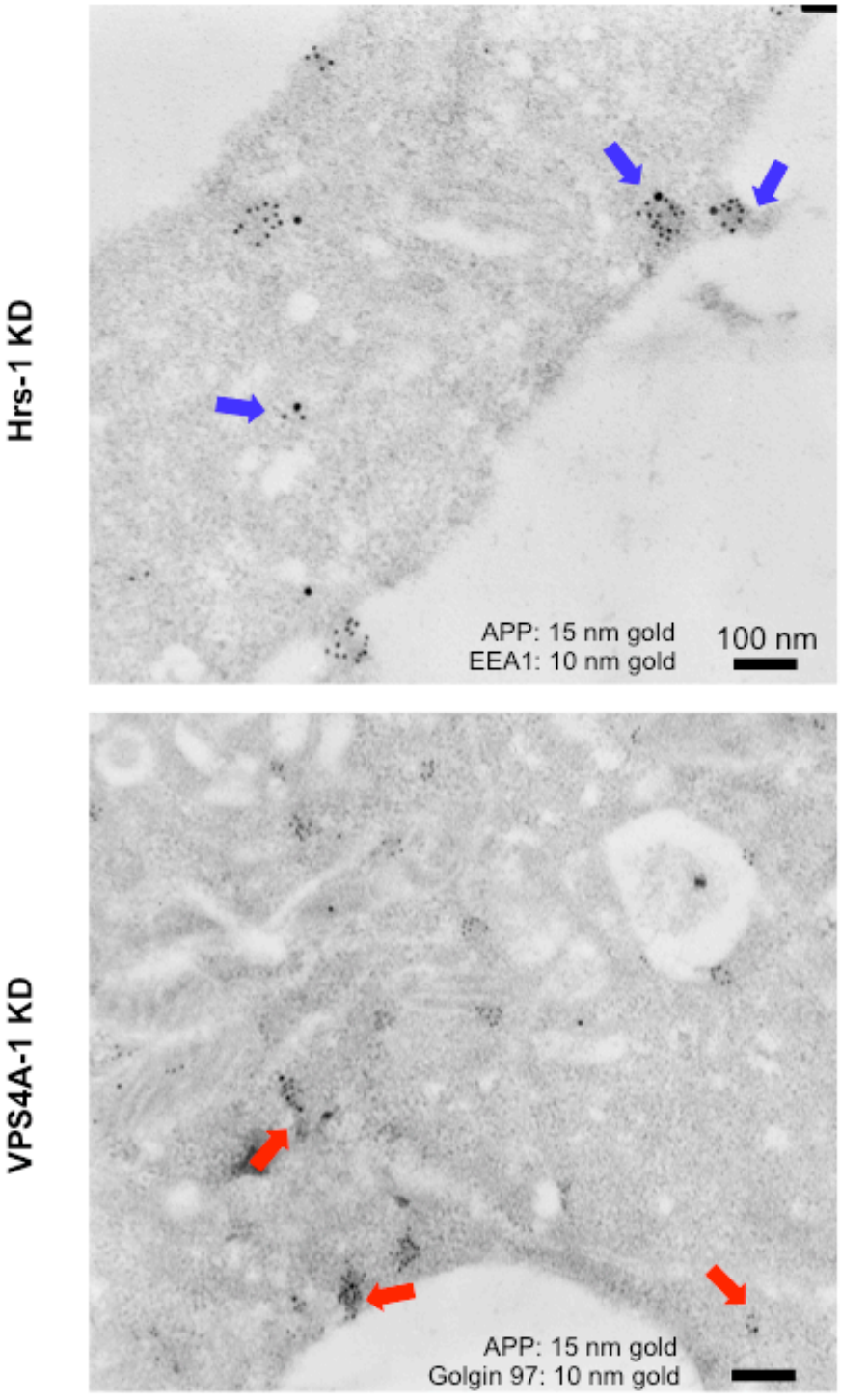
Hrs-1 KD
APP: 15 nm gold
EEA1: 10 nm gold
100 nm
VPS4A-1 KD
APP: 15 nm gold
Golgin 97: 10 nm gold

Figure 2-12. Double knockdown of Hrs and VPS4A reduced Aβ production.
HEK293 cells stably expressing APP_{695} were transfected with empty vector (control) or pooled shRNA constructs (Hrs-1 and VPS4A-1) directed to Hrs and VPS4A (KD). (A) Cells were lysed at 120 h post-transfection and proteins were analyzed by immunoblot. Actin was used as loading control. (B) Relative protein level of Hrs and VPS4A in double knockdown cells as a percentage of the control (set as 100%) was quantified by the LI-COR Odyssey Infrared Imaging System (mean ± SEM; $n \geq 3$). (C) Culture media conditioned from 96 h to 120 h post-transfection of shRNA were subjected to $A\beta_{40}$ ELISA analysis. Relative normalized $A\beta_{40}$ levels as a percentage of the control (set as 100%) were plotted as mean ± SEM ($n \geq 3$). * $p < 0.05$

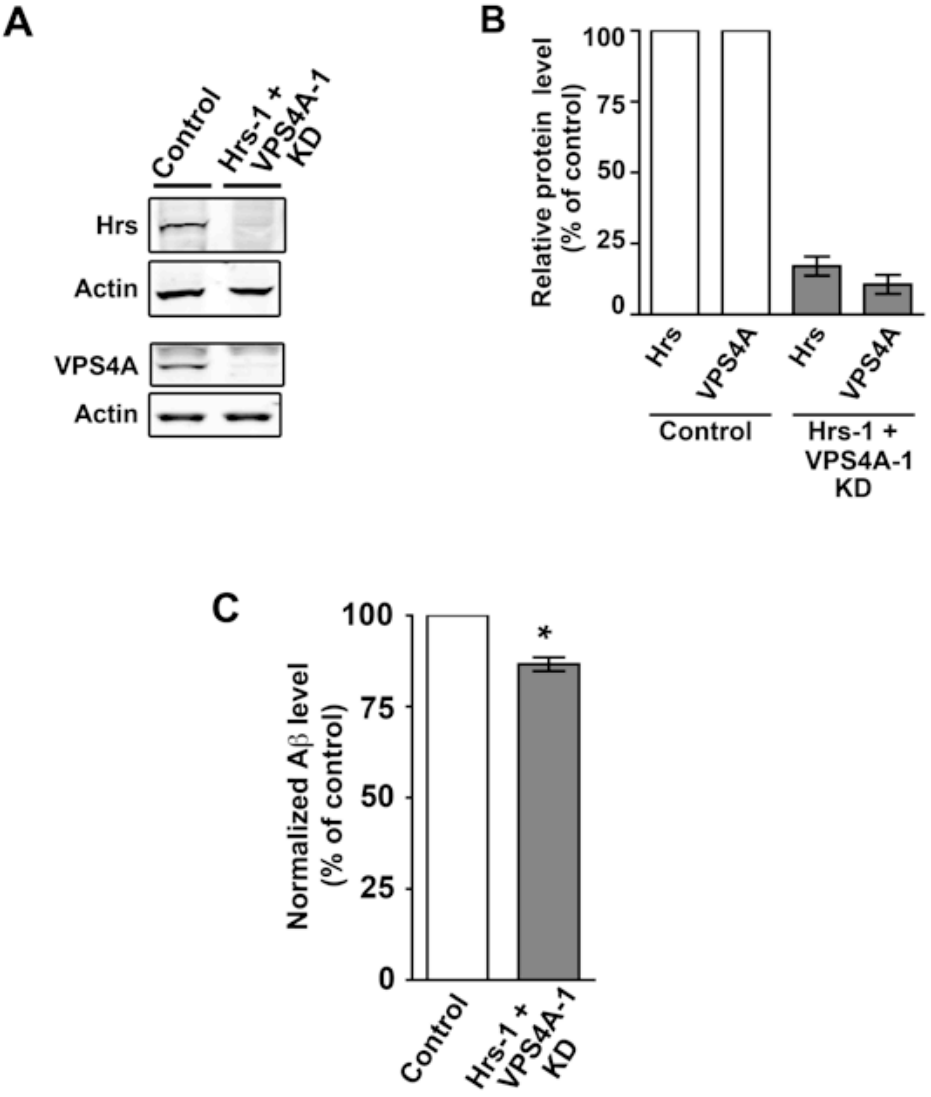
A
Control
Hrs-1 + VPS4A-1 KD
Hrs
Actin
VPS4A
Actin
B
Relative protein level (% of control)
100
75
50
25
0
Hrs
VPS4A
Hrs
VPS4A
Control
Hrs-1 + VPS4A-1 KD
C
Normalized Aβ level (% of control)
100
75
50
25
0
*
Control
Hrs-1 + VPS4A-1 KD

Figure 2-13. APP localized to enlarged early endosomes upon double knockdown of Hrs and VPS4A. HEK293 cells stably expressing APP_{695} were transfected with empty vector (control) or pooled shRNA constructs (Hrs-1 and VPS4A-1) directed to Hrs and VPS4A (KD). Cells were fixed at 120 h post-transfection and stained for APP, and subcellular markers Golgin 97 or EEA1. (A) Cells were transfected with pSUPER.puro shRNA targeting Hrs, and pSUPER+GFP shRNA construct targeting VPS4A. (B) Cell were transfected with pSUPER.puro shRNA targeting VPS4, and pSUPER+GFP shRNA construct targeting Hrs. Because pSUPER+GFP vector co-expressed both the shRNA and GFP, GFP signals were used to indicate cells with knockdown. Representative cells with GFP signals are shown. Merged images were generated from the Alexa 568 channel (APP signals indicated by red) and the Alexa 647 channel (Golgin 97 or EEA signals indicated by green), or 2D-deconvolved images from each channel; colocalization indicated by yellow. Scale bars = 10 μm.

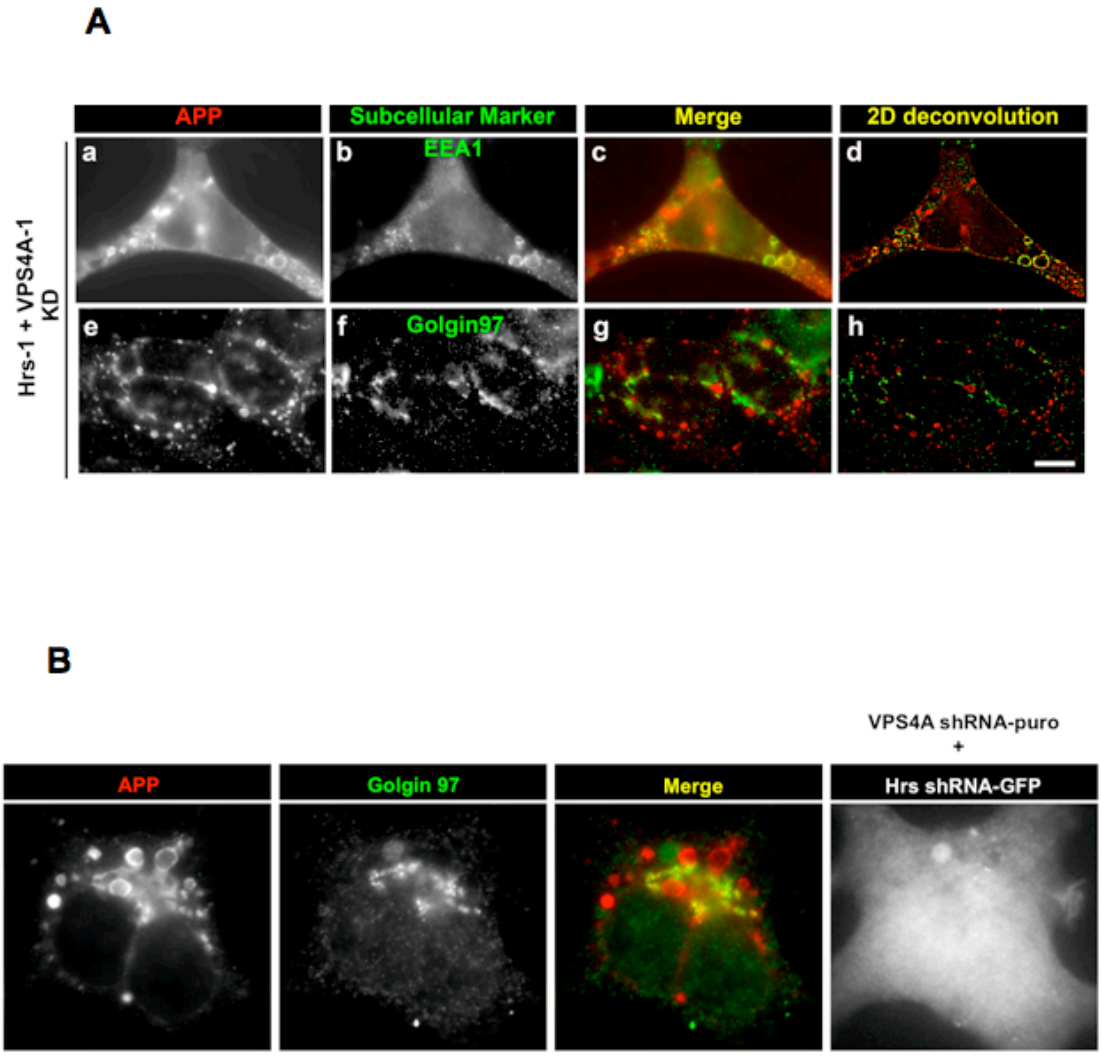
A
APP
Subcellular Marker
Merge
2D deconvolution
a
b
EEA1
c
d
Hrs-1 + VPS4A-1 KD
e
f
Golgin97
g
h
B
VPS4A shRNA-puro
+
APP
Golgin 97
Merge
Hrs shRNA-GFP

CHAPTER THREE
RETROMER-MEDIATED RECYCLING OF APP IS REQUIRED FOR Aβ PRODUCTION

INTRODUCTION

Retrograde transport of proteins from the endosomes to the TGN flow from early endosomes via recycling endosomes, or transit from late endosomes in a Rab9-dependent manner (Ganley et al., 2008; Pfeffer, 2009). Recently, it has been shown that endosome-to-TGN recycling of APP was retromer-dependent (Sullivan et al., 2011; Vieira et al., 2010). Based on the findings of ESCRT knockdown experiments in Chapter Two (Fig. 2-12 and 2-13), I hypothesized that endosome-to-TGN recycling may play a role in Aβ production by re-directing APP from the endocytic pathway to the TGN for proteolytic processing. Here, I investigated the importance of different recycling pathways on Aβ production.

RESULTS

To confirm whether the retrieval of APP from endosomes to the TGN was important in the production of Aβ, I examined both the early and late recycling routes by knockdown of VPS35 and Rab9, respectively (Fig. 3-1). Depletion of a retromer core subunit VPS35 redistributed APP from the TGN to puncta that partially colocalized with EEA1 (33 ± 4%) (Fig. 3-1 *e-h*), but to a lesser extent with Golgin 97 (20 ± 3%) (Fig. 3-1 *a-d*), suggesting that recycling of APP from the early endosomes to the TGN was defective. These partially EEA1-labeled puncta could represent recycling compartments between early endosomes and the TGN formed when the retromer pathway is defective. A decrease in the $A\beta_{40}$ level was measured in VPS35-depleted cells (Fig. 3-2) which correlated well with the reduced localization of APP to the TGN. However, steady-state APP colocalized with Golgin 97 in Rab9-depleted cells (57 ± 3%) (Fig. 3-1 *i-l*), with a subset of APP colocalizing with EEA (12 ± 2%) (Fig. 3-1 *m-p*), which was comparable to the control cells (Fig. 2-8), suggesting the retrograde transport of APP to the TGN was not impaired upon Rab9 depletion. No significant change in the $A\beta_{40}$ level (Fig. 3-2) was observed in Rab9 knockdown. My results demonstrated that the majority of the endosomal population of APP was retrieved to the TGN via the early pathway that was dependent on retromer, consistent with the findings reported by other groups (Sullivan et al., 2011; Vieira et al., 2010), rather than the late Rab9-dependent recycling pathway. In addition, the delay in Aβ production upon retromer depletion further supported the notion that the TGN could be the subcellular site for efficient Aβ production because delaying APP trafficking back to the TGN decreased the formation of Aβ peptides.

In Chapter Two, I speculated the increase in Aβ production upon depletion of late ESCRT components such as CHMP6, VPS4A, and VPS4B was attributable to the rerouting of more APP from endosomes back to the TGN (Fig. 2-7 and 2-10), because Aβ production was reduced when APP was retained in early endosomes in a double knockdown of Hrs and VPS4A (Fig. 2-12 and 2-13). To further confirm the notion that increased production of Aβ in late ESCRT knockdown is dependent on endosome-to-TGN recycling of APP, I performed a double knockdown of retromer and late ESCRT components (Fig. 3-3 and 3-4). Rather than accumulating predominantly in the TGN as observed in single knockdown of these late ESCRT components, steady-state APP in VPS35 and CHMP6 double-depleted cells, VSP35 and VPS4A double-depleted cells, and

VPS35 and VPS4B double-depleted cells all showed a significant decrease in TGN localization when compared to the control or single late ESCRT knockdown cells (Fig. 3-3). Similar to the phenotypes observed in single VPS35 depletion (Fig. 3-1), APP localization was shifted from the TGN to small puncta at the perinuclear area, which were presumably some intermediate recycling compartments with only partial colocalization with EEA1 (Fig. 3-3). As expected, the levels of $A\beta_{40}$ were also reduced in these double-knockdown cells with a defective retromer pathway (Fig. 3-4). These data suggested an important role of functional retromer-mediated endosome-to TGN recycling pathway in Aβ production.

DISCUSSION

My findings in Chapter Two based on the double-knockdown of Hrs and VPS4 suggested that the retromer pathway that retrieved endosomal APP to the TGN plays a role in Aβ production (Fig. 2-12 and 2-13). Endosomal proteins that recycled to the TGN could take two major routes, either via the retromer-dependent pathway from early endosomes, or the Rab9-dependent pathway from late endosomes (Ganley et al., 2008; Pfeffer, 2009). Recent evidence (Sullivan et al., 2011; Vieira et al., 2010) and my data (Fig. 3-1 and 3-2) consistently suggest that the retrograde transport of APP from early endosomes to the TGN is retromer-dependent. I also demonstrated that APP was less likely to take the Rab9-dependent recycling route from late endosomes back to the TGN (Fig. 3-1 and 3-2). I showed that impeding the retromer-mediated recycling pathway by depletion of VPS35 leads to a decrease in Aβ production (Fig. 3-2), which is consistent with the finding of a recent study using a similar cell line (Sullivan et al., 2011). I demonstrated that in VPS35-depleted cells the steady state distribution of APP shifted from the TGN to distinct puncta that could possibly be intermediate recycling compartments (Fig. 3-1 *a-h*). In addition, I also demonstrated that upon double knockdown of retromer (VPS35) and late ESCRT components (CHMP6, VPS4A and VPS4B), APP could no longer be recycled from early endosomes to the TGN, leading to reduced APP processing (Fig. 3-3 and 3-4). This also confirmed that the increase in Aβ production in late ESCRT knockdown was due to more endocytic APP re-directed to the TGN but not some general effect that retained biosynthetic APP in the TGN. My findings demonstrated the importance of functional retromer-dependent retrograde pathway in Aβ production.

MATERIALS AND METHODS

Antibodies

Mouse monoclonal antibodies used were: anti-Rab9 (mab9, EMD chemicals), anti-Golgin 97 (CDF4, Life Technologies), anti-EEA1 (14, BD Transduction Laboratories), and anti-Actin (C4, MP Biomedicals). Rabbit polyclonal antibodies used were anti-CHMP6 (gift from W. I. Sundquist, University of Utah), anti-VPS4A (gift from W. I. Sundquist, University of Utah), anti-VPS4B (gift from W. I. Sundquist, University of Utah), anti-β subunit of AP-4 (gift from M. S. Robinson; University of Cambridge, UK), anti-SEC23A (gift from J. P. Paccaud; Drugs of Neglected Diseases Initiative, Geneva, Switzerland) and anti-APP C-terminus (Sigma-Aldrich). Goat polyclonal anti-VPS35 antibody was

obtained from Imgenex. IRDye 680 and 800 secondary antibodies (LICOR) were used for immunoblotting analysis. Alexa Fluor 568 and 647-conjugated secondary antibodies (Life Technologies) were used for immunofluorescence microscopy.

RNAi constructs

The mRNA sequences of human VPS35, and Rab9A were used to design short hairpin RNA (shRNA) for specific gene silencing as described in the Materials and Methods of Chapter Two.

Two pairs of complementary oligonucleotides directed towards distinct regions of mRNA sequences of each knockdown target was synthesized (Integrated DNA Technologies), as follows:

5'-
GATCGACATGCCTTCAGAGGATGTTCAAGAGACATCCTCTGAAGGCATGTCT
TTTTTGGAAA-3' and 5'-
AGCTTTTCCAAAAAAGACATGCCTTCAGAGGATGTCTCTTGAACATCCTCTGA
AGGCATGTC-3' for VPS35-1;

5'-
GATCAGTGGCAGATCTCTACGAATTCAAGAGATTCGTAGAGATCTGCCACTTT
TTTTGGAAA-3' and

5'-
AGCTTTTCCAAAAAAAGTGGCAGATCTCTACGAATCTCTTGAATTCGTAGAG
ATCTGCCACT-3' for VPS35-2;

5'-
GATCGTTTGATACCCAGCTCTTCTTCAAGAGAGAAGAGCTGGGTATCAAACTT
TTTTGGAAA-3' and 5'-
AGCTTTTCCAAAAAAGTTTGATACCCAGCTCTTCTCTCTTGAAGAAGAGCTGG
GTATCAAAC-3' for Rab9A-1;

5'-
GATCTCAACATGGGGATGGAGAATTCAAGAGATTCTCCATCCCCATGTTGATT
TTTTGGAAA-3' and 5'-
AGCTTTTCCAAAAAATCAACATGGGGATGGAGAATCTCTTGAATTCTCCATCC
CCATGTTGA-3' for Rab9A-2.

ELISA, Protein Determination, and Immunoblotting

Experiments were done as described in the Materials and Methods of Chapter Two.

Immunofluorescence Microscopy and Quantification

as described in the Materials and Methods of Chapter Two.

Figure 3-1. VPS35 depletion delayed retromer-mediated retrieval of APP to the TGN. HEK293 cells stably expressing APP_{695} were transfected with pSUPER+GFP shRNA directed to VPS35 or Rab9A (KD). Cells were fixed at 120 h post-transfection and stained for subcellular markers Golgin 97 or EEA1. Because the pSUPER+GFP vector co-expressed both the shRNA and GFP, GFP signals were used to indicate knockdown cells. Representative cells with GFP signals are shown. Merged images were generated from the Alexa 568 channel (APP signals indicated by red) and the Alexa 647 channel (Golgin 97 or EEA signals indicated by green), or 2D-deconvolved images from each channel; colocalization indicated by yellow. Scale bars = 10 μm

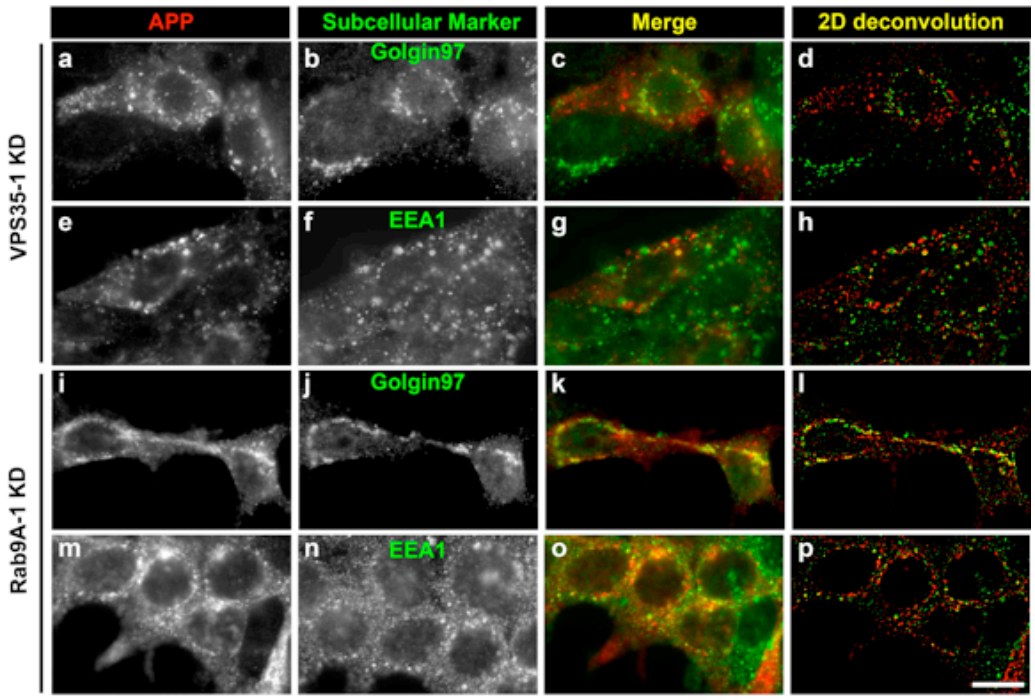
APP
Subcellular Marker
Merge
2D deconvolution
VPS35-1 KD
Rab9A-1 KD
a
b
Golgin97
c
d
e
f
EEA1
g
h
i
j
Golgin97
k
l
m
n
EEA1
o
p

Figure 3-2. Knockdown of retromer reduced Aβ production. (A) HEK293 cells stably expressing APP_{695} were transfected with empty vector (control) or two shRNA constructs directed to VPS35 or Rab9A (KD). Cells were lysed at 120 h post-transfection and proteins were analyzed by immunoblot. Actin or SEC23A were used as loading controls. (B) Relative protein levels in shRNA knockdown cells as a percentage of the control (set as 100%) were quantified by the LI-COR Odyssey Infrared Imaging System (mean ± SEM; $n \geq 3$). (C) Culture media conditioned from 96 h to 120 h post-transfection were subjected to $A\beta_{40}$ ELISA analysis. Relative normalized $A\beta_{40}$ levels as a percentage of the control (set as 100%) were plotted as mean ± SEM ($n \geq 3$). ** $p < 0.01$ and *** $p < 0.001$, only p values below 0.05 were shown.

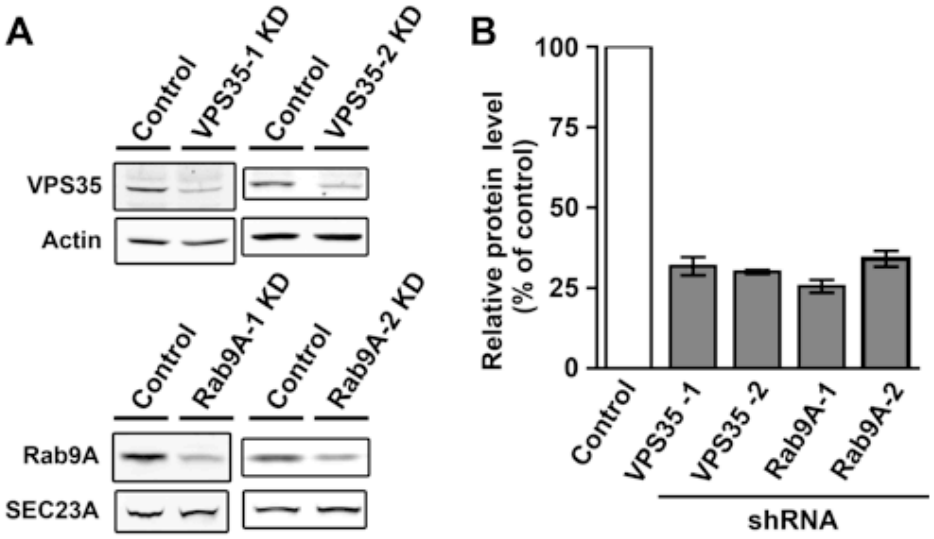
A
Control
VPS35-1 KD
Control
VPS35-2 KD
VPS35
Actin
Control
Rab9A-1 KD
Control
Rab9A-2 KD
Rab9A
SEC23A
B
Relative protein level
(% of control)
100
75
50
25
0
Control
VPS35 -1
VPS35 -2
Rab9A-1
Rab9A-2
shRNA

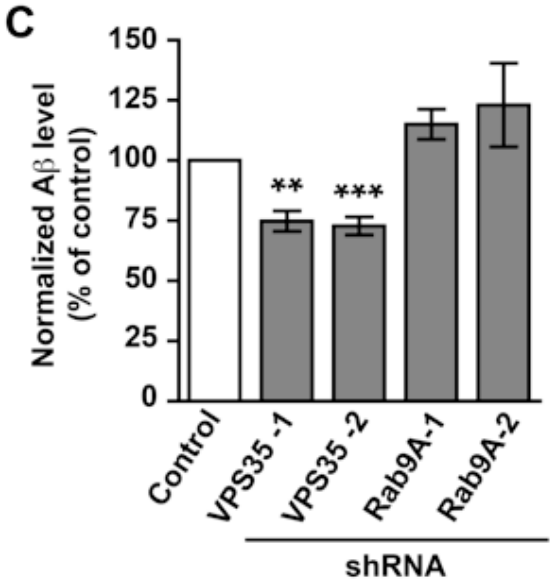
C
Normalized Aβ level
(% of control)
150
125
100
75
50
25
0
**
***
Control
VPS35 -1
VPS35 -2
Rab9A-1
Rab9A-2
shRNA

Figure 3-3. Double knockdown of retromer and late ESCRT components delayed retromer-mediated retrieval of APP to the TGN. HEK293 cells stably expressing APP_{695} were transfected with empty vector (control) or pooled shRNA constructs directed to both VPS35 and late ESCRT components (CHMP6, VPS4A or VPS4B) at the same time. Two shRNA constructs of VPS35 (VPS35-1 and VPS35-2) were used simultaneously to ensure efficient knockdown of VPS35. Cells were fixed at 120 h post-transfection and stained for subcellular markers Golgin 97 or EEA1. Because the pSUPER+GFP vector co-expressed both the shRNA and GFP, GFP signals were used to indicate the knockdown cells. Representative cells with GFP signals are shown. Merged images were generated from the Alexa 568 channel (APP signals indicated by red) and the Alexa 647 channel (Golgin 97 or EEA signals indicated by green); colocalization indicated by yellow. Scale bars = 10 μm

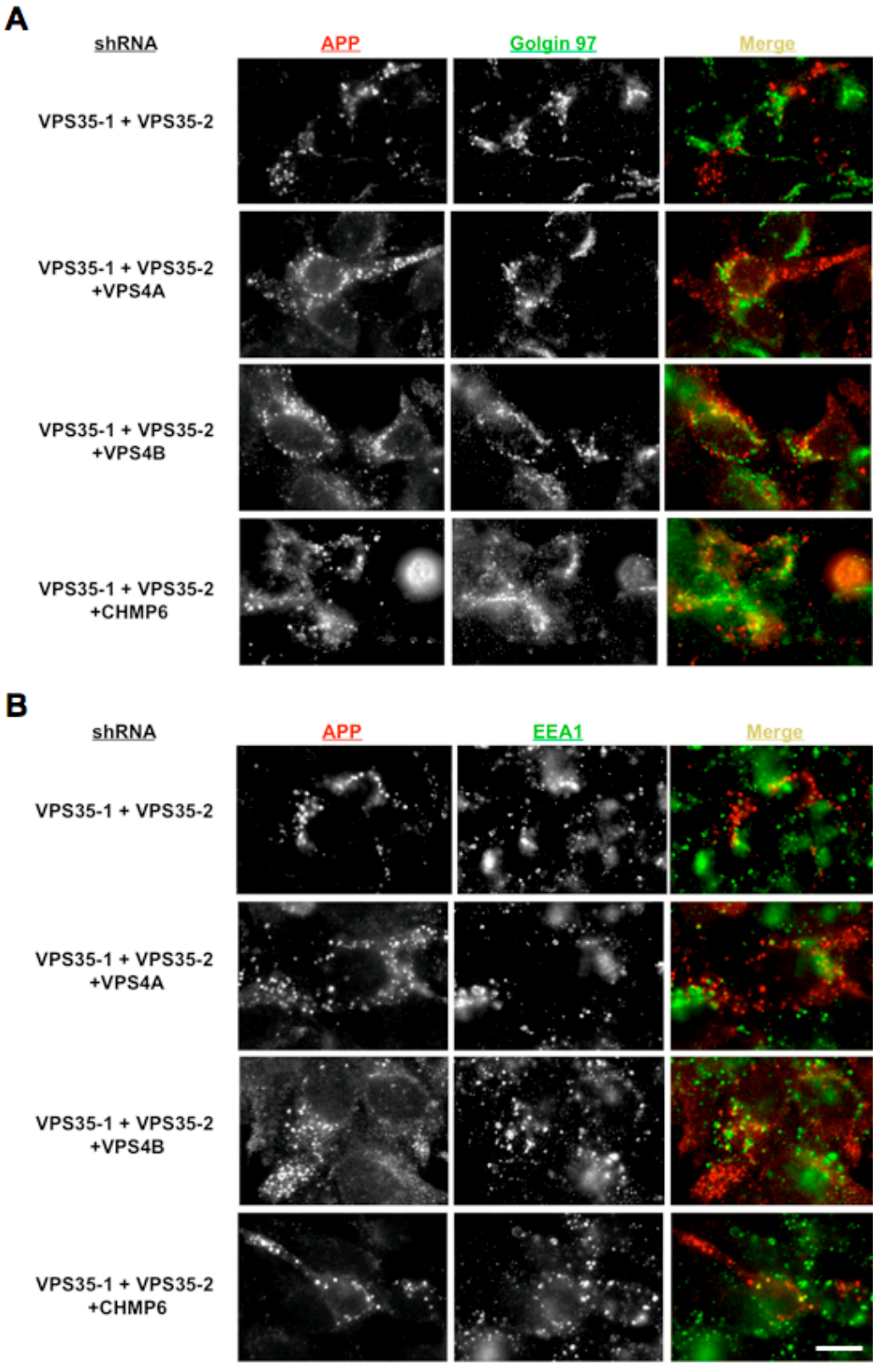
A
shRNA
APP
Golgin 97
Merge
VPS35-1 + VPS35-2
VPS35-1 + VPS35-2 +VPS4A
VPS35-1 + VPS35-2 +VPS4B
VPS35-1 + VPS35-2 +CHMP6
B
shRNA
APP
EEA1
Merge
VPS35-1 + VPS35-2
VPS35-1 + VPS35-2 +VPS4A
VPS35-1 + VPS35-2 +VPS4B
VPS35-1 + VPS35-2 +CHMP6

Figure 3-4. Double knockdown of retromer and late ESCRT components reduced Aβ production. HEK293 cells stably expressing APP_{695} were transfected with empty vector (control) or pooled shRNA constructs directed to VPS35 and late ESCRT components (CHMP6, VPS4A or VPS4B) at the same time. Two shRNA constructs of VPS35 (VPS35-1 and VPS35-2) were used simultaneously to ensure efficient knockdown of VPS35. Culture media conditioned from 96 h to 120 h post-transfection of shRNA were subjected to $A\beta_{40}$ ELISA analysis. Relative normalized $A\beta_{40}$ levels as a percentage of the control (set as 100%) were plotted.

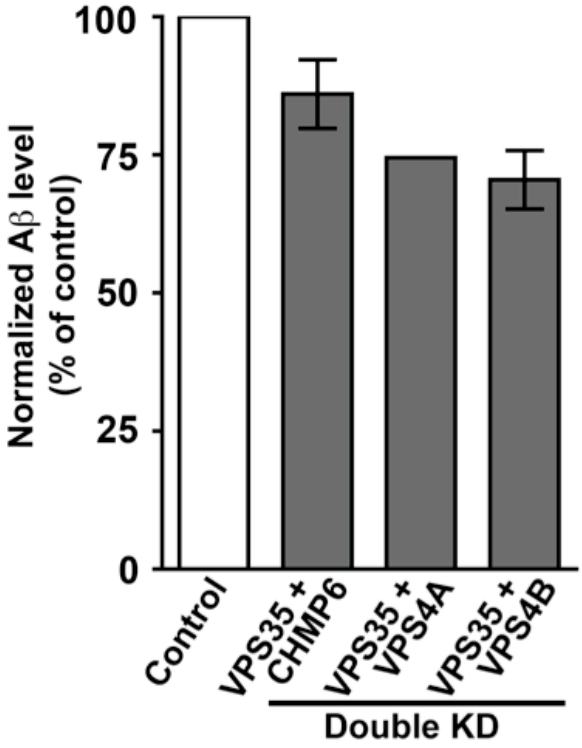
100
75
50
25
0
Normalized Aβ level
(% of control)
Control
VPS35 +
CHMP6
VPS35 +
VPS4A
VPS35 +
VPS4B
Double KD

CHAPTER FOUR
ENDOCYTOSED APP IS RECYCLED TO THE TGN FOR Aβ PRODUCTION

INTRODUCTION

Although my data suggested that APP accumulation in the TGN upon depletion of late ESCRT subunits was likely to come from the endosomal population of APP that underwent retromer-mediated retrograde transport (Fig. 2-12 and 2-13), I had to determine whether the recycled APP were originated from the endocytosed population from the cell surface or from the biosynthetic population of APP that trafficked to the endosomes directly from the TGN. A TGN-to-endosome route for APP has been described that is mediated by the direct interaction of APP with the adaptor protein complex-4 (AP-4) (Burgos et al., 2010). Disruption of the interaction between the μ subunit of AP-4 complex (AP-4 μ) and APP or depletion of AP-4 μ shifted the steady-state distribution of APP to the TGN with an increase in the Aβ level, consistent with my findings that the TGN is the site for Aβ production (Burgos et al., 2010). In this study, I investigated the effects on APP localization as well as Aβ production after depletion of AP-4 μ to block direct TGN-to-endosome trafficking, or double-knockdown of AP-4 μ and VPS35 to interrupt the bi-directional APP trafficking between the TGN and endosomes.

RESULTS

I first repeated the knockdown experiment of AP-4 μ in HEK293 cells expressing APP_{695} (Fig. 4-1 A and B), and I observed similar results of increased Aβ production (Fig. 4-1 C) and steady-state localization of APP to the TGN (55 ± 4%) (Fig. 4-2 *a-d*). This result is consistent with but not necessarily demonstrate that APP cleaved in the TGN was derived from the biosynthetic pathway. To examine whether the recycled APP came from the cell surface-derived endocytic pool or from the biosynthetic pool, I performed a double knockdown of both the AP-4 μ and the retromer subunit VPS35, to block the forward and retrograde trafficking between the TGN and the endosomes. If the majority of APP cleaved in the TGN were the biosynthetic population of APP that had never reached the cell surface, I would expect the double-knockdown to behave as the single knockdown of AP-4 μ. On the contrary, I would expect that APP would be retained in the endosomal pathway if it was derived from the endocytic population of APP. Strikingly, APP was redistributed at steady state to enlarged (with varying sizes), ring-like EEA1-positive structures upon the double knockdown of AP-4 μ and VPS35 (35 ± 14%) (Fig. 4-2 *i-l*), similar to the phenotypes I observed upon depletion of Hrs or Tsg101, which were never seen in single knockdown of either AP-4 μ or VPS35 alone. I observed a decrease in APP localization in the TGN (10 ± 1%) (Fig. 4-2 *e-h*). Thus, disruption of the bidirectional trafficking of APP between the TGN and endosomes resulted in a majority of APP transitioning the secretory pathway to the cell surface following internalization to and accumulation in early endosomes. As expected, with the redistribution of APP to enlarged early endosomes upon double-depletion of AP-4 μ and VPS35, I measured a decrease in Aβ production (Fig. 4-1), supporting my earlier interpretation Aβ is not produced in early endosomes. I concluded that the production of Aβ occurs predominantly in the TGN, and the majority of APP that was cleaved in the TGN originated at the cell surface and required endocytosis and recycling back to the TGN for efficient proteolytic processing.

DISCUSSION

In this study, I explored the relative contributions of endocytosis versus biosynthesis in the delivery of APP to the TGN for proteolytic processing. If the biosynthetic population of APP represents the majority of substrate to generate Aβ, blocking the bidirectional pathways that link the TGN and early endosomes should produce the same result as inhibitions of trafficking of APP from the TGN to early endosomes. However, I showed by double knockdown of AP-4 μ and VPS35 that Aβ production was reduced (Fig. 4-1), and APP was redistributed to enlarged early endosomes (Fig. 4-2); suggesting the majority of APP transits to the plasma membrane is internalized, and then recycles from early endosomes to the TGN for Aβ production. Of course I would expect that some biosynthetic APP traffics from the TGN to endosomes and back (Burgos et al., 2010), but this appears to be less relevant to Aβ production.

Why must APP traffic all to the plasma membrane before being retrieved via the retromer complex to the TGN given that the TGN is the major subcellular compartment which generates Aβ? Given that BACE is believed to process APP into β-CTF in early endosomes after its internalization (Huse et al., 2000; Kinoshita et al., 2003), the itinerary of APP may uptake and traffic through the endosome to produce a substrate suitable for the action of γ-secretase in the TGN. Once APP is processed by BACE in early endosomes, APP β-CTF could then be transported to the TGN via the retromer-dependent recycling pathway for Aβ production.

With regard to the importance of trafficking between the TGN and the endosomes on APP processing, the sortilin-related receptor SorLA was identified to be a genetic risk factor for late-onset Alzheimer's disease (Rogaeva et al., 2007). SorLA has been localized to the TGN and endosomes where it may serve to mediate the traffic of APP (Andersen et al., 2005; Offe et al., 2006). Depletion of SorLA increases Aβ production (Rogaeva et al., 2007). It is not clear if SorLA mediates the transport of APP from the TGN to endosomes or retrieves endocytic APP from endosomes back to the TGN (Andersen et al., 2005; Offe et al., 2006). A thorough investigation on how SorLA regulates APP trafficking between the TGN and endosomes using various cell types including polarized and neuronal cells is crucial to identifying the actual subcellular compartment in which Aβ is produced.

In summary, I demonstrated that the retromer-dependent recycling pathway is important in the process of Aβ production, possibly by maintaining the balance of the bidirectional trafficking between the TGN and the endosomes, so that APP with proper modifications in the endocytic pathway could gain access to the TGN where Aβ production occurs (Fig. 4-3).

MATERIALS AND METHODS

Antibodies

Mouse monoclonal antibodies used were anti-Golgin 97 (CDF4, Life Technologies), anti-EEA1 (14, BD Transduction Laboratories), and anti-Actin (C4, MP Biomedicals). Rabbit polyclonal antibodies used were anti-β subunit of AP-4 (gift from M. S. Robinson; University of Cambridge, UK), anti-SEC23A (gift from J. P. Paccaud; Drugs of Neglected Diseases Initiative, Geneva, Switzerland) and anti-APP C-terminus (Sigma-Aldrich). Goat polyclonal anti-VPS35 antibody was obtained from Imgenex. IRDye 680 and 800 secondary antibodies (LICOR) were used for immunoblotting analysis. Alexa Fluor 568 and 647-conjugated secondary antibodies (Life Technologies) were used for immunofluorescence microscopy.

RNAi constructs

For human AP-4 μ knockdown, the siRNA target sequence reported by Burgos et al (Burgos et al., 2010) was used to design complementary oligonucleotides as follows:
5'-
GATCGTCTCGTTTCACAGCTCTGTTCAAGAGACAGAGCTGTGAAACGAGACT
TTTTTGGAAA-3' and
5'-
AGCTTTTCCAAAAAAGTCTCGTTTCACAGCTCTGTCTCTTGAACAGAGCTGTG
AAACGAGAC-3' for AP-4 μ.
The complementary pair of DNA oligonucleotides was annealed and ligated into the linearized pSUPER.retro.puro (pSUPER) shRNA or pSUPER.retro.gfp+neo (pSUPER+GFP) expression vectors (OligoEngine) in between the BglII and HindIII sites.

ELISA, Protein Determination, and Immunoblotting

Experiments were done as described in the Materials and Methods of Chapter Two.

Immunofluorescence Microscopy and Quantification

Experiments were done as described in the Materials and Methods of Chapter Two.

Figure 4-1. Double knockdown of AP-4 μ and VPS35 and reduced Aβ production. HEK293 cells stably expressing APP_{695} were transfected with empty vector (control) or shRNA directed to AP-4 μ, or pooled shRNA constructs (AP-4 μ and VPS35-1) directed to AP-4 μ and VPS35-1 (KD) for double knockdown. (A) Cells were lysed at 120 h post-transfection and proteins were analyzed by immunoblot. Antibody against the β subunit of AP-4 was used to evaluate the β,μ complex of AP-4. Actin or SEC23A were used as loading controls. (B) Relative protein level of AP-4 and VPS35 in shRNA knockdown cells as a percentage of the control (set as 100%) was quantified by the LI-COR Odyssey Infrared Imaging System (mean ± SEM; n = 3). (C) Culture media conditioned from 96 h to 120 h post-transfection of shRNA were subjected to $A\beta_{40}$ ELISA analysis. Relative normalized $A\beta_{40}$ levels as a percentage of the control (set as 100%) were plotted as mean ± SEM (n = 3). * $p < 0.05$, ** $p < 0.01$.

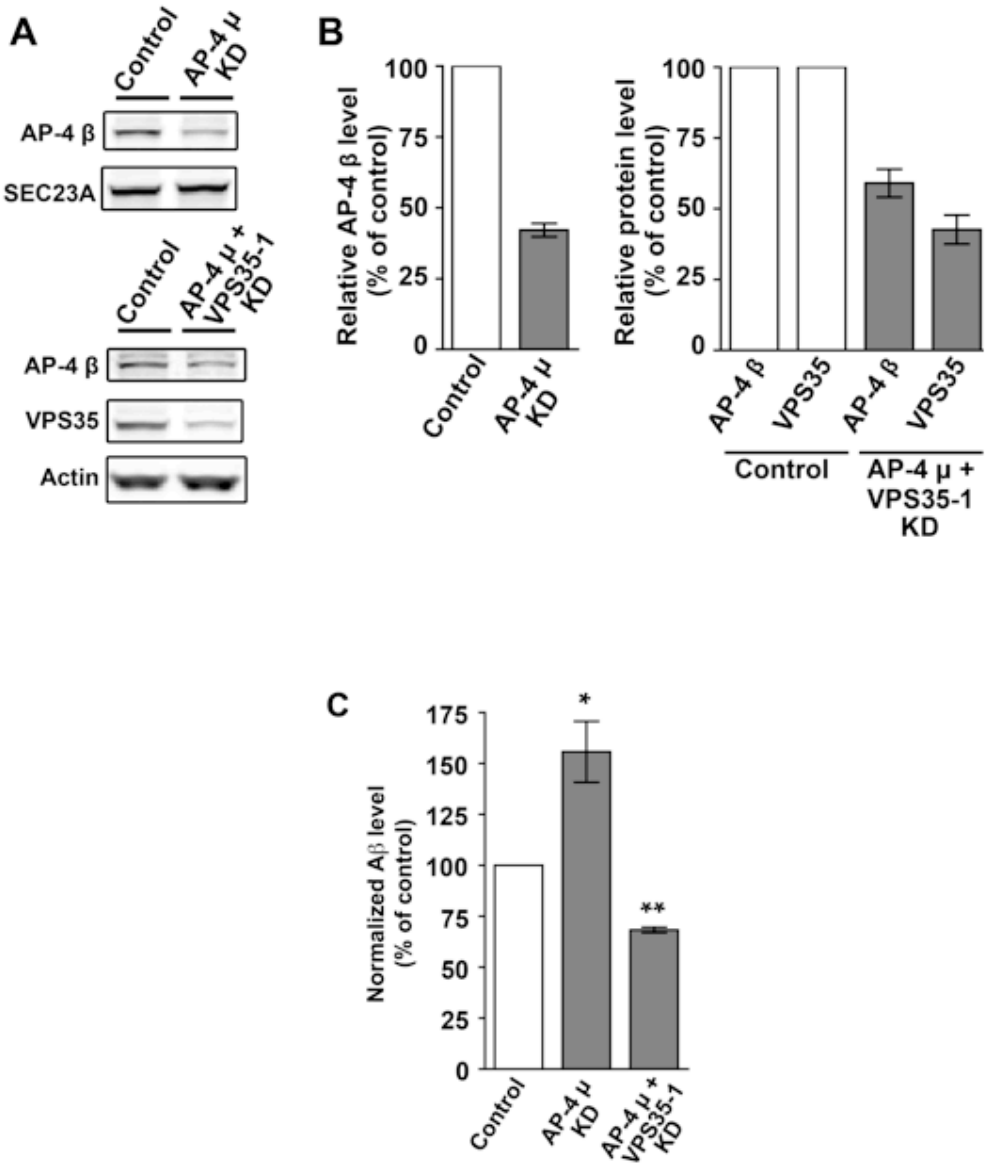
A
Control
AP-4 μ KD
AP-4 β
SEC23A
Control
AP-4 μ + VPS35-1 KD
AP-4 β
VPS35
Actin
B
Relative AP-4 β level (% of control)
100
75
50
25
0
Control
AP-4 μ KD
Relative protein level (% of control)
AP-4 β
VPS35
AP-4 β
VPS35
Control
AP-4 μ + VPS35-1 KD
C
Normalized Aβ level (% of control)
175
150
125
100
75
50
25
0
*
**
Control
AP-4 μ KD
AP-4 μ + VPS35-1 KD

Figure 4-2. Double knockdown of AP-4 μ and VPS35 retained APP in the early endosomes. HEK293 cells stably expressing APP_{695} were transfected with pSUPER+GFP shRNA directed to AP-4 μ or pooled shRNA constructs (AP-4 μ and VPS35-1) directed to AP-4 μ and VPS35-1 (KD). Cells were fixed at 120 h post-transfection and stained for subcellular markers Golgin 97 or EEA1. Because the pSUPER+GFP vector co-expressed both the shRNA and GFP, GFP signals were used to indicate which cell sustained knockdown. Representative cells with GFP signals are shown. Merged images were generated from the Alexa 568 channel (APP signals indicated by red) and the Alexa 647 channel (Golgin 97 or EEA signals indicated by green), or 2D-deconvolved images from each channel; colocalization indicated by yellow. Scale bars = 10 μm

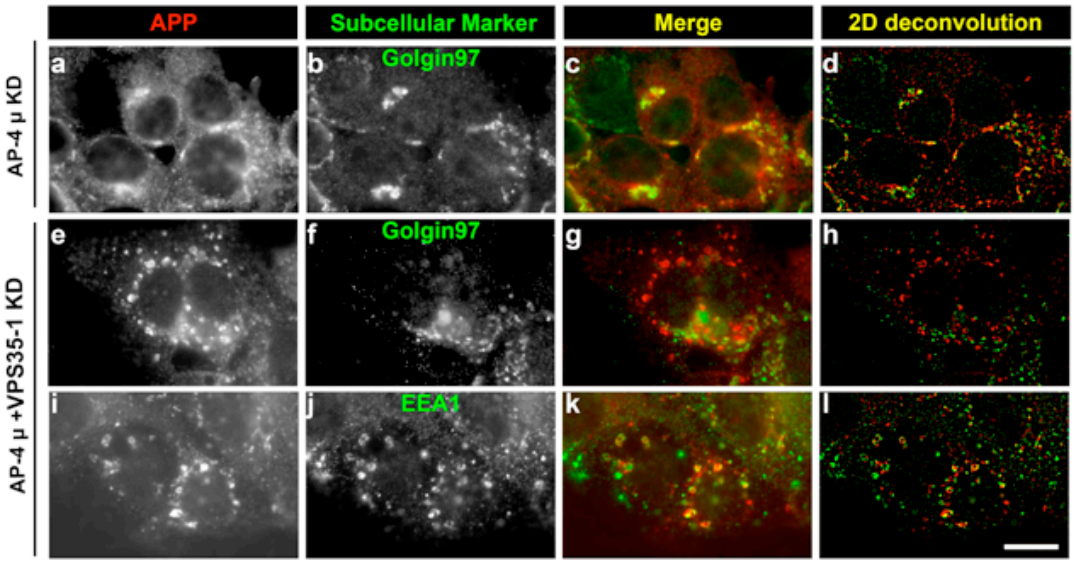
APP
Subcellular Marker
Merge
2D deconvolution
AP-4 μ KD
AP-4 μ +VPS35-1 KD
a
b
Golgin97
c
d
e
f
Golgin97
g
h
i
j
EEA1
k
l

Figure 4-3. Model for APP trafficking in Aβ production. (A) In order for APP to be cleaved efficiently into Aβ in the TGN, newly-synthesized APP at the ER first traffics along the secretory pathway via the TGN to the plasma membrane. (B) APP is then internalized via endocytosis to reach early endosomes. (C) Next, the endosomal pool of APP is recycled to the TGN in a retromer-dependent manner, where Aβ is produced. (D) The biosynthetic pool of APP in the TGN can also traffic directly to endosomes which is mediated by the AP-4 complex, (C) and be retrieved back to the TGN in a retromer-dependent manner for Aβ production. APP is indicated as red.

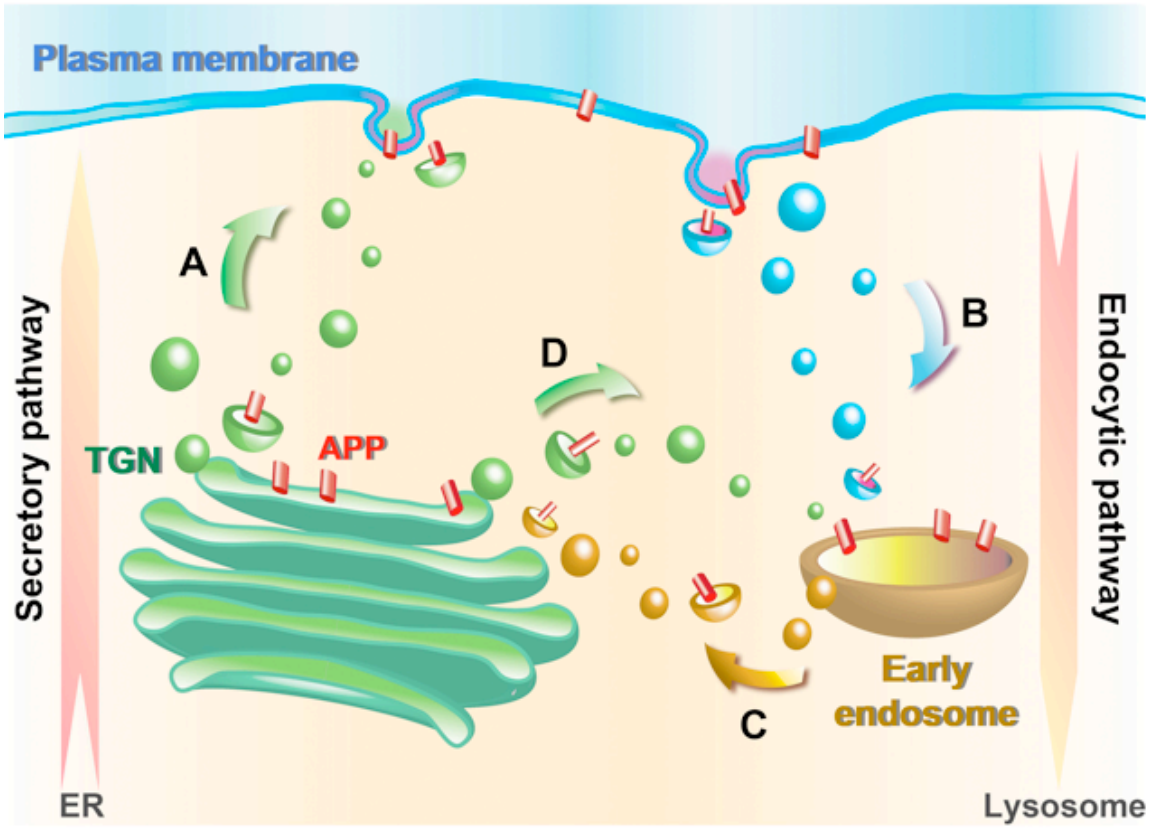
Plasma membrane
A
B
D
TGN
APP
C
Early endosome
Secretory pathway
Endocytic pathway
ER
Lysosome

CHAPTER FIVE
DEVELOPMENT OF A CELL SURFACE STREPTAVIDIN UPTAKE ASSAY TO MONITOR ENDOCYTIC APP TRAFFICKING

INTRODUCTION

By disrupting different intracellular trafficking pathways using an RNAi approach, I have confirmed the essential role of the endocytic pathway in Aβ production and demonstrated the importance of an endosome-to-TGN recycling pathway in APP processing. Although steady-state localization studies provided me with useful information on how APP distribution was affected upon the depletion of different trafficking regulators, one major limitation of this analysis is that I am unable to distinguish between proteins coming from the secretory and endocytic pathways, in which APP staining represented a mixed population of APP that were derived from different trafficking pathways. In order to dissect these trafficking pathways and focus on the endocytic population of APP, a cell surface uptake assay of APP would be useful to follow APP trafficking after internalization from the plasma membrane. Cell surface uptake or internalization assays are widely used in studying endocytosis as well as other post-endocytic trafficking pathways. For instance, transferrin (Tfn) uptake assays are performed extensively to determine the efficiency of endocytosis and endosome-to-plasma membrane recycling. Cholera toxin B subunit (CTxB) uptake assays are used to study the retrograde transport of internalized cholera toxin from the endosomal system to the Golgi and the ER. Receptor-mediated endocytosis can also be studied by surface uptake of antibodies that specifically recognize the extracellular domain of the receptors. In order to follow the post-endocytic trafficking of cell surface APP, specific anti-APP antibodies recognizing the N-terminus of APP can be used for the uptake assay; yet, choosing a suitable antibody for APP uptake assay could be tricky. Only antibodies against the N-terminus of the Aβ sequence should be used to avoid the loss of antibody due to the shredding of the extracellular domain of APP after BACE cleavage in the amyloidogenic pathway. However, it is still possible for the antibody to be dissociated from APP at anytime after endocytosis due to the increasing acidic environment along the endosomal system.

An alternative method to label cell surface membrane proteins using biotin-streptavidin interaction has been described by Ting and colleagues (Chen et al., 2005; Howarth et al., 2005). A 15-amino acid biotin acceptor peptide (AP) sequence, GLNDIFEAQKIEWHE (Beckett et al., 1999; Schatz, 1993), can be inserted in the extracellular domain of the protein of interest (Chen et al., 2005; Howarth et al., 2005). Proteins with this AP sequence can be biotinylated with *Escherichia coli* biotin ligase (BirA) either *in vitro* with exogenous recombinant BirA or *in vivo* by co-expressing BirA in the cell (Chen et al., 2005; Howarth et al., 2005). The AP sequence is specifically recognized by bacterial BirA but not the mammalian biotin ligase holocarboxylase synthetase (Chapman-Smith and Cronan, 1999; de Boer et al., 2003). This method is preferable to the conventional antibody uptake assay because the linkage between the biotin streptavidin is the strongest non-covalent interaction in nature and is unlikely to dissociate even in the acidic endosomal environment. Here, I described the development and optimization of a cell surface uptake of APP by inserting the 15-amino acid AP tag within the Aβ region of APP for biotinylation and streptavidin-labeling of the APP population residing on the plasma membrane (Fig 5-1).

RESULTS

Generation of a new functional APP construct tagged internally with AP sequence

A 15-amino acid AP sequence was inserted within the Aβ region of wildtype APP to generate an APP-AP1 construct. Insertion of the AP sequence eliminated α-secretase cleavage of APP in the non-amyloidogenic pathway. I showed that APP-AP1 was functional APP and generated and secreted Aβ at a level comparable to the wildtype APP as monitored by ELISA. However, APP-AP2, another APP construct with 2 tandem repeats of AP sequences inserted, showed less efficient production of Aβ when compared to the wildtype APP (Fig. 5-2).

Biotinylation of APP-AP *in vivo* is more efficient than *in vitro* reaction

Because the AP tag was inserted within the short extracellular region of the Aβ sequence within APP, it was positioned very close to the transmembrane region which could impede accessibility to BirA, leading to a lower biotinylation efficiency. *In vitro* biotinylation of APP-AP1 was performed using purified recombinant GST-tagged BirA biotin ligase (BirA-GST) at 37^{o}C for 90 min with the addition of biotin and ATP (Chen et al., 2005; Tran et al., 2009). Biotinylated APP could not be detected in reactions containing 0.3 μM BirA-GST, whereas 2 μM BirA-GST produced a weak signal of biotinylated APP (Fig. 5-3). The inefficient *in vitro* biotinylation of APP-AP1 may be complicated by the optimum 37^{o}C reaction conditions where cell surface APP may continue to be internalized. Using a higher concentration of BirA-GST or incubating the reaction at a lower temperature for a longer time may help to enhance the *in vitro* biotinylation efficiency of APP-AP1.

Protein with an AP tag can also be biotinylated in vivo by co-expressing a construct of BirA containing an N-terminal signal sequence and a C-terminal ER retention signal (BirA-ER) (Chen et al., 2005). Although all AP-tagged proteins are now biotinylated in the ER, the cell surface population of biotinylated APP-AP may be selected by addition of exogenous streptavidin at low temperature. In the *in vivo* biotinylation assay, I co-transfected BirA-ER together with APP-AP1 or APP-AP2. Wildtype APP (without the AP tag) was used as a negative control. CFP-TM-AP, a robustly biotinylated chimera, was used as a positive control (Chen et al., 2005). APP biotinylation was easily detected in cells transfected with APP-AP1 or APP-AP2, even though the biotinylation efficiency was significantly lower when compared to the CFP-TM-AP control which contained a highly accessible AP tag at the N-terminus (Fig. 5-4). As expected, APP-AP2 had a higher biotinylation efficiency than APP-AP1 due to the extra AP tag present in APP-AP2. The addition of extra biotin to the culture medium at 24 h post-transfection helped to boost the biotinylation efficiency slightly. I used the APP-AP1 construct to monitor post-endocytic trafficking of APP.

Cell surface streptavidin uptake assay to monitor APP-AP1 trafficking

The cell surface population of *in vivo* biotinylated APP-AP1 can be labeled by streptavidin conjugated to fluorophores such as Alexa Fluor (Ax) or Quantum dot (Qdot). Streptavidin-Qdot labeling of CFP-TM-AP was used as a positive control. Without co-

transfecting with BirA-ER, no streptavidin-Qdot labeling of CFP-TM-AP was detected, demonstrating the specificity and low background of this surface labeling reaction (Fig. 5-5 A). When CFP-TM-AP was co-transfected with BirA-ER, a strong labeling with streptavidin-Qdot was observed on the cell surface at time 0, which remained on the cell surface with few internalized puncta after shifting the temperature to 37^{o}C to initiate endocytosis (Fig. 5-5 A). Specific labeling of APP-AP1 was also observed as shown by the absence of streptavidin-Qdot signal in negative control cells that did not experess BirA-ER (Fig. 5-5 B). In cells that were co-transfected with APP-AP1 and BirA-ER, I observed cell surface streptavidin-Qdot labeling at time 0, with a significantly lower signal when compared to CFP-TM-AP, probably due to the lower biotinylation efficiency of APP-AP1. Most of the streptavidin-Qdot labeled APP-AP1 was internalized after shifting the temperature to 37^{o}C for 15 min, with more intracellular punctate labeling after 45 min of uptake (Fig. 5-5 B). This experiment demonstrated that cell surface streptavidin labeling of APP-AP1 was specific, and further confirmed that APP-AP1 was a functional APP that could be constitutively internalized by endocytosis.

Live cell imaging of APP-AP1 uptake from the cell surface

Live cell imaging of streptavidin-Alexa labeled APP-AP1 uptake was performed to monitor the trafficking routes of APP at different time points following endocytosis. Cells co-transfected with BirA-ER and APP-AP1 were labeled with streptavidin-Alexa and then subjected to internalization at 37^{o}C in a temperature controlled heated tissue culture dish. At time 0, cell surface APP-AP1 was labeled with streptavidin-Alexa. After 5 min of uptake, a major population of APP-AP1 was internalized and detected as intracellular puncta that localized near the peripheral region of the cell, which were likely to be in early endosomes. From approximately 15-20 min onwards up to 2 h within the time course of this study, APP-AP1 was localized and concentrated in one distinct perinuclear region (Fig. 5-6).

To study the localization of APP-AP1 following internalization from the cell surface in live cells, I examined other organelles in real time using various fluorescent marker proteins. Well-defined trafficking routes have been established for some cell surface cargoes that undergo endocytosis. For instance, endocytosed cholera toxin B subunit (CTxB) has been demonstrated to be retrieved from endosomes to the TGN followed by retrograde transport from the Golgi to the ER (Chinnapen et al., 2007; Montesano et al., 1982; Nichols, 2002; Sandvig and van Deurs, 2002). Transferrin (Tfn) has been shown to be internalized into early endosomes and then recycled back to the plasma membrane directly via recycling compartments without going through the TGN (Dautry-Varsat, 1986; Hopkins and Trowbridge, 1983; Mayle et al., 2011). To understand more about the trafficking routes of endocytosed APP, I performed co-uptake assays of APP-AP1 and either CTxB-Alexa or Tfn-Alexa. Labeling of the Golgi apparatus in live cells can be done simultaneously by co-uptake and transduction with a BacMam CellLight reagent which expresses a GFP-fusion protein of a Golgi resident enzyme, N-acetylgalactosaminyltransferase 2 (GalNAc-T2). As shown in Fig. 5-7, both streptavidin-Alexa bound APP-AP1 and CTxB-Alexa co-labeled the cell surface at 4^{o}C at

time 0. After a 5 min of temperature shift to 37^{o}C, both APP-AP1 and CTxB were internalized into puncta near the cell periphery, which were likely to be early endosomes. From approximately 15 to 20 min onwards up to 90 min, both cargoes had exited the early endosomal-like compartments and were localized to the perinuclear region. During this time, although both APP-AP1 and CtxB were concentrated at the perinuclear region, the two signals only partially colocalized within the center core of the perinuclear structure, with CTxB in a more spread out distribution and APP-AP1 in a more concentrated and confined localization.

To further study the subcellular localization of APP-AP1 and CTxB during these time points, I used GalNAc-T2-GFP as a live cell Golgi marker (Fig. 5-8). From approximately 15 to 20 min onwards up to 90 min post-internalization, APP-AP1 and CTxB showed a partial colocalization in the perinuclear region which was consistent with the data shown in Fig 5-7. All of the APP-AP1 signals colocalized with a portion of CTxB that was concentrated and confined within the center core of the perinuclear structure and was completely devoid of the Golgi marker GalNAc-T2 (Fig. 5-8). However, the remaining portion of CTxB which did not colocalize with APP-AP1 showed a strong colocalization of GalNAc-T2 in the outer region surrounding the APP-AP1 positive core region of the perinuclear structure (Fig. 5-8). This result suggested that once APP-AP1 arrived at these perinuclear compartments, it did not move out of the compartments rapidly such as CTxB to reach the Golgi during these time points. In the co-uptake assay of streptavidin-Alexa bound APP-AP1 and Tfn-Alexa, from 15 to 20 min onwards, both APP-AP1 and Tfn were colocalized significantly in the same confined perinuclear compartment that was devoid of the Golgi marker GalNAc-T2. These GalNAc-T2 negative perinuclear compartments that contain APP derived from early endosomes could be intermediate recycling compartments; yet, further experiments using other live cell imaging markers and longer uptake times would be necessary to gain a better understanding of the post-endocytic trafficking of APP.

DISCUSSION

Cell surface uptake assay to study APP trafficking

One of the limitations of steady-state localization analysis to study the intracellular trafficking of APP is that the mixed population of APP originating from the secretory and endocytic pathways could not be easily distinguished, and the dynamics of APP trafficking could not be followed in steady state since equilibrium has been established. In order to specifically study the post-endocytic trafficking events of APP, I sought a method to label only the cell surface population of APP and devoid of the intracellular APP pool that might cause confusion in the analysis. This can be done by performing a cell surface uptake assay to monitor trafficking of cell surface APP following endocytosis. In this study, I developed and optimized an APP uptake assay based on streptavidin labeling of biotinylated APP using a novel APP construct (APP-AP1) that contained an internal 15-amino acid biotin acceptor peptide (AP) sequence within the Aβ region. I found that APP-AP1 was biotinylated more efficiently *in vivo* by co-expressing a bacterial BirA than *in vitro* biotinylation using a recombinant BirA (Fig.

5-3 and 5-4). I also followed the real-time trafficking of endocytosed APP using live cell imaging. Cell surface APP-AP1 was labeled with fluorophore-conjugated streptavidin, and was internalized into early endosomes within 5 min at 37^{o}C. At approximately 15 to 20 min, APP-AP1 moved further to a perinuclear compartment labeled with co-internalized CTxB and Tfn but was devoid of the Golgi marker GalNAc-T2. APP remained in these "non-Golgi" compartments for up to 2 h during the course of this study, further time points have yet to be performed. As labeled by internalized Tfn, these APP-containing compartments could possibly be some intermediate recycling compartments/recycling endosomes that were derived from early endosomes. From my previous findings, however, APP was shown to be predominantly localized to the TGN at steady state (Fig. 2-2). How do I reconcile the findings in the cell surface assay with the steady-state localization data? Does the surface uptake assay reveal the normal physiological situation in which endocytosed APP is required to remain in recycling compartments for a relatively longer period of time before being transported back to the TGN? Would it be possible that endocytosed APP may actually be processed in recycling compartments? Were the results of the cell surface uptake assays only the artifact of abnormal or altered trafficking of APP-AP1 attributed to the binding of the bulky tetrameric streptavidin to APP? These are some of the important and interesting questions that needed to be addressed.

Linking APP trafficking to Aβ production by a combined microscopy and biochemical approach

Now that I have developed an uptake assay that allows us to follow the post-endocytosis trafficking fate of APP, more specifically Aβ, one could apply it to studying the detailed molecular mechanisms of APP trafficking in relation to its processing. My results suggest that APP has to traffic through the endocytic and recycling pathways before being cleaved in the TGN. The APP uptake assay may be used to confirm that the changes in APP localization upon knockdown of different trafficking mediators are dynamic and direct effects of knockdown rather than a secondary effect or adaptation of the cells. In a preliminary experiment (Fig. 5-10), I performed an APP uptake assay in APP-AP1 and BirA co-expressing HEK293 cells that were transiently transfected with shRNA targeting Hrs, and analyzed the post-endocytosis trafficking of APP-AP1 under Hrs-depleted condition. I fixed cells at different time points during the uptake assay and stained for subcellular markers for immunofluorescence analysis. Consistent with the steady-state analysis, I showed that newly internalized APP-AP1 was retained in EEA1-postive enlarged early endosomal compartments even after 90 min of uptake (Fig. 5-10). Further uptake experiments may be done similarly for other knockdowns. However, it is important to be aware of the fixation procedure might affect or shift the localization of the streptavidin conjugates that have been internalized into the cell (preliminary data not shown). The results of live cell imaging of internalized streptavidin conjugates must be compared to those of fixed cells evaluated by immunofluorescence microscopy. The use of live cell markers in real-time imaging may be preferable to fixation given artifacts. Further optimization of APP uptake assay in knockdown cells is required. The efficiency of transient transfection of the 3 plasmids, shRNA, APP-AP1 and BirA, at the same time

is low and causes high cell death. During the APP uptake assay after a 120 h knockdown, only very few cells with both the knockdown (as indicated by GFP signal from pSUPER+GFP) and streptavidin signals could be identified and analyzed. One potential solution for transfection efficiency and cytotoxicity issues would be to generate stable cell lines that can express inducible shRNA or co-express APP-AP1 and BirA. Alternatively, GFP-positive cells with shRNA knockdown could be enriched by fluorescence-activated cell sorting (FACS) before performing the uptake assay. The combination of RNAi and the uptake assay will be useful to understand more about the endocytic trafficking of APP.

The ability to label specifically the Aβ region of APP on the cell surface allows one to monitor real-time trafficking of APP and to capture the time frame when APP processing into Aβ peptides occurs. Because APP-AP1 can be labeled by streptavidin, it is possible to detect endocytosed APP-AP1 in parallel streptavidin uptake experiments using the fluorescence microscopy and biochemical assays. It may be possible to isolate newly-generated streptavidin-Aβ using affinity purification from the cell lysates harvested from different time points of the uptake assay (Fig. 5-11). It should then be possible to correlate the streptavidin-Aβ signal to the fluorescence-based streptavidin signal to determine the exact subcellular location for Aβ production.

FRET analysis to study APP and γ-secretase interaction

In addition, fluorescence resonance energy transfer (FRET) analysis may also be used to detect the real-time interaction between the endocytosed APP and the Aβ-generating γ-secretase complex (Fig. 5-12). In a preliminary study, I have fused tdTomato (Shaner et al., 2004), a red fluorescent protein (RFP) variant, to different extracellular loops of the γ-secretase catalytic subunit PSEN-1 (Fig. 5-13). PSEN-1-tdTomato may form a good FRET acceptor-donor pair with streptavidin-Qdot525 if they come into sufficiently close and properly oriented proximity after internalization of streptavidin labeled APP-AP1. I have generated 4 different extracellular tagged PSEN-1-tdTomato constructs and tested whether these PSEN-1 could undergo endoproteolysis to form CTF and NTF, which was a prerequisite for the formation of an active γ-secretase (Fig. 5-13). PSEN-1-tdTomato constructs #1 and #2 with tdTomato inserted in the first long extracellular loop from the N-terminus, showed a robust production of NTF, whereas constructs #3 and #4 with tdTomato inserted in shorter loops showed relatively low levels of NTF production (Fig. 5-13). Both PSEN-1-tdTomato constructs #1 and #2 showed normal steady-state localization in the ER labeled with the ER marker, protein disulfide isomerase (PDI), colocalizing with the functional PSEN-1-GFP (Fig. 5-14). These PSEN-1-tDTomato constructs may be suitable for FRET analysis with the streptavidin-Qdot525 APP-AP1 construct.

MATERIALS AND METHODS

Antibodies and constructs

Mouse monoclonal antibodies used were anti-GFP (7.1 and 13.1, Roche), anti-Golgin 97 (CDF4, Life Technologies), anti-EEA1 (14, BD Transduction Laboratories), and anti-Actin (C4, MP Biomedicals). Rabbit polyclonal antibodies were anti-APP C-terminus (Sigma-Aldrich), anti-PDI (Santa Cruz Biotechnology) and anti-GFP (Torrey Pines). IRDye 680 and 800 secondary antibodies (LICOR) were used for immunoblotting analysis. Alexa Fluor 568 and 647-conjugated secondary antibodies (Life Technologies) were used for immunofluorescence microscopy. A 15-amino acid biotin acceptor peptide (AP) sequence, GLNDIFEAQKIEWHE, (Beckett et al., 1999; Schatz, 1993), was inserted within the Aβ region of full length APP in a pCI-neo mammalian expression vector (Promega) to generate the APP-AP1 construct. Two tandem repeats of AP tag, GLNDIFEAQKIEWHE, were inserted within the Aβ region of full length APP in pCI-neo to generate the APP-AP2 construct. Full length cDNA of human PSEN-1 was cloned into a pCMV-tdTomato mammalian expression vector (Clontech) for the expression of fusion proteins of tdTomato PSEN-1. The tdTomato tag was inserted into the first extracellular loop of PSEN-1 for constructs #1 and #2; the second extracellular loop for construct #3, and the fourth extracellular loop for construct #4.

In vitro biotinylation using recombinant BirA

Purification of recombinant GST-tagged BirA biotin ligase (BirA-GST) was performed as described (Tran et al., 2009). In vitro biotinylation was performed as described (Chen et al., 2005). Cells were transfected in 6-well plates with 3.5 μg of AP-tagged construct APP-AP1 using Lipofectamine 2000 (Life Technologies) in serum-free Opti-MEM (Life Technologies) for 24 h. Transfection media were replaced by complete media at 24 h post-transfection. At 48 h post-transfection, cells were washed gently with PBS pH 7.4 (Life Technologies) with 5 mM $MgCl_2$, and incubated with either 0.3 μM or 2 μM of recombinant BirA-GST, 1 mM ATP (Sigma-Aldrich), and 10 μM biotin (Avidity) in PBS for 90 min in a humidified incubator with 5% CO_2 at 37^{o}C. pDisplay BirA-ER and CFP-TM-AP constructs were gifts AY Ting from Massachusetts Institute of Technology (Chen et al., 2005). Cells were lysed for immunoblot analysis.

In vivo biotinylation by expression of BirA-ER

Cells were co-transfected in 6-well plates with 1.75 μg BirA-ER together with AP-tagged constructs, APP-AP1, APP-AP2, or CFP-AP-TM, using Lipofectamine 2000 (Life Technologies) in serum-free Opti-MEM (Life Technologies) for 24 h. At 24 h post-transfection, transfection media were replaced by complete media supplemented with 10 μM biotin. Cells were seeded on glass coverslips or imaging dishes for fluorescence microscopy in the following day, or lysed for immunoblot analysis at 48 h post-transfection.

Streptavidin uptake assay and fluorescence microscopy

In vivo biotinylation was performed as described by coexpressing both BirA-ER and APP-AP1 constructs. At 24 h post-transfection, cells were trypsinized and plated at 30%

confluent on poly-D-lysine hydrobromide (Sigma-Aldrich)-coated 0.17 mm Delta T dishes (Fisher Scientific) for live cell imaging, or on 25 mm glass coverslips for immunofluorescence analysis. A steptavidin uptake assay was performed based on previously described protocol (Chen et al., 2005) with modifications. Cells were washed with ice cold PBS 3 times on ice to remove any remaining biotin-containing media. Cells were incubated on ice for 30 min to slow down endocytosis and to accumulate APP-AP1 on the cell surface. After the pre-incubation, cells were incubated on ice with streptavidin-Alexa568 (Life Technologies) for 10 min in the dark. Unbound streptavidin-Alexa568 was removed by rinsing twice with ice cold PBS. For live cell imaging, 1.5 mL of imaging buffer (Phenol red-free DMEM/5% FBS/10 mM HEPES/GlutaMAX) pre-warmed to 37°C was added to streptavidin-labeled cells in the Delta T dishes (designated as time 0). Cells were maintained at constant temperature at 37°C by using placing the Delta T dishes in a Biotechs Delta T Controlled Culture Dish System (AutoMate Scientific) for controlled heating while imaging in real-time using a wide-field fluorescence microscope (AxioObserver Z1, Carl Zeiss). To express live Golgi marker GalNAc-T2-GFP in the cells, I added BacMam CellLight Golgi-GFP (Life Technologies) together with biotin to the cells at 24 h post-transfection. For immunofluorescence analysis of the uptake assay, pre-warmed complete culture media were added to streptavidin-labeled cells on coverslips (designated as time 0). Cells were incubated in a humidified incubator with 5% CO_2 at 37^{o}C, fixed at different time points, and analyzed by immunostaining of subcellular markers.

Co-uptake assay of cholera toxin subunit B or transferrin with streptavidin

Co-uptake of cholera toxin subunit B **(**CTxB) with streptavidin from the cell surface was done exactly as described in the streptavidin uptake assay, with an exception that CTxB-Alexa488 or CTxB-Alexa647 (Life Technologies) were first added to pre-cooled cells for 20 min before co-incubating with streptavidin-Alexa568 for additional 10 min. For transferrin (Tfn)/streptavidin co-uptake assays, cells were first starved in serum-free starving media (DMEM/BSA/10 mM HEPES/GlutaMAX) for 1 h in a humidified incubator with 5% CO_2 at 37^{o}C. Cells were washed and incubated on ice before cold binding as described in the streptavidin uptake assay, with an exception that Tfn-Alexa647 (Life Technologies) was first added to pre-cooled cells for 20 min before co-incubating with streptavidin-Alexa568 for additional 10 min.

ELISA, Protein Determination, and Immunoblotting

Experiments were done as described in the Materials and Methods of Chapter Two.

Immunofluorescence Microscopy and Quantification

Experiments were done as described in the Materials and Methods of Chapter Two.

Figure 5-1. Schematic illustration of APP uptake assay using APP tagged with biotin acceptor peptide sequence labeled by fluorescently-conjugated streptavidin. A 15-amino acid biotin acceptor peptide (AP) sequence was inserted into the extracellular exposed region of the Aβ sequence to generate the APP-AP construct. APP-AP and bacterial biotin ligase BirA were co-expressed in HEK293 cells, resulting in *in vivo* biotinylation of APP-AP. After cold binding of fluorescently-conjugated streptavidin to cell surface APP, internalization of streptavidin-labeled APP was initiated by shifting the temperature to 37^{o}C. The post-endocytic trafficking of APP is followed at different time points.

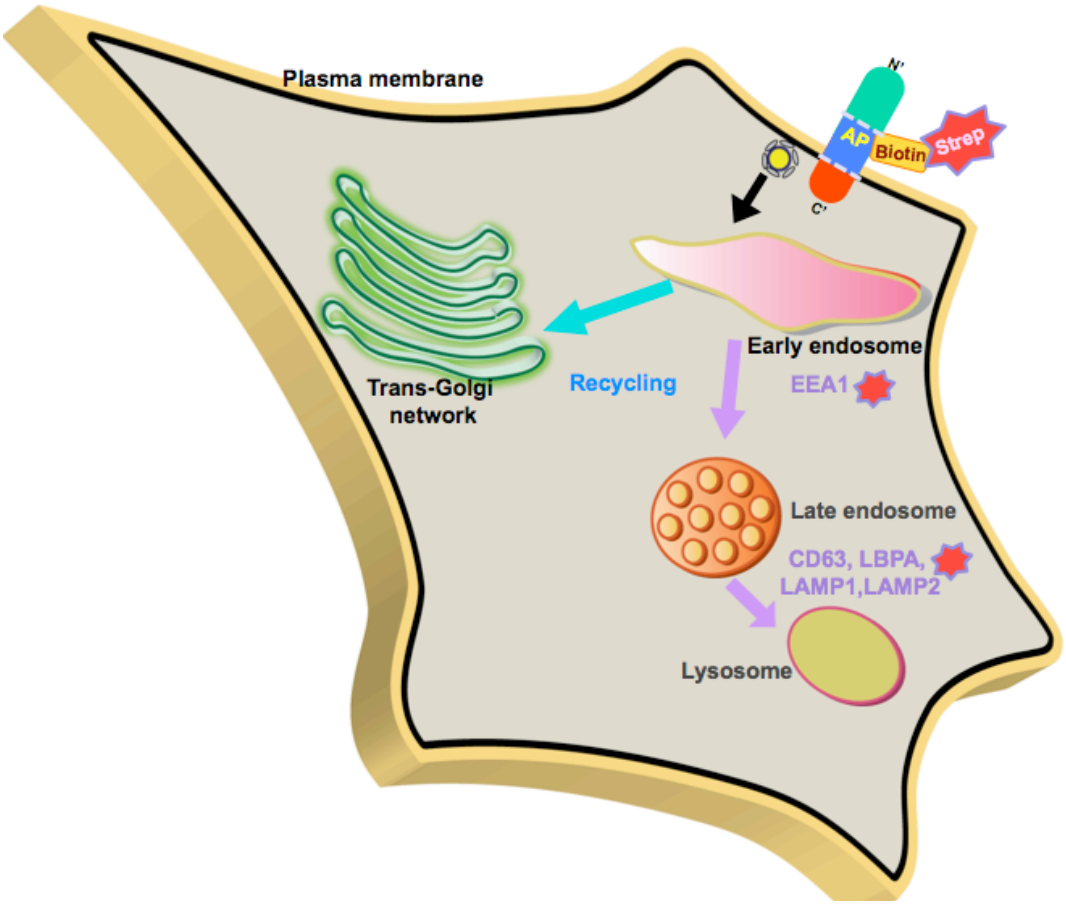
Plasma membrane
N'
AP
Biotin
Strep
C'
Early endosome
EEA1
Recycling
Trans-Golgi network
Late endosome
CD63, LBPA, LAMP1,LAMP2
Lysosome

Figure 5-2. ELISA analysis of $A\beta_{40}$ level in transiently transfected APP-AP cells. Culture media conditioned from 48 h post-transfection of empty vector control, wildtype APP (APP), and the AP-tagged APP constructs APP-AP1 and APP-AP2 were subjected to $A\beta_{40}$ ELISA analysis. Mock-transfected cells by Lipofectamine only were also included as a control.

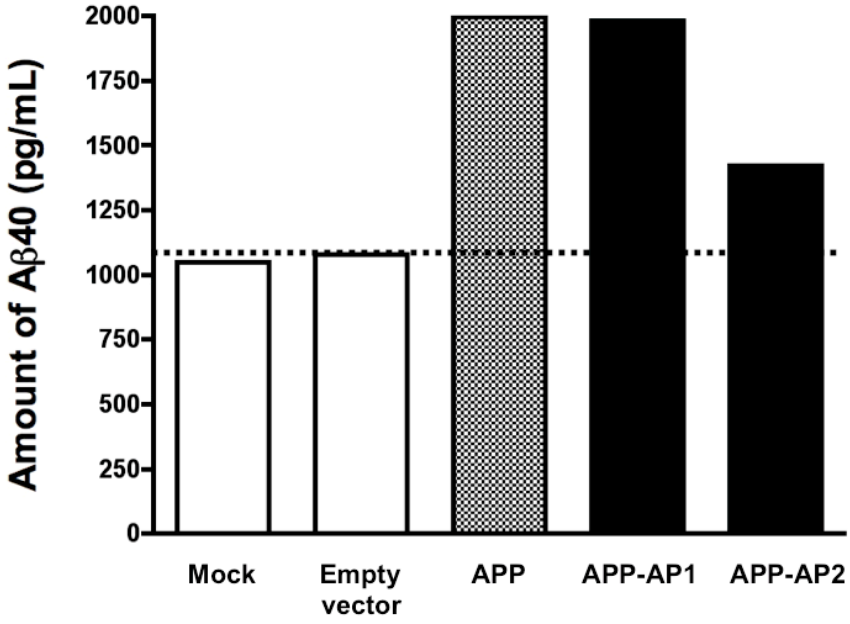
Amount of Aβ40 (pg/mL)
2000
1750
1500
1250
1000
750
500
250
0
Mock
Empty vector
APP
APP-AP1
APP-AP2

Figure 5-3. ***In vitro*** **biotinylation of APP-AP1 using recombinant BirA**. HEK293 cells transfected with APP-AP1 for 48 h were subjected to *in vitro* biotinylation using purified recombinant GST-tagged BirA (BirA-GST) at different concentrations in the absence or presence of additional biotin and ATP. The reaction was performed at 37^{o}C for 90 min. Cells were lysed at and proteins were analyzed by immunoblot.

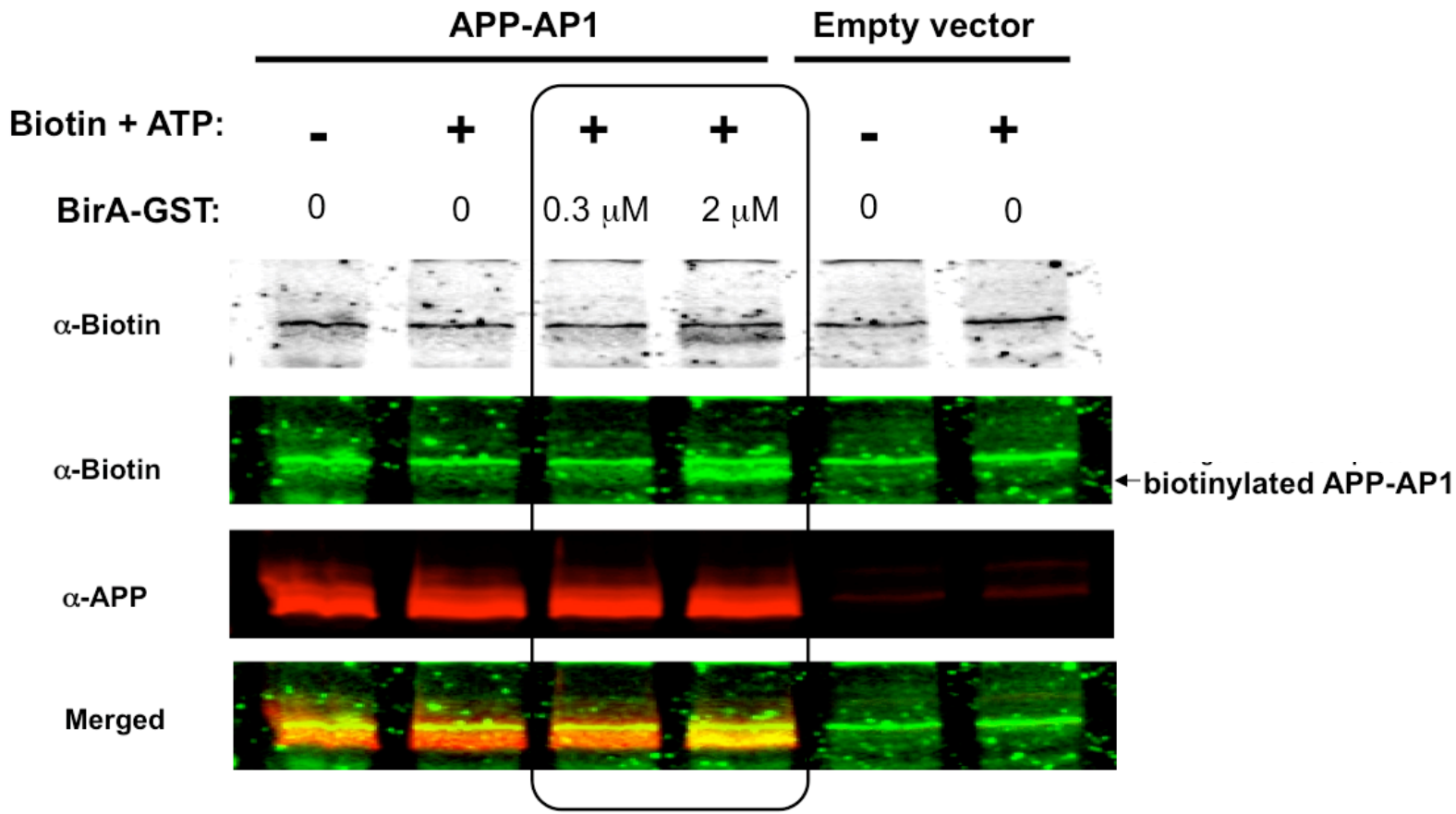
APP-AP1
Empty vector
Biotin + ATP:
- + + + - +
BirA-GST:
0 0 0.3 μM 2 μM 0 0
α-Biotin
α-Biotin
biotinylated APP-AP1
α-APP
Merged

Figure 5-4. ***In vivo*** **biotinylation of APP-AP1 and APP-AP2 by co-expressing BirA in the cells.** HEK293 cells were co-transfected with bacterial biotin ligase fused to a signal sequence and an ER retention signal (BirA-ER), together with wildtpe APP (APP), AP-tagged APP constructs APP-AP1 or APP-AP2, or the positive control CFP-TM-AP consisting of an AP sequence N-terminal to cyan fluorescent protein (CFP) fused to the transmembrane helix of platelet-derived growth factor receptor. At 24 h post-transfection, additional biotin was added to the culture media. Cells were lysed 48 h post-transfection, and proteins were analyzed by immunoblot.

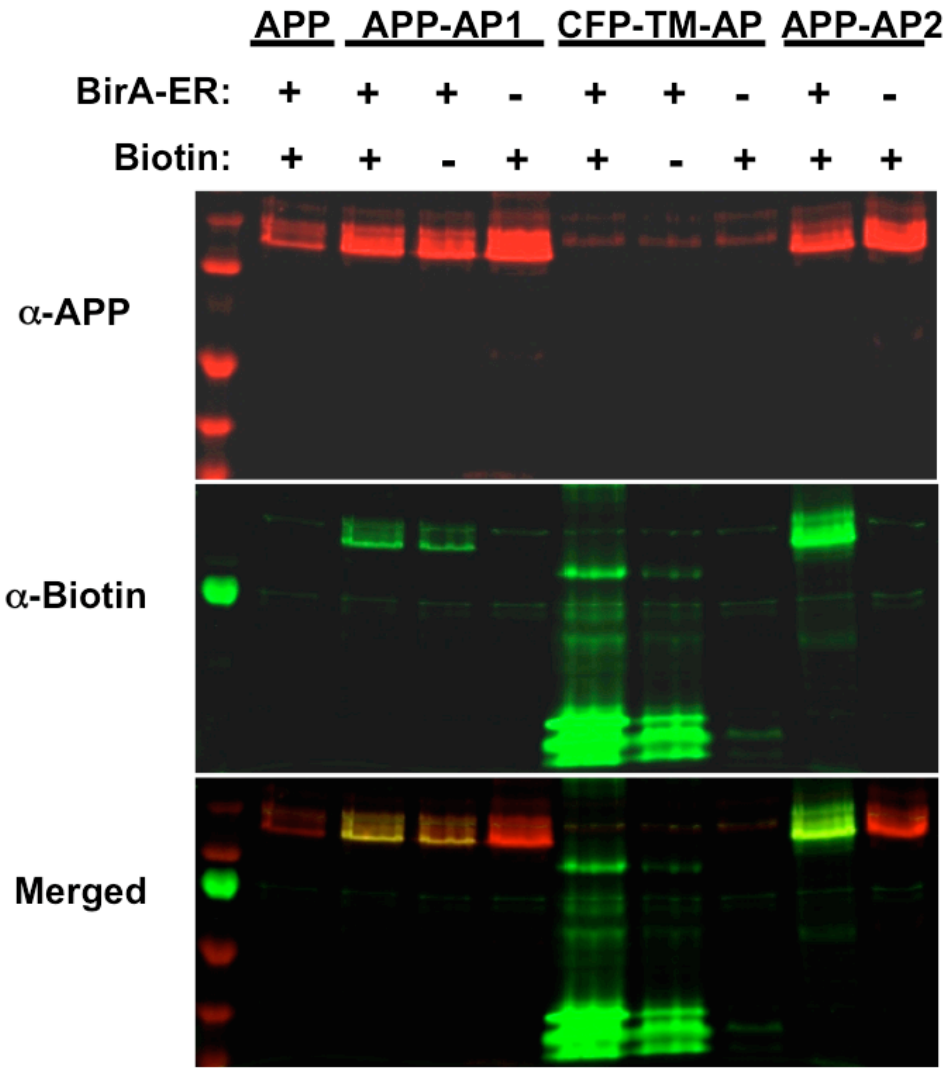
APP
APP-AP1
CFP-TM-AP
APP-AP2
BirA-ER: + + + - + + - + -
Biotin: + + - + + - + + +
α-APP
α-Biotin
Merged

Figure 5-5. Cell surface labeling of APP-AP1 with streptavidin-Qdot. HEK293 cells were co-transfected BirA-ER together with (A) APP-AP1 or (B) the positive control CFP-TM-AP. Cells without co-transfection of BirA-ER were used as negative controls to demonstrate the specificity of the labeling reaction. At 24 h post-transfection, additional biotin was added to the culture media. At 48 h post-transfection, pre-equilibrated cells were incubated with streptavidin-Qdot605 for 10 min at 4^{o}C (time 0). Unbound streptavidin-Qdot605 was washed off and labeled cells were then incubated at 37^{o}C for uptake to occur. Cells were fixed at different time points and analyzed by fluorescence microscopy. 2D deconvolved images were shown. Scale bars = 10 μm.

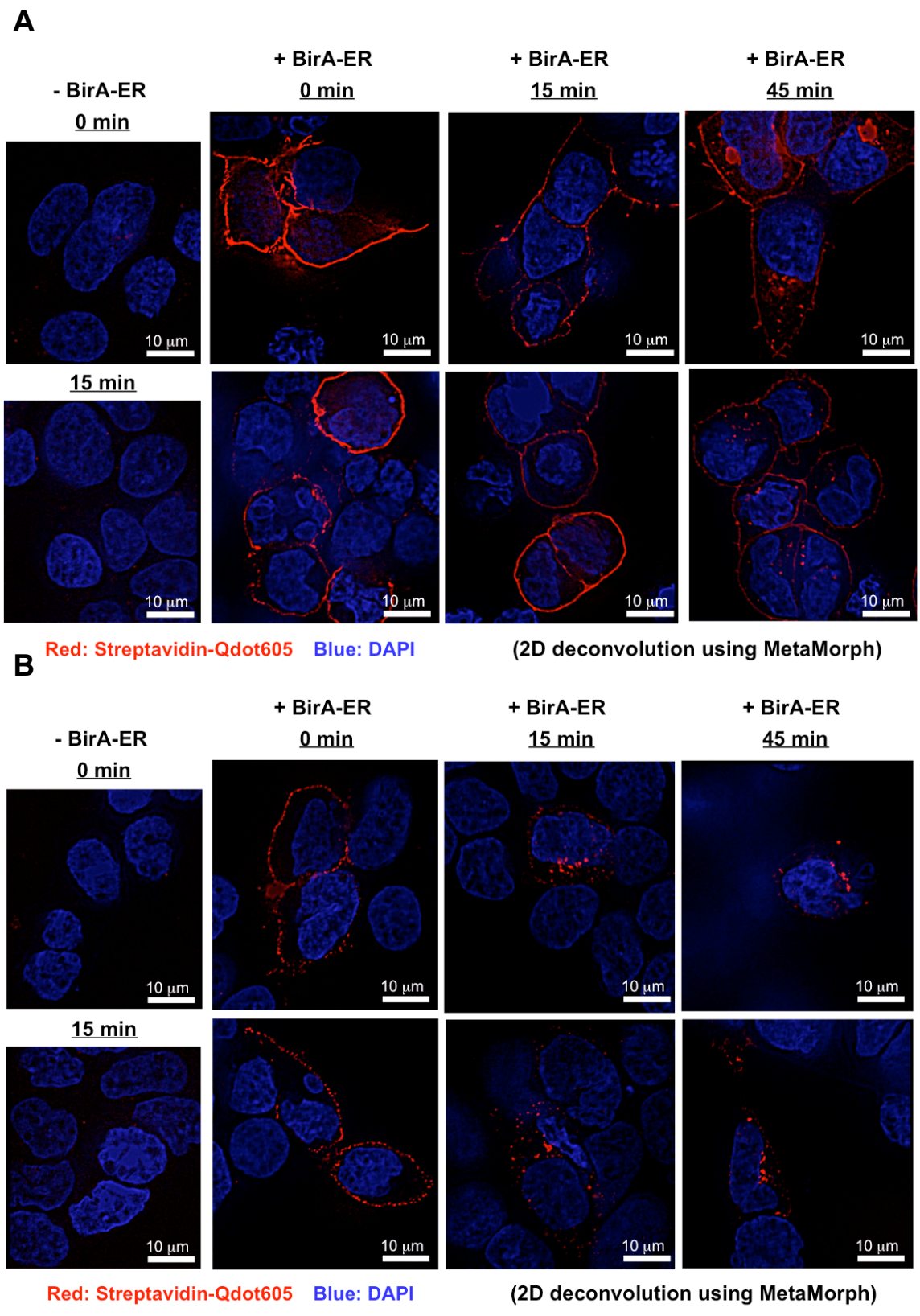
A
- BirA-ER
0 min
+ BirA-ER
0 min
+ BirA-ER
15 min
+ BirA-ER
45 min
15 min
10 μm
Red: Streptavidin-Qdot605 Blue: DAPI
(2D deconvolution using MetaMorph)
B
- BirA-ER
0 min
+ BirA-ER
0 min
+ BirA-ER
15 min
+ BirA-ER
45 min
15 min
10 μm
Red: Streptavidin-Qdot605 Blue: DAPI
(2D deconvolution using MetaMorph)

Figure 5-6. Live cell imaging of APP-AP1 uptake. HEK293 cells were co-transfected with BirA-ER and APP-AP1. At 24 h post-transfection, additional biotin was added to the culture media. At 48 h post-transfection, pre-equilibrated cells were incubated with streptavidin-Alexa568 for 10 min at 4^{o}C (time 0). Unbound streptavidin-Alexa568 was washed off, and fresh phenol red-free culture media was added to the cells to allow uptake at 37^{o}C in a temperature-controlled dish. Images were captured every minute in different cells. Scale bars = 10 μm.

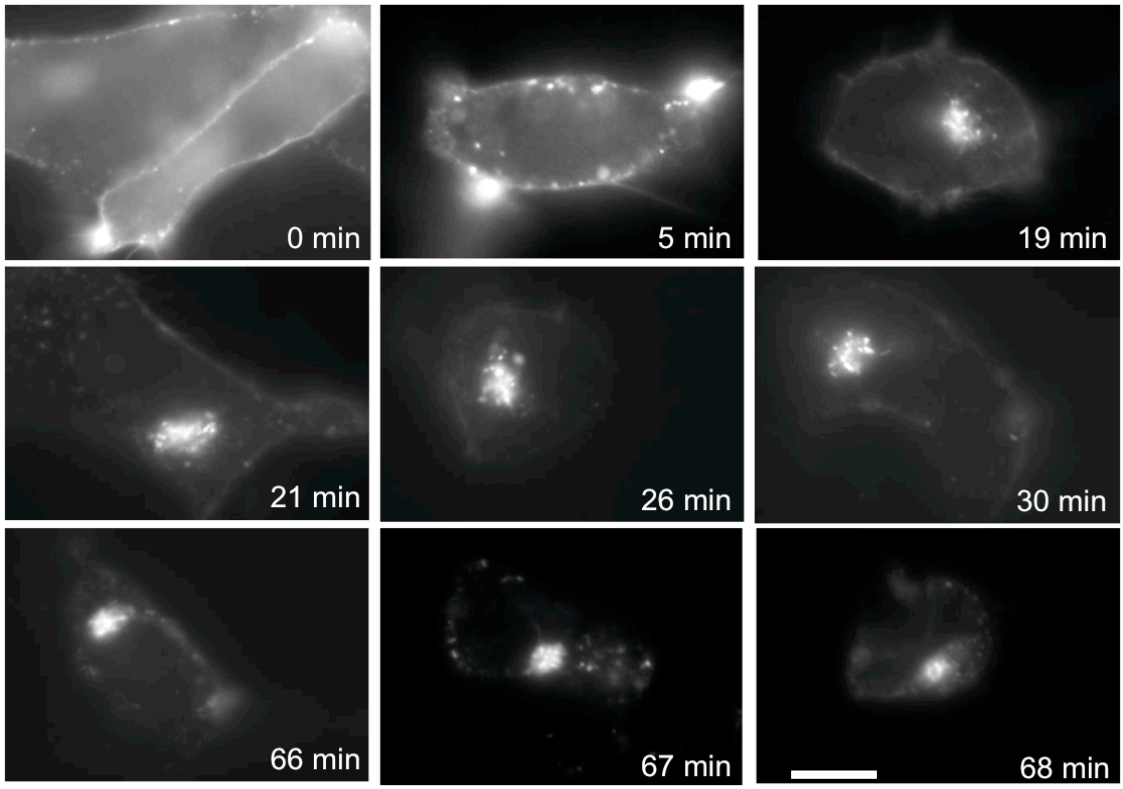
0 min
5 min
19 min
21 min
26 min
30 min
66 min
67 min
68 min

Figure 5-7. Live cell imaging of APP-AP1 and cholera toxin B subunit co-uptake. HEK293 cells were co-transfected with BirA-ER and APP-AP1. At 24 h post-transfection, additional biotin was added to the culture media. At 48 h post-transfection, pre-equilibrated cells were incubated at 4^{o}C first with CTxB-Alexa488 for 20min and then with streptavidin-Alexa568 for 10 min (time 0). Unbound CTxB-Alexa488 and streptavidin-Alexa568 was washed off and fresh phenol red-free culture media was added to the cell to allow uptake at 37^{o}C in a temperature-controlled dish. Images were captured at different time points after internalization.

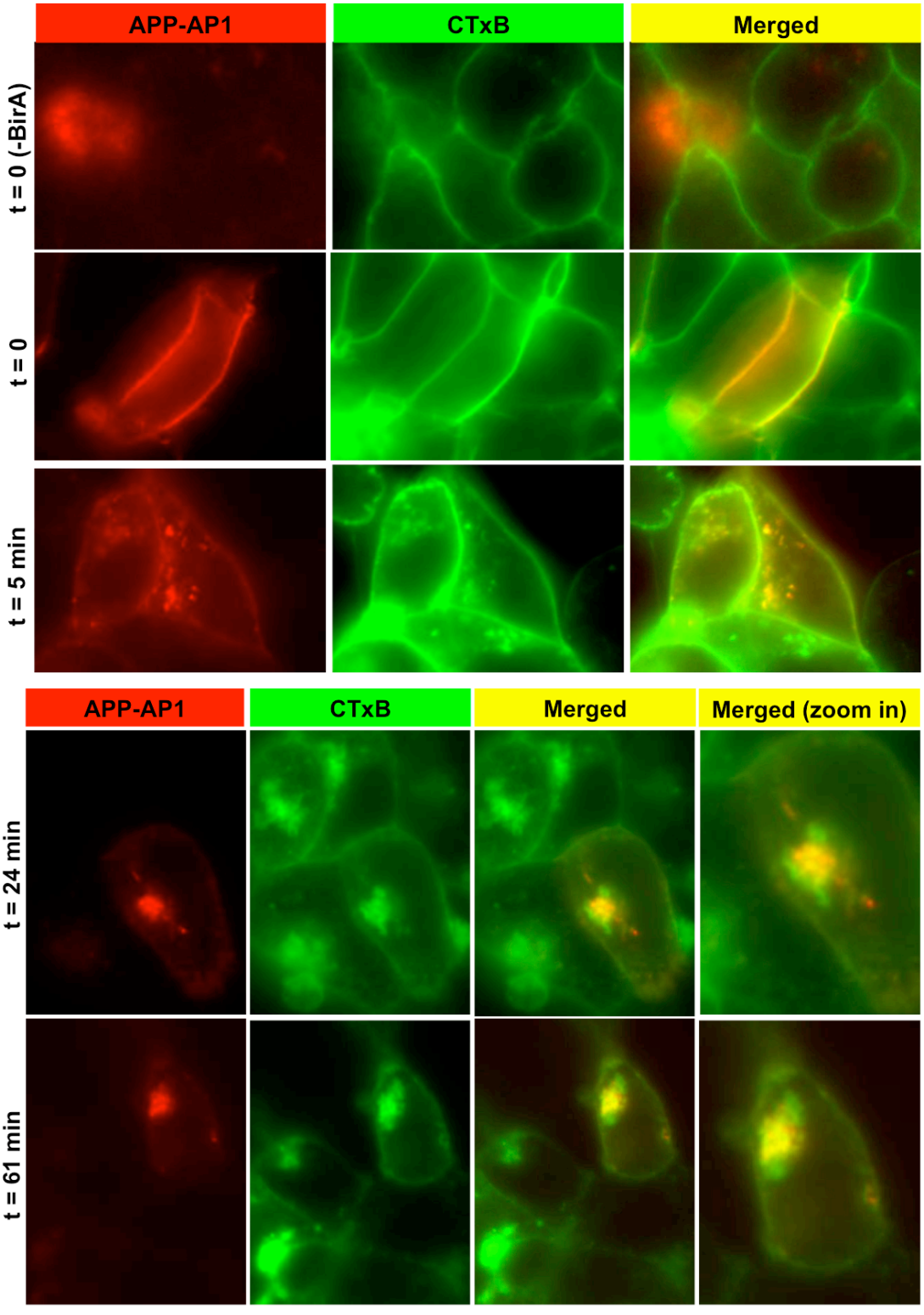
APP-AP1
CTxB
Merged
t = 0 (-BirA)
t = 0
t = 5 min
APP-AP1
CTxB
Merged
Merged (zoom in)
t = 24 min
t = 61 min

Figure 5-8. Live cell imaging of APP-AP1 and cholera toxin B subunit co-uptake and colocalization analysis with Golgi marker. HEK293 cells were co-transfected with BirA-ER and APP-AP1. At 24 h post-transfection, additional biotin and BacMam CellLight GalNAc-T2-GFP reagent were added to the culture media. At 48 h post-transfection, pre-equilibrated cells were incubated at 4^{o}C with CTxB-Alexa647 for 20 min and then with streptavidin-Alexa568 for 10 min (time 0). Unbound CTxB-Alexa488 and streptavidin-Alexa568 was washed off, and fresh phenol red-free culture media was added to the cells to allow uptake at 37^{o}C in a temperature-controlled dish. Representative images from time points of (A) 36 min and (B) 50 min post-internalization were shown.

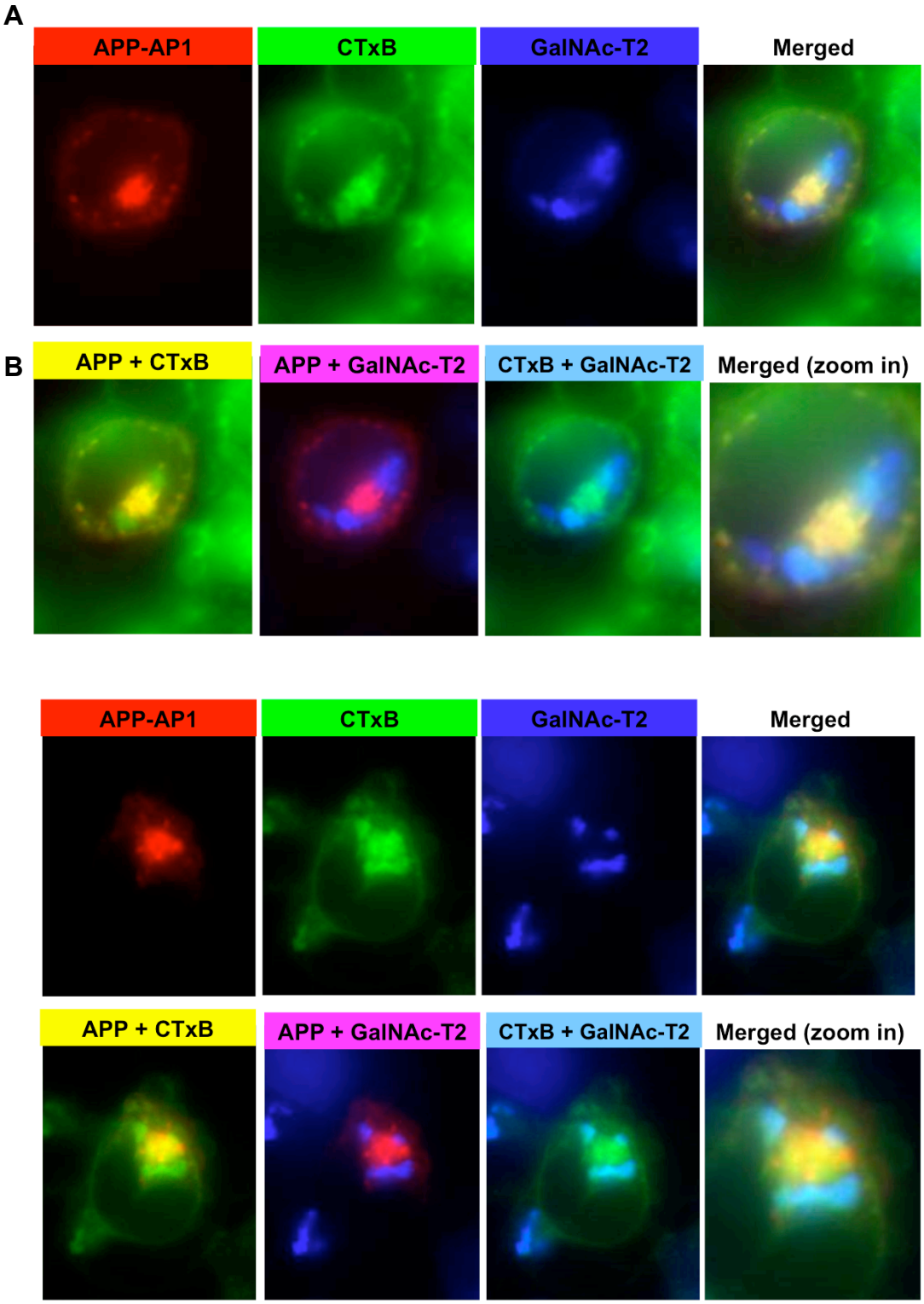
A
APP-AP1
CTxB
GalNAc-T2
Merged
B
APP + CTxB
APP + GalNAc-T2
CTxB + GalNAc-T2
Merged (zoom in)
APP-AP1
CTxB
GalNAc-T2
Merged
APP + CTxB
APP + GalNAc-T2
CTxB + GalNAc-T2
Merged (zoom in)

Figure 5-9. Live cell imaging of APP-AP1 and transferrin co-uptake and colocalization analysis with Golgi marker. HEK293 cells were co-transfected with BirA-ER and APP-AP1. At 24 h post-transfection, additional biotin and BacMam CellLight GalNAc-T2-GFP Golgi reagent were added to the culture media. At 48 h post-transfection, pre-equilibrated cells were incubated at 4^{o}C first with Tfn-Alexa647 for 20 min and then with streptavidin-Alexa568 for 10 min (time 0). Unbound CTxB-Alexa488 and streptavidin-Alexa568 was washed off, and fresh phenol red-free culture media was added to the cell to allow uptake at 37^{o}C in a temperature-controlled dish. Representative images from time points of (A) 32 min and (B) 41 min post-internalization are shown.

A

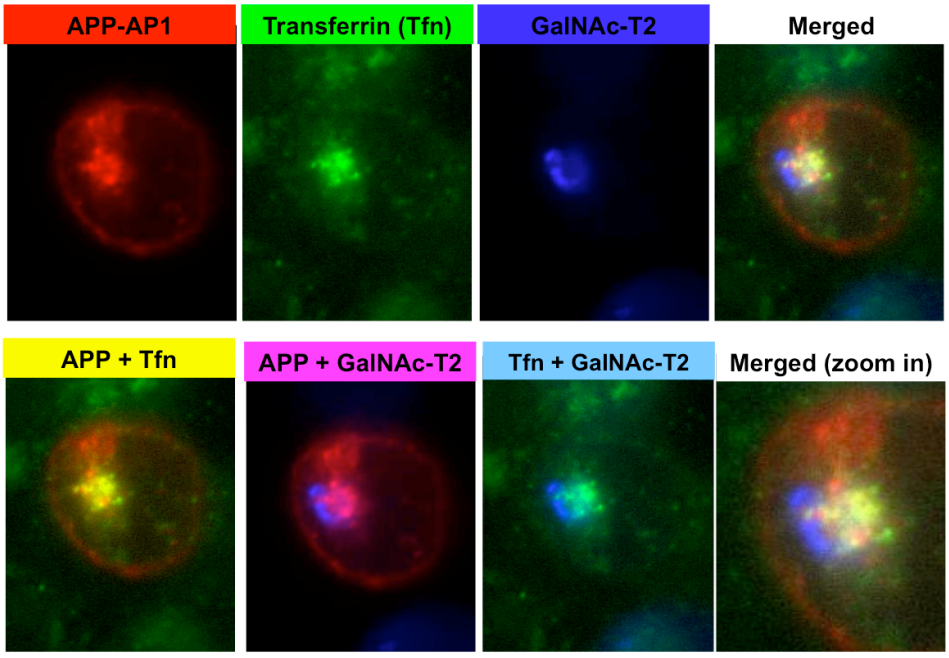
APP-AP1
Transferrin (Tfn)
GalNAc-T2
Merged
APP + Tfn
APP + GalNAc-T2
Tfn + GalNAc-T2
Merged (zoom in)

B

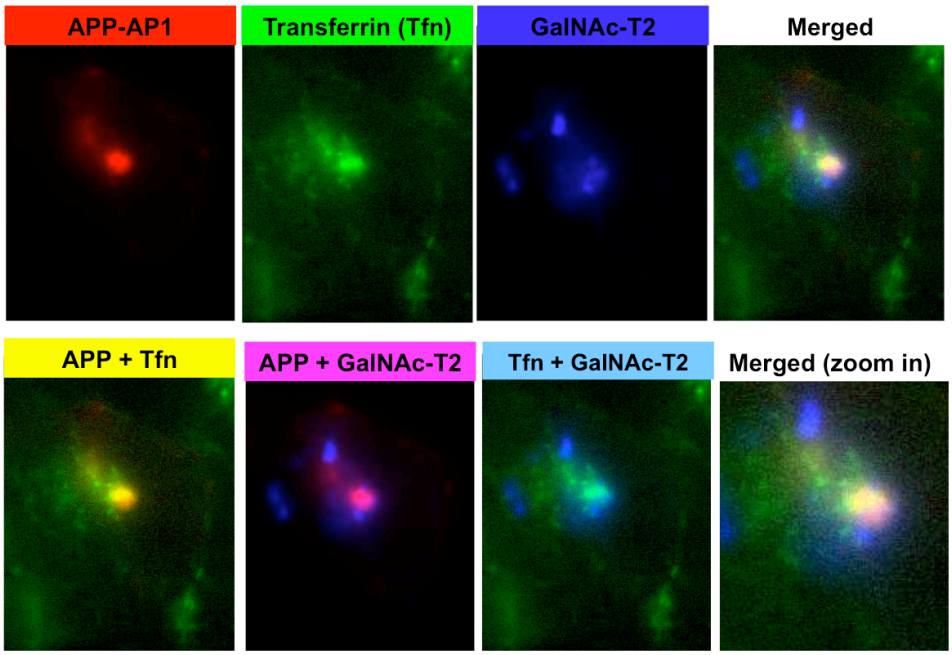
APP-AP1
Transferrin (Tfn)
GalNAc-T2
Merged
APP + Tfn
APP + GalNAc-T2
Tfn + GalNAc-T2
Merged (zoom in)

Figure 5-10. APP uptake assay in Hrs-depleted cells shows APP accumulation in enlarged early endosomes. HEK293 cells were transfected with pSUPER+GFP shRNA directed towards Hrs. At 72 h post-transfection, the cells were co-transfected with BirA-ER and APP-AP1 in a second round of transfection. At 120 h post-transfection of shRNA, pre-equilibrated cells were incubated at 4^{o}C with streptavidin-Alexa568 for 10 min. Unbound streptavidin-Alexa568 was washed off, and fresh culture media was added to the cells to allow uptake at 37^{o}C for 90 min. Cells were fixed and stained for the subcellular markers EEA1 or LAMP2. Because pSUPER+GFP vector co-expressed both the shRNA and GFP, GFP signals were used to indicate cells which cells experiences Hrs knockdown. Representative cells with GFP signals are shown. Merged 2D-deconvolved images were generated from the Alexa 568 channel (APP-AP1 signal indicated by red) and the Alexa 647 channel (EEA or LAMP2 signals indicated by green). Colocalization indicated by yellow. Scale bars = 10 μm.

HRSshRNA-GFP
Merged
EEA1
APP
HRSshRNA-GFP
Merged
LAMP2
APP

Figure 5-11. Flow chart showing the biochemical approach to isolate newly generated Aβ peptides from the cell surface APP uptake assay.

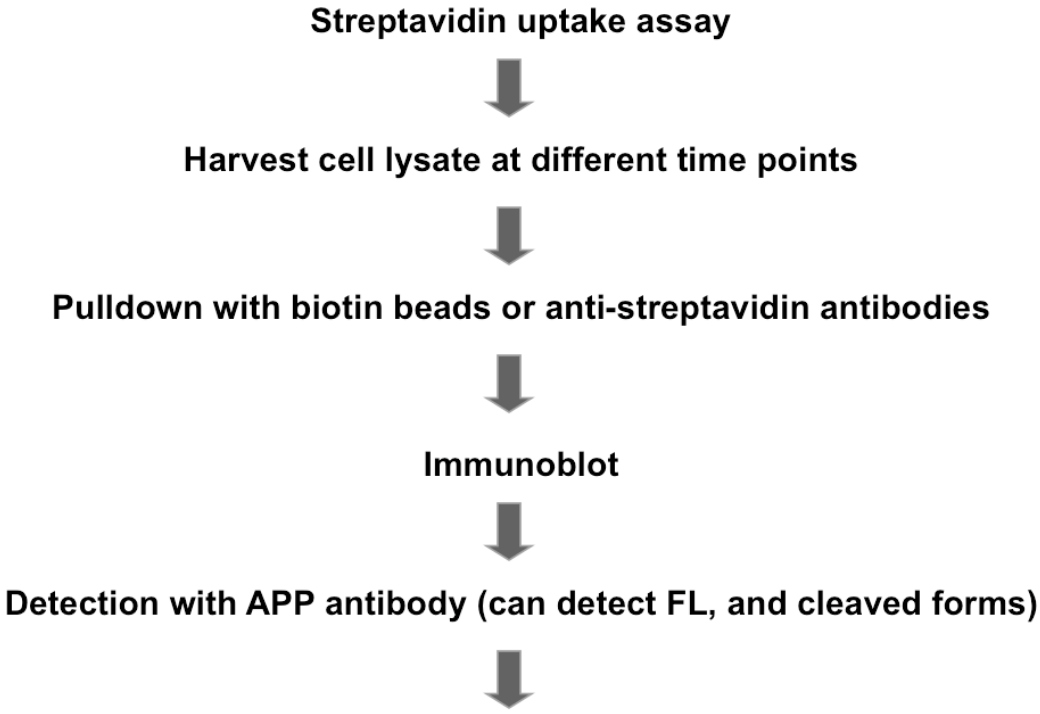
Streptavidin uptake assay
Harvest cell lysate at different time points
Pulldown with biotin beads or anti-streptavidin antibodies
Immunoblot
Detection with APP antibody (can detect FL, and cleaved forms)
Correlation of appearance of Aβ and imaging data

Figure 5-12. Schematic illustration of FRET analysis of APP and γ-secretase. Fluorescence resonance energy transfer (FRET) analysis may be used to detect a real-time interaction between endocytosed APP and the Aβ-generating γ-secretase complex. During the cell surface uptake assay, PSEN-1-tdTomato may form a good FRET acceptor-donor pair with streptavidin-Qdot525 APP=AP1 when they are in close proximity at the time of Aβ production.

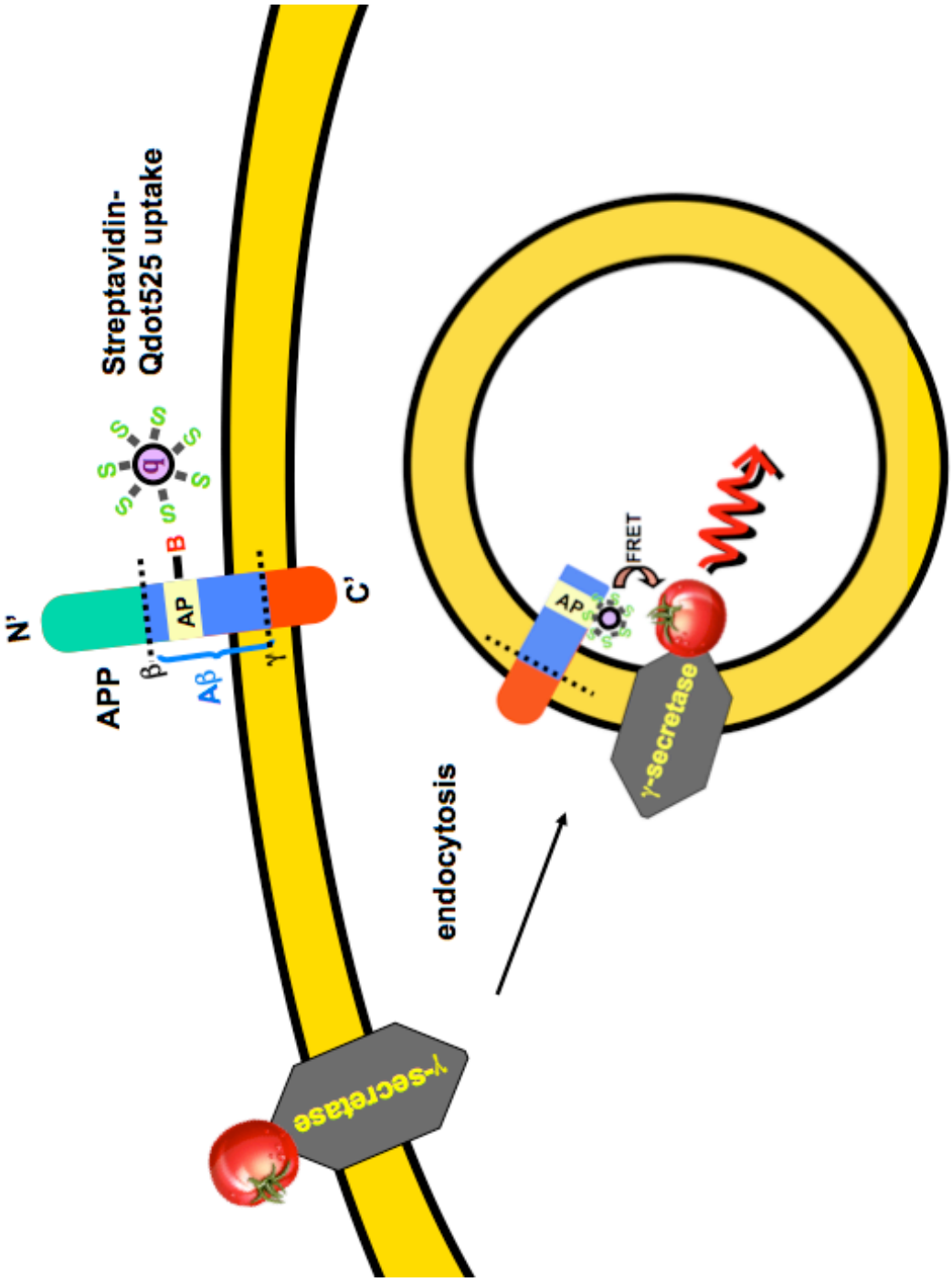
Streptavidin-
Qdot525 uptake
N'
C'
APP
AP
B
β
Aβ
γ
γ-secretase
endocytosis
FRET
AP
γ-secretase

Figure 5-13. Insertion of tdTomato tag within the extracellular loop of PSEN-1. (A) RFP-derived tdTomato tag was inserted into different extracellular loops of PSEN-1, constructs #1 and #2 in the first loop, #3 in the second loop, and #4 in the forth loop. (B) HEK293 cells were transfected with PSEN-1-tdTomato constructs. Cells were lysed 48 h post-transfection and proteins were analyzed by immunoblot. Full length (FL) and N-terminus fragment (NTF) of PSEN-1 were detected by PSEN-1 antibody recognizing the NTF.

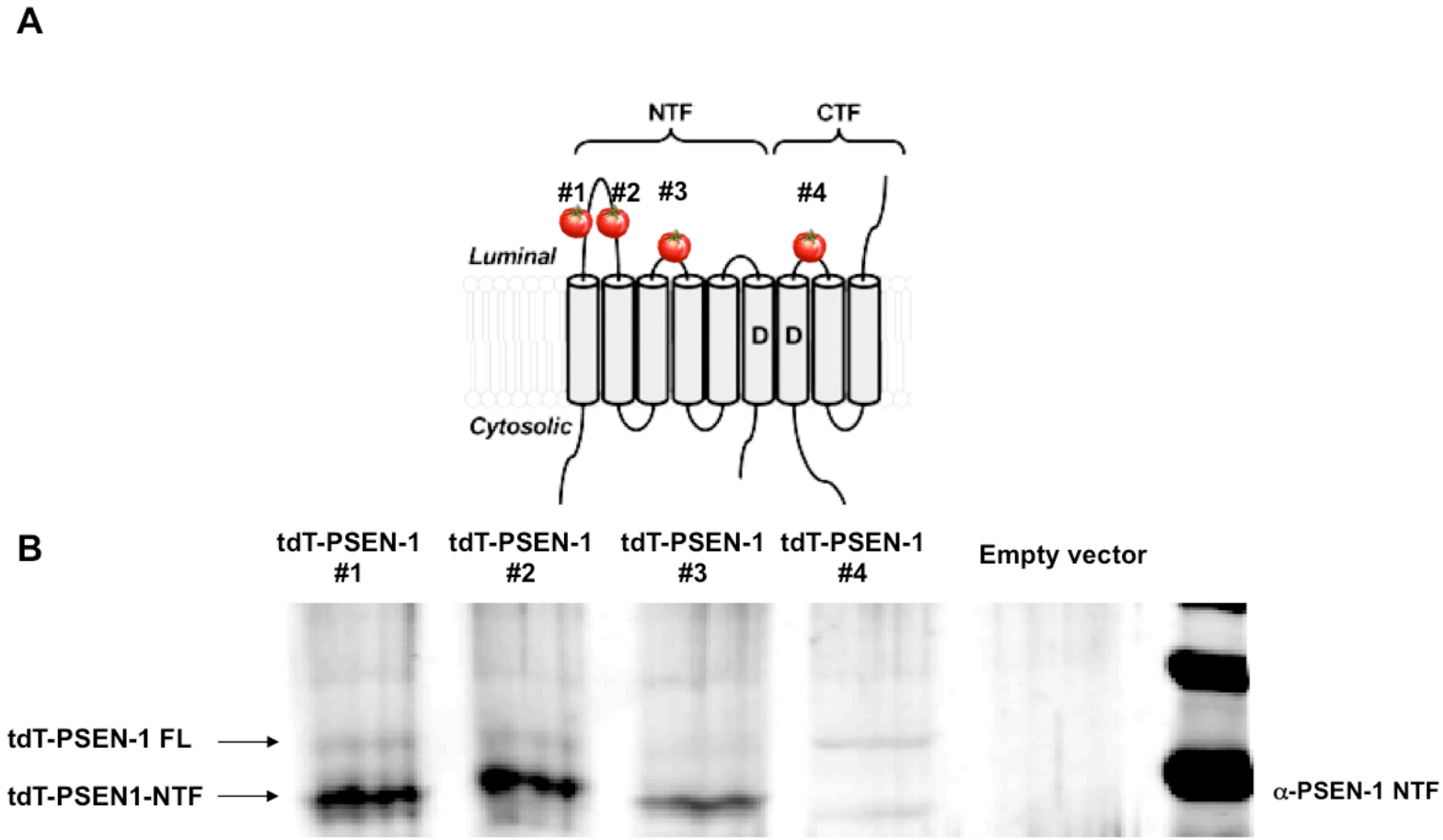
A
NTF
CTF
#1
#2
#3
#4
Luminal
Cytosolic
D
D
B
tdT-PSEN-1 #1
tdT-PSEN-1 #2
tdT-PSEN-1 #3
tdT-PSEN-1 #4
Empty vector
tdT-PSEN-1 FL
tdT-PSEN1-NTF
α-PSEN-1 NTF

Figure 5-14. PSEN-1-tdTomato localized normally in the ER. HEK293 cells were co-transfected with PSEN-1-GFP together with PSEN-1-tdTomato constructs #1 or #2. At 48 h post-transfection, cells were fixed and stained with PDI. Scale bars = 10 μm.

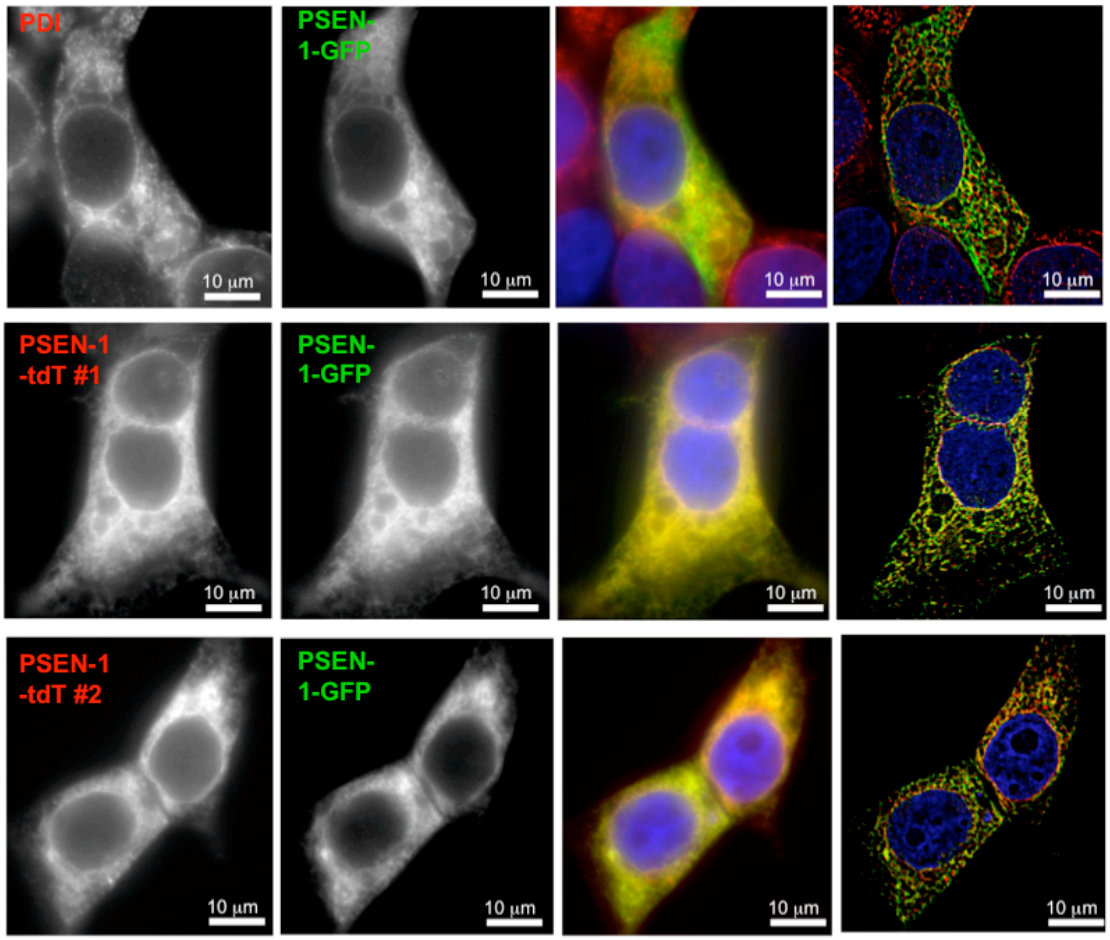
PDI
PSEN-1-GFP
PSEN-1-tdT #1
PSEN-1-GFP
PSEN-1-tdT #2
PSEN-1-GFP
10 µm

REFERENCES

Andersen, O.M., Reiche, J., Schmidt, V., Gotthardt, M., Spoelgen, R., Behlke, J., von Arnim, C.A., Breiderhoff, T., Jansen, P., Wu, X.*, et al.* (2005). Neuronal sorting protein-related receptor sorLA/LR11 regulates processing of the amyloid precursor protein. Proc Natl Acad Sci U S A *102*, 13461-13466.

Babst, M., Katzmann, D.J., Estepa-Sabal, E.J., Meerloo, T., and Emr, S.D. (2002). Escrt-III: an endosome-associated heterooligomeric protein complex required for mvb sorting. Dev Cell *3*, 271-282.

Bache, K.G., Raiborg, C., Mehlum, A., and Stenmark, H. (2003). STAM and Hrs are subunits of a multivalent ubiquitin-binding complex on early endosomes. J Biol Chem *278*, 12513-12521.

Barlowe, C., Orci, L., Yeung, T., Hosobuchi, M., Hamamoto, S., Salama, N., Rexach, M.F., Ravazzola, M., Amherdt, M., and Schekman, R. (1994). COPII: a membrane coat formed by Sec proteins that drive vesicle budding from the endoplasmic reticulum. Cell *77*, 895-907.

Beckett, D., Kovaleva, E., and Schatz, P.J. (1999). A minimal peptide substrate in biotin holoenzyme synthetase-catalyzed biotinylation. Protein Sci *8*, 921-929.

Bertrand, C.A., and Frizzell, R.A. (2003). The role of regulated CFTR trafficking in epithelial secretion. Am J Physiol Cell Physiol *285*, C1-18.

Boyadjiev, S.A., Fromme, J.C., Ben, J., Chong, S.S., Nauta, C., Hur, D.J., Zhang, G., Hamamoto, S., Schekman, R., Ravazzola, M.*, et al.* (2006). Cranio-lenticulo-sutural dysplasia is caused by a SEC23A mutation leading to abnormal endoplasmic-reticulum-to-Golgi trafficking. Nat Genet *38*, 1192-1197.

Burgos, P.V., Mardones, G.A., Rojas, A.L., daSilva, L.L., Prabhu, Y., Hurley, J.H., and Bonifacino, J.S. (2010). Sorting of the Alzheimer's disease amyloid precursor protein mediated by the AP-4 complex. Dev Cell *18*, 425-436.

Burns, A., Byrne, E.J., and Maurer, K. (2002). Alzheimer's disease. Lancet *360*, 163-165.

Buxbaum, J.D., Liu, K.N., Luo, Y., Slack, J.L., Stocking, K.L., Peschon, J.J., Johnson, R.S., Castner, B.J., Cerretti, D.P., and Black, R.A. (1998). Evidence that tumor necrosis factor alpha converting enzyme is involved in regulated alpha-secretase cleavage of the Alzheimer amyloid protein precursor. J Biol Chem *273*, 27765-27767.

Cai, H., Wang, Y., McCarthy, D., Wen, H., Borchelt, D.R., Price, D.L., and Wong, P.C. (2001). BACE1 is the major beta-secretase for generation of Abeta peptides by neurons. Nat Neurosci *4*, 233-234.

Carey, R.M., Balcz, B.A., Lopez-Coviella, I., and Slack, B.E. (2005). Inhibition of dynamin-dependent endocytosis increases shedding of the amyloid precursor protein ectodomain and reduces generation of amyloid beta protein. BMC Cell Biol *6*, 30.

Cartier, E.A., Conti, L.R., Vandenberg, C.A., and Shyng, S.L. (2001). Defective trafficking and function of KATP channels caused by a sulfonylurea receptor 1 mutation associated with persistent hyperinsulinemic hypoglycemia of infancy. Proc Natl Acad Sci U S A *98*, 2882-2887.

Chapman-Smith, A., and Cronan, J.E., Jr. (1999). In vivo enzymatic protein biotinylation. Biomol Eng *16*, 119-125.

Chen, I., Howarth, M., Lin, W., and Ting, A.Y. (2005). Site-specific labeling of cell surface proteins with biophysical probes using biotin ligase. Nat Methods *2*, 99-104.

Chinnapen, D.J., Chinnapen, H., Saslowsky, D., and Lencer, W.I. (2007). Rafting with cholera toxin: endocytosis and trafficking from plasma membrane to ER. FEMS Microbiol Lett *266*, 129-137.

Citron, M., Oltersdorf, T., Haass, C., McConlogue, L., Hung, A.Y., Seubert, P., Vigo-Pelfrey, C., Lieberburg, I., and Selkoe, D.J. (1992). Mutation of the beta-amyloid precursor protein in familial Alzheimer's disease increases beta-protein production. Nature *360*, 672-674.

Cruts, M., and Van Broeckhoven, C. (1998a). Molecular genetics of Alzheimer's disease. Ann Med *30*, 560-565.

Cruts, M., and Van Broeckhoven, C. (1998b). Presenilin mutations in Alzheimer's disease. Hum Mutat *11*, 183-190.

Cupers, P., Bentahir, M., Craessaerts, K., Orlans, I., Vanderstichele, H., Saftig, P., De Strooper, B., and Annaert, W. (2001). The discrepancy between presenilin subcellular localization and gamma-secretase processing of amyloid precursor protein. J Cell Biol *154*, 731-740.

Dautry-Varsat, A. (1986). Receptor-mediated endocytosis: the intracellular journey of transferrin and its receptor. Biochimie *68*, 375-381.

de Boer, E., Rodriguez, P., Bonte, E., Krijgsveld, J., Katsantoni, E., Heck, A., Grosveld, F., and Strouboulis, J. (2003). Efficient biotinylation and single-step purification of tagged transcription factors in mammalian cells and transgenic mice. Proc Natl Acad Sci U S A *100*, 7480-7485.

De Strooper, B., Saftig, P., Craessaerts, K., Vanderstichele, H., Guhde, G., Annaert, W., Von Figura, K., and Van Leuven, F. (1998). Deficiency of presenilin-1 inhibits the normal cleavage of amyloid precursor protein. Nature *391*, 387-390.

Dennis, A.M., and Bao, G. (2008). Quantum dot-fluorescent protein pairs as novel fluorescence resonance energy transfer probes. Nano Lett *8*, 1439-1445.

Deretic, D., Williams, A.H., Ransom, N., Morel, V., Hargrave, P.A., and Arendt, A. (2005). Rhodopsin C terminus, the site of mutations causing retinal disease, regulates trafficking by binding to ADP-ribosylation factor 4 (ARF4). Proc Natl Acad Sci U S A *102*, 3301-3306.

Doyotte, A., Russell, M.R., Hopkins, C.R., and Woodman, P.G. (2005). Depletion of TSG101 forms a mammalian "Class E" compartment: a multicisternal early endosome with multiple sorting defects. J Cell Sci *118*, 3003-3017.

Fliegauf, M., Benzing, T., and Omran, H. (2007). When cilia go bad: cilia defects and ciliopathies. Nat Rev Mol Cell Biol *8*, 880-893.

Fromme, J.C., Ravazzola, M., Hamamoto, S., Al-Balwi, M., Eyaid, W., Boyadjiev, S.A., Cosson, P., Schekman, R., and Orci, L. (2007). The genetic basis of a craniofacial disease provides insight into COPII coat assembly. Dev Cell *13*, 623-634.

Ganley, I.G., Espinosa, E., and Pfeffer, S.R. (2008). A syntaxin 10-SNARE complex distinguishes two distinct transport routes from endosomes to the trans-Golgi in human cells. J Cell Biol *180*, 159-172.

Hardy, J., and Selkoe, D.J. (2002). The amyloid hypothesis of Alzheimer's disease: progress and problems on the road to therapeutics. Science *297*, 353-356.

Hardy, J.A., and Higgins, G.A. (1992). Alzheimer's disease: the amyloid cascade hypothesis. Science *256*, 184-185.

Harold, D., Abraham, R., Hollingworth, P., Sims, R., Gerrish, A., Hamshere, M.L., Pahwa, J.S., Moskvina, V., Dowzell, K., Williams, A.*, et al.* (2009). Genome-wide association study identifies variants at CLU and PICALM associated with Alzheimer's disease. Nat Genet *41*, 1088-1093.

Henne, W.M., Buchkovich, N.J., and Emr, S.D. (2011). The ESCRT pathway. Dev Cell *21*, 77-91.

Hollingworth, P., Harold, D., Sims, R., Gerrish, A., Lambert, J.C., Carrasquillo, M.M., Abraham, R., Hamshere, M.L., Pahwa, J.S., Moskvina, V.*, et al.* (2011). Common variants at ABCA7, MS4A6A/MS4A4E, EPHA1, CD33 and CD2AP are associated with Alzheimer's disease. Nat Genet *43*, 429-435.

Hopkins, C.R., and Trowbridge, I.S. (1983). Internalization and processing of transferrin and the transferrin receptor in human carcinoma A431 cells. J Cell Biol *97*, 508-521.

Howarth, M., Takao, K., Hayashi, Y., and Ting, A.Y. (2005). Targeting quantum dots to surface proteins in living cells with biotin ligase. Proc Natl Acad Sci U S A *102*, 7583-7588.

Hurley, J.H., and Hanson, P.I. (2010). Membrane budding and scission by the ESCRT machinery: it's all in the neck. Nat Rev Mol Cell Biol *11*, 556-566.

Huse, J.T., Pijak, D.S., Leslie, G.J., Lee, V.M., and Doms, R.W. (2000). Maturation and endosomal targeting of beta-site amyloid precursor protein-cleaving enzyme. The Alzheimer's disease beta-secretase. J Biol Chem *275*, 33729-33737.

Jensen, D., and Schekman, R. (2011). COPII-mediated vesicle formation at a glance. J Cell Sci *124*, 1-4.

Jin, H., White, S.R., Shida, T., Schulz, S., Aguiar, M., Gygi, S.P., Bazan, J.F., and Nachury, M.V. (2010). The conserved Bardet-Biedl syndrome proteins assemble a coat that traffics membrane proteins to cilia. Cell *141*, 1208-1219.

Jones, B., Jones, E.L., Bonney, S.A., Patel, H.N., Mensenkamp, A.R., Eichenbaum-Voline, S., Rudling, M., Myrdal, U., Annesi, G., Naik, S.*, et al.* (2003). Mutations in a Sar1 GTPase of COPII vesicles are associated with lipid absorption disorders. Nat Genet *34*, 29-31.

Kaether, C., Haass, C., and Steiner, H. (2006). Assembly, trafficking and function of gamma-secretase. Neurodegener Dis *3*, 275-283.

Kang, J., Lemaire, H.G., Unterbeck, A., Salbaum, J.M., Masters, C.L., Grzeschik, K.H., Multhaup, G., Beyreuther, K., and Muller-Hill, B. (1987). The precursor of Alzheimer's disease amyloid A4 protein resembles a cell-surface receptor. Nature *325*, 733-736.

Karten, B., Peake, K.B., and Vance, J.E. (2009). Mechanisms and consequences of impaired lipid trafficking in Niemann-Pick type C1-deficient mammalian cells. Biochim Biophys Acta *1791*, 659-670.

Kehoe, P.G., Russ, C., McIlory, S., Williams, H., Holmans, P., Holmes, C., Liolitsa, D., Vahidassr, D., Powell, J., McGleenon, B.*, et al.* (1999). Variation in DCP1, encoding ACE, is associated with susceptibility to Alzheimer disease. Nat Genet *21*, 71-72.

Kim, J., Hamamoto, S., Ravazzola, M., Orci, L., and Schekman, R. (2005). Uncoupled packaging of amyloid precursor protein and presenilin 1 into coat protein complex II vesicles. J Biol Chem *280*, 7758-7768.

Kim, J., Kleizen, B., Choy, R., Thinakaran, G., Sisodia, S.S., and Schekman, R.W. (2007). Biogenesis of gamma-secretase early in the secretory pathway. J Cell Biol *179*, 951-963.

Kinoshita, A., Fukumoto, H., Shah, T., Whelan, C.M., Irizarry, M.C., and Hyman, B.T. (2003). Demonstration by FRET of BACE interaction with the amyloid precursor protein at the cell surface and in early endosomes. J Cell Sci *116*, 3339-3346.

Kollmann, K., Pohl, S., Marschner, K., Encarnacao, M., Sakwa, I., Tiede, S., Poorthuis, B.J., Lubke, T., Muller-Loennies, S., Storch, S.*, et al.* (2010). Mannose phosphorylation in health and disease. Eur J Cell Biol *89*, 117-123.

LaFerla, F.M. (2002). Calcium dyshomeostasis and intracellular signalling in Alzheimer's disease. Nat Rev Neurosci *3*, 862-872.

Lambert, J.C., Heath, S., Even, G., Campion, D., Sleegers, K., Hiltunen, M., Combarros, O., Zelenika, D., Bullido, M.J., Tavernier, B.*, et al.* (2009). Genome-wide association study identifies variants at CLU and CR1 associated with Alzheimer's disease. Nat Genet *41*, 1094-1099.

Langelier, C., von Schwedler, U.K., Fisher, R.D., De Domenico, I., White, P.L., Hill, C.P., Kaplan, J., Ward, D., and Sundquist, W.I. (2006). Human ESCRT-II complex and its role in human immunodeficiency virus type 1 release. J Virol *80*, 9465-9480.

Laudon, H., Hansson, E.M., Melen, K., Bergman, A., Farmery, M.R., Winblad, B., Lendahl, U., von Heijne, G., and Naslund, J. (2005). A nine-transmembrane domain topology for presenilin 1. J Biol Chem *280*, 35352-35360.

Lee, V.M., Balin, B.J., Otvos, L., Jr., and Trojanowski, J.Q. (1991). A68: a major subunit of paired helical filaments and derivatized forms of normal Tau. Science *251*, 675-678.

Levy-Lahad, E., Wasco, W., Poorkaj, P., Romano, D.M., Oshima, J., Pettingell, W.H., Yu, C.E., Jondro, P.D., Schmidt, S.D., Wang, K.*, et al.* (1995). Candidate gene for the chromosome 1 familial Alzheimer's disease locus. Science *269*, 973-977.

Lin, X., Koelsch, G., Wu, S., Downs, D., Dashti, A., and Tang, J. (2000). Human aspartic protease memapsin 2 cleaves the beta-secretase site of beta-amyloid precursor protein. Proc Natl Acad Sci U S A *97*, 1456-1460.

Liou, W., Geuze, H.J., and Slot, J.W. (1996). Improving structural integrity of cryosections for immunogold labeling. Histochem Cell Biol *106*, 41-58.

Ludwig, M., Doroszewicz, J., Seyberth, H.W., Bokenkamp, A., Balluch, B., Nuutinen, M., Utsch, B., and Waldegger, S. (2005). Functional evaluation of Dent's disease-causing mutations: implications for ClC-5 channel trafficking and internalization. Hum Genet *117*, 228-237.

Luo, Y., Bolon, B., Kahn, S., Bennett, B.D., Babu-Khan, S., Denis, P., Fan, W., Kha, H., Zhang, J., Gong, Y.*, et al.* (2001). Mice deficient in BACE1, the Alzheimer's beta-

secretase, have normal phenotype and abolished beta-amyloid generation. Nat Neurosci *4*, 231-232.

Lutsenko, S., and Petris, M.J. (2003). Function and regulation of the mammalian copper-transporting ATPases: insights from biochemical and cell biological approaches. J Membr Biol *191*, 1-12.

Ma, J., Yee, A., Brewer, H.B., Jr., Das, S., and Potter, H. (1994). Amyloid-associated proteins alpha 1-antichymotrypsin and apolipoprotein E promote assembly of Alzheimer beta-protein into filaments. Nature *372*, 92-94.

Mahley, R.W., and Rall, S.C., Jr. (2000). Apolipoprotein E: far more than a lipid transport protein. Annu Rev Genomics Hum Genet *1*, 507-537.

Matsuoka, K., Morimitsu, Y., Uchida, K., and Schekman, R. (1998). Coat assembly directs v-SNARE concentration into synthetic COPII vesicles. Mol Cell *2*, 703-708.

Mayle, K.M., Le, A.M., and Kamei, D.T. (2011). The intracellular trafficking pathway of transferrin. Biochim Biophys Acta.

Mellman, I., and Nelson, W.J. (2008). Coordinated protein sorting, targeting and distribution in polarized cells. Nat Rev Mol Cell Biol *9*, 833-845.

Merte, J., Jensen, D., Wright, K., Sarsfield, S., Wang, Y., Schekman, R., and Ginty, D.D. (2010). Sec24b selectively sorts Vangl2 to regulate planar cell polarity during neural tube closure. Nat Cell Biol *12*, 41-46; sup pp 41-48.

Montesano, R., Roth, J., Robert, A., and Orci, L. (1982). Non-coated membrane invaginations are involved in binding and internalization of cholera and tetanus toxins. Nature *296*, 651-653.

Ni, Y., Zhao, X., Bao, G., Zou, L., Teng, L., Wang, Z., Song, M., Xiong, J., Bai, Y., and Pei, G. (2006). Activation of beta2-adrenergic receptor stimulates gamma-secretase activity and accelerates amyloid plaque formation. Nat Med *12*, 1390-1396.

Nichols, B.J. (2002). A distinct class of endosome mediates clathrin-independent endocytosis to the Golgi complex. Nat Cell Biol *4*, 374-378.

O'Brien, R.J., and Wong, P.C. (2011). Amyloid precursor protein processing and Alzheimer's disease. Annu Rev Neurosci *34*, 185-204.

Offe, K., Dodson, S.E., Shoemaker, J.T., Fritz, J.J., Gearing, M., Levey, A.I., and Lah, J.J. (2006). The lipoprotein receptor LR11 regulates amyloid beta production and amyloid precursor protein traffic in endosomal compartments. J Neurosci *26*, 1596-1603.

Perez, R.G., Soriano, S., Hayes, J.D., Ostaszewski, B., Xia, W., Selkoe, D.J., Chen, X., Stokin, G.B., and Koo, E.H. (1999). Mutagenesis identifies new signals for beta-amyloid precursor protein endocytosis, turnover, and the generation of secreted fragments, including Abeta42. J Biol Chem *274*, 18851-18856.

Pericak-Vance, M.A., Bebout, J.L., Gaskell, P.C., Jr., Yamaoka, L.H., Hung, W.Y., Alberts, M.J., Walker, A.P., Bartlett, R.J., Haynes, C.A., Welsh, K.A.*, et al.* (1991). Linkage studies in familial Alzheimer disease: evidence for chromosome 19 linkage. Am J Hum Genet *48*, 1034-1050.

Pfeffer, S.R. (2009). Multiple routes of protein transport from endosomes to the trans Golgi network. FEBS Lett *583*, 3811-3816.

Puertollano, R., Aguilar, R.C., Gorshkova, I., Crouch, R.J., and Bonifacino, J.S. (2001). Sorting of mannose 6-phosphate receptors mediated by the GGAs. Science *292*, 1712-1716.

Razi, M., and Futter, C.E. (2006). Distinct roles for Tsg101 and Hrs in multivesicular body formation and inward vesiculation. Mol Biol Cell *17*, 3469-3483.

Rogaeva, E., Meng, Y., Lee, J.H., Gu, Y., Kawarai, T., Zou, F., Katayama, T., Baldwin, C.T., Cheng, R., Hasegawa, H.*, et al.* (2007). The neuronal sortilin-related receptor SORL1 is genetically associated with Alzheimer disease. Nat Genet *39*, 168-177.

Sandvig, K., and van Deurs, B. (2002). Transport of protein toxins into cells: pathways used by ricin, cholera toxin and Shiga toxin. FEBS Lett *529*, 49-53.

Sato, C., Takagi, S., Tomita, T., and Iwatsubo, T. (2008). The C-terminal PAL motif and transmembrane domain 9 of presenilin 1 are involved in the formation of the catalytic pore of the gamma-secretase. J Neurosci *28*, 6264-6271.

Schatz, P.J. (1993). Use of peptide libraries to map the substrate specificity of a peptide-modifying enzyme: a 13 residue consensus peptide specifies biotinylation in Escherichia coli. Biotechnology (N Y) *11*, 1138-1143.

Scheuner, D., Eckman, C., Jensen, M., Song, X., Citron, M., Suzuki, N., Bird, T.D., Hardy, J., Hutton, M., Kukull, W.*, et al.* (1996). Secreted amyloid beta-protein similar to that in the senile plaques of Alzheimer's disease is increased in vivo by the presenilin 1 and 2 and APP mutations linked to familial Alzheimer's disease. Nat Med *2*, 864-870.

Schmechel, D.E., Saunders, A.M., Strittmatter, W.J., Crain, B.J., Hulette, C.M., Joo, S.H., Pericak-Vance, M.A., Goldgaber, D., and Roses, A.D. (1993). Increased amyloid beta-peptide deposition in cerebral cortex as a consequence of apolipoprotein E genotype in late-onset Alzheimer disease. Proc Natl Acad Sci U S A *90*, 9649-9653.

Schwarz, K., Iolascon, A., Verissimo, F., Trede, N.S., Horsley, W., Chen, W., Paw, B.H., Hopfner, K.P., Holzmann, K., Russo, R.*, et al.* (2009). Mutations affecting the secretory COPII coat component SEC23B cause congenital dyserythropoietic anemia type II. Nat Genet *41*, 936-940.

Seubert, P., Vigo-Pelfrey, C., Esch, F., Lee, M., Dovey, H., Davis, D., Sinha, S., Schlossmacher, M., Whaley, J., Swindlehurst, C.*, et al.* (1992). Isolation and quantification of soluble Alzheimer's beta-peptide from biological fluids. Nature *359*, 325-327.

Shaner, N.C., Campbell, R.E., Steinbach, P.A., Giepmans, B.N., Palmer, A.E., and Tsien, R.Y. (2004). Improved monomeric red, orange and yellow fluorescent proteins derived from Discosoma sp. red fluorescent protein. Nat Biotechnol *22*, 1567-1572.

Shaw, G., Morse, S., Ararat, M., and Graham, F.L. (2002). Preferential transformation of human neuronal cells by human adenoviruses and the origin of HEK 293 cells. Faseb J *16*, 869-871.

Sherrington, R., Rogaev, E.I., Liang, Y., Rogaeva, E.A., Levesque, G., Ikeda, M., Chi, H., Lin, C., Li, G., Holman, K.*, et al.* (1995). Cloning of a gene bearing missense mutations in early-onset familial Alzheimer's disease. Nature *375*, 754-760.

Siman, R., and Velji, J. (2003). Localization of presenilin-nicastrin complexes and gamma-secretase activity to the trans-Golgi network. J Neurochem *84*, 1143-1153.

Sinha, S., Anderson, J.P., Barbour, R., Basi, G.S., Caccavello, R., Davis, D., Doan, M., Dovey, H.F., Frigon, N., Hong, J.*, et al.* (1999). Purification and cloning of amyloid precursor protein beta-secretase from human brain. Nature *402*, 537-540.

Small, S.A., and Gandy, S. (2006). Sorting through the cell biology of Alzheimer's disease: intracellular pathways to pathogenesis. Neuron *52*, 15-31.

Spasic, D., Tolia, A., Dillen, K., Baert, V., De Strooper, B., Vrijens, S., and Annaert, W. (2006). Presenilin-1 maintains a nine-transmembrane topology throughout the secretory pathway. J Biol Chem *281*, 26569-26577.

St George-Hyslop, P.H., Tanzi, R.E., Polinsky, R.J., Haines, J.L., Nee, L., Watkins, P.C., Myers, R.H., Feldman, R.G., Pollen, D., Drachman, D.*, et al.* (1987). The genetic defect causing familial Alzheimer's disease maps on chromosome 21. Science *235*, 885-890.

Steiner, H., Fluhrer, R., and Haass, C. (2008). Intramembrane proteolysis by gamma-secretase. J Biol Chem *283*, 29627-29631.

Strittmatter, W.J., Saunders, A.M., Schmechel, D., Pericak-Vance, M., Enghild, J., Salvesen, G.S., and Roses, A.D. (1993). Apolipoprotein E: high-avidity binding to beta-

amyloid and increased frequency of type 4 allele in late-onset familial Alzheimer disease. Proc Natl Acad Sci U S A *90*, 1977-1981.

Sullivan, C.P., Jay, A.G., Stack, E.C., Pakaluk, M., Wadlinger, E., Fine, R.E., Wells, J.M., and Morin, P.J. (2011). Retromer disruption promotes amyloidogenic APP processing. Neurobiol Dis *43*, 338-345.

Takahashi, R.H., Milner, T.A., Li, F., Nam, E.E., Edgar, M.A., Yamaguchi, H., Beal, M.F., Xu, H., Greengard, P., and Gouras, G.K. (2002). Intraneuronal Alzheimer abeta42 accumulates in multivesicular bodies and is associated with synaptic pathology. Am J Pathol *161*, 1869-1879.

Takasugi, N., Tomita, T., Hayashi, I., Tsuruoka, M., Niimura, M., Takahashi, Y., Thinakaran, G., and Iwatsubo, T. (2003). The role of presenilin cofactors in the gamma-secretase complex. Nature *422*, 438-441.

Tamarappoo, B.K., and Verkman, A.S. (1998). Defective aquaporin-2 trafficking in nephrogenic diabetes insipidus and correction by chemical chaperones. J Clin Invest *101*, 2257-2267.

Thinakaran, G., and Koo, E.H. (2008). Amyloid precursor protein trafficking, processing, and function. J Biol Chem *283*, 29615-29619.

Tran, J.H., Chen, C.J., Emr, S., and Schekman, R. (2009). Cargo sorting into multivesicular bodies in vitro. Proc Natl Acad Sci U S A *106*, 17395-17400.

Vassar, R., Bennett, B.D., Babu-Khan, S., Kahn, S., Mendiaz, E.A., Denis, P., Teplow, D.B., Ross, S., Amarante, P., Loeloff, R*., et al.* (1999). Beta-secretase cleavage of Alzheimer's amyloid precursor protein by the transmembrane aspartic protease BACE. Science *286*, 735-741.

Vieira, S.I., Rebelo, S., Esselmann, H., Wiltfang, J., Lah, J., Lane, R., Small, S.A., Gandy, S., da Cruz, E.S.E.F., and da Cruz, E.S.O.A. (2010). Retrieval of the Alzheimer's amyloid precursor protein from the endosome to the TGN is S655 phosphorylation state-dependent and retromer-mediated. Mol Neurodegener *5*, 40.

Waguri, S., Dewitte, F., Le Borgne, R., Rouille, Y., Uchiyama, Y., Dubremetz, J.F., and Hoflack, B. (2003). Visualization of TGN to endosome trafficking through fluorescently labeled MPR and AP-1 in living cells. Mol Biol Cell *14*, 142-155.

Walsh, D.M., and Selkoe, D.J. (2004). Deciphering the molecular basis of memory failure in Alzheimer's disease. Neuron *44*, 181-193.

Wang, C.W., Hamamoto, S., Orci, L., and Schekman, R. (2006). Exomer: A coat complex for transport of select membrane proteins from the trans-Golgi network to the plasma membrane in yeast. J Cell Biol *174*, 973-983.

Wolfe, M.S., Xia, W., Ostaszewski, B.L., Diehl, T.S., Kimberly, W.T., and Selkoe, D.J. (1999). Two transmembrane aspartates in presenilin-1 required for presenilin endoproteolysis and gamma-secretase activity. Nature *398*, 513-517.

Xu, H., Sweeney, D., Wang, R., Thinakaran, G., Lo, A.C., Sisodia, S.S., Greengard, P., and Gandy, S. (1997). Generation of Alzheimer beta-amyloid protein in the trans-Golgi network in the apparent absence of vesicle formation. Proc Natl Acad Sci U S A *94*, 3748-3752.